**Deep Sea Research Part I: Oceanographic Research Papers**
January 2022, Volume 179, Pages 103630 (26p.)
https://doi.org/10.1016/j.dsr.2021.103630
https://archimer.ifremer.fr/doc/00728/84052/



# Extending the dataset of fluid geochemistry of the Menez Gwen, Lucky Strike, Rainbow, TAG and Snake Pit hydrothermal vent fields: Investigation of temporal stability and organic contribution

Konn Cécile [1, *], Donval Jean-Pierre [1], Guyader Vivien [1], Germain Yoan [1], Alix Anne-Sophie [1], Roussel Erwan [2], Rouxel Olivier [1]

[1] Ifremer, Laboratoire des Cycles Géochimiques et ressources, CS10070, F-29280, Plouzané, France
[2] Ifremer, Laboratoire de Microbiologie des Environments Extrêmes, CS10070, F-29280, Plouzané, France

* Corresponding author : Cécile Konn, email address : cecile.konn@lilo.org

**Abstract :**

The Menez Gwen, Lucky Strike, Rainbow, TAG (Transatlantic Geotraverse) and Snake Pit hydrothermal vent fields on the Mid-Atlantic Ridge were revisited and resampled for geochemical investigation during the BIOBAZ 2013 and BICOSE 2014 research cruises. Geochemical analysis of the major and minor elements of the hydrothermal fluid and concentrations of gases extends and complements the existing dataset. Our results are consistent with values previously reported and fall within the range of the analytical error. This indicates that the hydrothermal vent field system has remained relatively stable over the last few decades. However, some differences were observed and (i) suggested a recent eruption at Menez Gwen, (ii) supported the occurrence of low-temperature serpentinisation in this same site, (iii) supported a change in the reaction zone or axial magma chamber (AMC) depth at Lucky Strike, (iv) an increase of the temperature at depth at Snake Pit and (v) supported the hypothesis of large seawater entrainment through the TAG hydrothermal mound. Besides, it is possible that small temporal and spatial scale processes may control a significant part of the geochemistry, owing to the fact that some variations in the data could not be interpreted. However, our investigation of the organic geochemistry represents a pioneering addition to research for Menez Gwen, Snake Pit and TAG and a much more comprehensive study for Lucky Strike and Rainbow. Concentrations for a wide variety of semi volatile organic compounds (SVOCs) were obtained for the first time at all sites. Our results showed that a great part of the total organic carbon (TOC) could not be allocated by the total SVOCs studied here, suggesting that other processes/sources of organic carbon remain to be identified. The TAG organic geochemistry seemed entirely based on thermogenic processes whereas mixed processes may occur at the other vent field. The presence of n-alkanes suggested the contribution of a low-temperature fluid at all sites. An additional high-temperature organic matter degradation component was likely present at Menez Gwen and Lucky Strike. Our results also indicated that both abiogenic and biogenic processes produced organic compounds. Therefore, we suggest that a portion of the fatty acids at Menez Gwen and polyaromatic hydrocarbons (PAHs) at Rainbow may be derived from abiogenic processes, whereas biogenic processes could be responsible for the presence of n-fatty acids (n-FAs) at Lucky Strike and Rainbow. Moreover, organic geochemistry data appeared to be helpful in understanding some inorganic processes.

**Highlights**

► Organic compounds of MAR hydrothermal fluids: concentrations, interests and implications.

**Keywords** : Hydrothermal systems, Organic geochemistry, Fluid geochemistry, Gases, Major and minor elements

## 1 Introduction

The first submarine warm springs were discovered in the Pacific near the Galapagos exhibiting fluids at ~30°C above ambient seawater (Corliss *et al*., 1979). The existence of a ~350°C fluid was subsequently inferred and discovered a few years later at 21°N on the East Pacific Rise (EPR) (Edmond *et al*., 1979; Von Damm *et al*., 1985). Hydrothermal activity was associated with basaltic and highly active ridges. At that time, hydrothermal systems were not expected to be found on slow-spreading ridges, including the Mid-Atlantic Ridge (MAR). It was also believed that all hydrothermal fluids should have the same chemical composition deriving from seawater / basalt interactions. Subsequent research showed that the geochemistry of the fluids was as varied as the number of discovered vent fields which contributed to numerous research questions and notably the possibility for hydrothermal activity to occur in various environments. The first hydrothermal vent to be discovered on the MAR was the Transatlantic Geotraverse (TAG) in 1972 (Scott *et al*., 1974). Since then hydrothermal activity has been largely studied on the MAR and up to date 45 hydrothermal vents have been discovered and ~50 are inferred (Beaulieu and Szafranski, 2020). However, some vent fields have remained unstudied since their discovery. For example, the TAG and Snake Pit hydrothermal vent field had not been sampled since the late 1990s (Rudnicki and Eldelfield, 1992; Edmond *et al*., 1995; Edmonds *et al*., 1996; Charlou *et al*., 1996) while the last published data for the Menez Gwen hydrothermal mound dated from 2001 (Charlou *et al*., 2001). By contrast, other vent fields such as Rainbow and Lucky Strike have been the focus of many studies at somewhat regular time scales (last published data in Seyfried *et al*., 2011; Pester *et al*., 2012). Notably, Lucky Strike has been hosting a seafloor observatory since 2010 to monitor several physical and chemical parameters (Cannat *et al*., 2011). Time series data are of great importance to further understand chemical processes, the overall functioning of hydrothermal systems and temporal evolution of hydrothermal activity. Here

we report on concentrations of major and minor elements, gas species and isotopes, which extend existing datasets for 5 hydrothermal vent field of the MAR (Menez Gwen, Lucky Strike, Rainbow, TAG and Snake Pit).

Besides, the majority of studies on hydrothermal fluid composition focus on element and/or gas geochemistry while a few studies report on organic geochemistry and in most cases they dealt with small molecules (hydrocarbon gases, volatile fatty acids, amino acids). Very little data is available on semi-volatile organic compounds (SVOCs) and is hardly ever quantitative. Despite the growing interest for organic matter (OM) in the ocean and hydrothermal systems there is still a major lack in identification and quantification of organic compounds (Amon, 2016; Bennett *et al*., 2011; Hawkes *et al.*, 2016; Hawkes *et al*., 2015; Lang et al., 2006; Longnecker *et al*., 2018). A numbers of studies agree on the major ligand role of organics in metal stabilisation, transportation, bioavailability and ore-forming but there are hardly any clues on the nature of these ligands in hydrothermal environments (Breier *et al*., 2012; Brugger *et al*., 2016; Fitzsimmons *et al*., 2017; Gautier *et al*., 2015; Gerringa *et al*., 2015; Hawkes *et al*., 2013; Homoky, 2017; Sander and Koschinsky, 2011; Seward *et al*., 2014; Toner *et al*., 2009). Organic compounds in hydrothermal fluids may come from marine dissolved organic matter recycling (Hawkes *et al*., 2016; Hawkes *et al*., 2015), sub-surface biomass degradation (Konn *et al*., 2011), entrainment of organic detritus from local recharge zones and subsequent degradation, or abiotic formation in the deep sub-surface (Konn *et al*., 2009; Lang *et al*., 2010; McDermott *et al*., 2015; Reeves and Fiebig, 2020; Reeves *et al*., 2014). The latter is supported by many theoretical (e.g. Shock and Canovas, 2010; Shock, 1990; Shock, 1992) and experimental work summarised in two reviews (McCollom, 2013; McCollom and Seewald, 2007). Field data only exist for the Lost City, Rainbow, Lucky Strike and Fatu Kapa (Wallis & Futuna region) hydrothermal vent fields (Konn *et al*., 2009; McCollom *et al*., 2015; Konn *et al*., 2018). In the MAR area, organic compounds have been

reported and partly quantified in the fluids from the Lost City alkaline vent field (Konn *et al*., 2009; McCollom *et al*., 2015). Conversely, the presence of organic compounds in fluids from Rainbow and Lucky Strike appears more controversial according to those studies. Nevertheless, we report the presence of SVOCs in hydrothermal fluids from 5 vent fields of the MAR (Menez Gwen, Lucky Strike, Rainbow, TAG and Snake Pit). In addition, we provide the concentrations of a selection of extractable organic compounds that have been identified previously as hydrothermally derived (Konn *et al*., 2012; Konn *et al*., 2009; Konn *et al*., 2018): *n*-alkanes, *n*-fatty acids (*n*-FAs), mono- and poly- aromatic hydrocarbons (BTEXs and PAHs). These very first quantitative field data for the MAR area might feed thermodynamic models of abiotic synthesis, guide the design of experiments to better understand hydrothermal organic geochemistry, help assessing the importance of hydrothermally derived organic compounds in metal complexation and as a nutrient for microorganisms, complete fluxes calculation, and enter in the carbon cycle budget calculations.

## 2 Geological settings, site descriptions and sampling location

The slow spreading MAR is characterised by a deep, up to 15 km across, fault-bounded axial valley hosting sporadic volcanic edifices. Coupled magma-tectonic processes result in a variety of discontinuities in the ridge structure consisting in offsets of the rift axis as small as < 1 km and up to > 30 km. Near the largest transform faults that drive these deviations, the seafloor generally rises significantly (up to > 4000 m) over rather long distances (10-15 km) (Kelley *et al*., 2002 and references therein). Each segment of the rift valley is bounded by 2 discontinuities and has its own characteristics in terms of spreading rates, tectonics, rocks, and manifestations of hydrothermal activity. Hydrothermal systems have been found at a variety of locations including on-axis, off-axis, in the vicinity of faults, in the centre of a segment, on

detachment faults. The different vent fields sampled for the present study were all located in a slow-spreading context but were hosted in varied geological settings (Figure 1).

### 2.1 Menez Gwen

The Menez Gwen segment of the MAR is about 55 km long and marks the southern end of the Azores platform. The absence of a rift valley in this segment is notable. A large volcano of 850 m high with a mean diameter of 15 km is present near the centre of the segment. The top part is divided into two halves by a 2 km-wide and 9-km long axial graben that forms a 300 to 400 m-deep valley across the volcano. The graben hosts a lava lake in its deepest part consisting in fresh to very fresh lavas (pillars, pillows, lobate flows). Several recently formed minor volcanoes are scattered across the northern part of the graben and mark the intense volcanic activity of the Azores hotspot. The largest of them (central volcano) is about 700 m wide, up to 200 m high (Figure 2). The surface rocks of this young volcano are composed of fresh lava and some volcanic breccia (Fouquet *et al*., 1994; Ondréas *et al*., 1997). The lava has no sediment cover, and it has been suggested that the entire volcano developed during the latest eruptive episode (Ondréas *et al*., 1997). All lavas at Menez Gwen are enriched due to the contribution of the Azores hotspot (Marques *et al*., 2011).

The Menez Gwen hydrothermal field was discovered in 1994 and is the shallowest and youngest (<100 y) site known on the MAR lying at 800 m depth (Fouquet *et al*., 1994). Very little fauna was reported at Menez Gwen, yet our last visit in 2013 revealed large patches of the deep-sea bivalve, *Bathymodiolus*. The hydrothermal activity is mainly concentrated on 200 $m^2$ on the southern and eastern flanks of the central volcano at 800 m depth (Fouquet *et al*., 1994). In 1994, one site on the southern flank was characterized by a 50 m-wide mound with a low elevation and 2 m-high anhydrite chimneys, which was surrounded by diffusive barite-rich small and flat mounds (Fouquet *et al*., 1994). Today these mounds are capped by small sulphides chimney venting shimmering fluids (Marques *et al*., 2011). The other site

148 was an escarpment topped by a chimney, which was bordered by pillow lavas and crumbled rocks.

150 Samples were taken at the summit of the White Flames area in a short anhydrite chimney expelling a translucent fluid (Figure 2). Mussels were present as large patches nearby the 152 sampled chimney. The reference water sample was taken at 3.4 m altitude, ~160 m away from the active mound.

154 **2.2 Lucky Strike**

The Lucky Strike segment and hydrothermal vent fields have been well mapped and 156 described elsewhere (Ondréas *et al*., 2009), and therefore only some of the main features are described here. The segment stretches on ~60 km between 37°03'N and 37°37'N, just south 158 of the Menez Gwen segment and is bounded by non-transform offsets. A fairly constant width of 10-15 km is maintained all along the segment and the spreading rate is ~22 mm/yr. 160 At the middle of the segment, a central volcano rises to 1660 m water depth. It is mostly comprised of volcanic breccia and pillow lavas (which are cut by a number of 162 faults/lineaments). Outside of the central volcano only fresh lobate and sheet-flow lavas have been observed. Most of the MORBs (Mid-Oceanic Ridge Basalts) present in the centre of the 164 segment are enriched in incompatible elements (E-MORBs), consistent with an influence of the Azores hotspot (Wanless *et al*., 2015).

166 The Lucky Strike hydrothermal vent field was first discovered in 1992 during the FAZAR cruise and has been revisited a large amount of times since (Langmuir *et al*., 1997). 168 It occurs in the summit basin, infilled by lava from the central volcano that nearly extends across the rift. At some time after its formation, it has been rifted in two parts separated by a 3 170 to 5 km wide and 50 to 100 m-deep graben. The present-day summit of the volcano is infilled by lava and is formed of three volcanic cones that surround a 1 km-diameter, 100 m-deep 172 depression, which hosts most of the venting sites at 1700 m depth (Humphris *et al*., 2002;

Ondréas *et al*., 1997) (Figure 3). Notably two other active vents have recently been discovered (Escartin *et al*., 2015). The peculiarity of the Lucky Strike hydrothermal vent field is the variety of fluid chemistries as nearly each vent exhibits a different chemistry (Chavagnac *et al*., 2018). Consistently, substrates exposed on the seafloor also show a great diversity with lavas, sulphides, basalts and sediments (Langmuir *et al*., 1997). Lucky Strike is one of the 3 hydrothermal systems where a local axial magma chamber (AMC) could be imaged (Singh *et al*., 2006). It is located ~3 km beneath the vent field and is thought to sustain hydrothermal activity and circulation along permeable faults that have been shown to penetrate down to the AMC (Crawford *et al*., 2013; Escartin *et al*., 2015; Singh *et al*., 2006).

Our study focused on the Montsegur and Tour Eiffel vents in the southeastern area of the main field where the seafloor is dominated by slabs of cemented breccia comprising of basaltic glass, plagioclase crystals, sulphides, barite and silica (Figure 3) (Langmuir *et al*., 1997). Montsegur is representative of the venting type in that area which comprises of small active black smokers (< 50 cm high and < 10 cm outer diameter) on top of small sulphide mounds. Fluid samples were collected from a greyish fluid expelling short chimney surrounded by mussels and bacterial mats (Figure 3). By contrast Tour Eiffel consists of a tall tapered spire of ~20 m high expelling focused hot fluids. The mineralogy of the chimneys was reported to be typical of black smokers i.e. massive chalcopyrite for the inner wall; pyrite, anhydrite and small amounts of sphalerite and marcasite for the outer wall (Langmuir *et al*., 1997). Greyish fluids were sampled from a small group of chimneys on the flank of the edifice which was nearly lacking fauna; a few juvenile shrimp were observed. The reference water sample was taken at 5 m altitude at ~140 m and ~70 m west of the Montsegur and Tour Eiffel vents, respectively.

196 **2.3 Rainbow**

The Rainbow massif is located south of the Azores, at an offset between the Azores Mid-
198 Atlantic Ridge (AMAR) and South-AMAR segments and at the intersection of the non-transform fault system and the ridge fault system. The particular location is most likely due
200 to local tectonics that would have extruded the massif like an oceanic core complex (Ildefonse *et al*., 2007). The present-day full spreading rate of this MAR region is ~21.5 mm/yr.

202 The Rainbow hydrothermal field is located at 36°14'N and 2300 m depth, on the west-facing flank of the Rainbow massif (Figure 4) (Charlou *et al*., 2002a). The vent field size is
204 about 250 m (E-W) by 100 m (N-S) and consists of at least 10 groups of highly active black smokers, which are distributed over the entire field. Chimneys at Rainbow are typically made
206 of sulphides enriched in Co, Ni, Zn, Cu (e.g., Fouquet *et al*., 1998). In contrast to the other vent fields studied in this work, the Rainbow hydrothermal vent field is hosted on ultramafic
208 peridotite-rich mantle rocks (Charlou *et al*., 1998; Fouquet *et al*., 1998). Only a small veneer of old basalts has been found on the Rainbow ridge, 1 km away from the active field.
210 Hydrothermal circulation was thought to be controlled by tectonics, however, until 2013 the heat source(s) capable of sustaining the high temperatures observed at Rainbow was (were)
212 uncertain (Seyfried Jr *et al*., 2011). Recent seismic imaging has revealed that the ultramafic rocks composing the Rainbow massif are intruded by a large number of magmatic sills,
214 distributed throughout the massif at depths of ~2–10 km. These sills can supply the heat needed to drive high-temperature hydrothermal circulation (Canales *et al*., 2017).

216 The Rainbow hydrothermal vent field has been the focus of many studies and thus sampled for fluids every 2-4 years between its discovery in 1997 during the FLORES cruise
218 and the BIOBAZ cruise in 2013. During the latest, fluid samples were recovered from the IRIS 3 and USB/TAC vents which are typical strongly active black smokers of the Rainbow
220 field (Figure 4). They are located, respectively, west and east of the major edifice

Thermitière. They consist of a series of short and aligned black smokers. In contrast to the Thermitière area (where swarms of *Rimicaris exoculata* shrimp thrive), this particular site showed no evidence of fauna. The reference water sample was collected at ~250 m northwestward of the active vents, in the inactive zone.

### 2.4 Snake Pit

The Snake Pit hydrothermal vent field is located in the MARK (MAR Kane Fracture Zone) area which corresponds to the area immediately south of the eastern intersection of the Kane fracture zone (FZ) and a 40 km-long segment of the MAR with an accretion rate of 25 mm/y (Fouquet *et al*., 1993; Karson and Brown, 1988) (Figure 1). Tectonised basaltic lavas constitute the seafloor of the rift valley, whereas walls contain gabbros, basalts and serpentinised peridotites. Grabbroic rocks are exposed near the ridge-transform intersection as well as off axis and in the southern wall of the FZ (Auzende *et al*., 1994; Cannat *et al*., 1995). Notably, exhumed mantle rocks are present south of the Kane FZ at 50 km of the rift axis but also at the axis in the shape of a 2 km-wide and 20 km-long band of peridotite spreading to the south of the FZ (Alt and Shanks, 2003; Gente *et al*., 1991).

The Snake Pit hydrothermal field was discovered and sampled in 1985 (Kong *et al*., 1985). It lies at 23°23'N, 3500 m depth and at the axis of a neovolcanic ridge located in the centre of the rift valley. It has not been the focus of many studies and indeed had not been sampled for fluids since 1995. The scarce occurrence of sediments and the age of the most ancient sulphurs (4000 years) suggest that the formation of the Snake Pit hydrothermal system is fairly recent (Lalou *et al*., 1993). The site comprises 3 coalescent East-West trending mounds and covers about 0.45 $km^2$ in which distinct active zones can be described. The most active vents from the Snake Pit system are Moose and Beehive (Figure 5). More details can be found in a comprehensive study by Fouquet and collaborators (1993).

Fluid samples were collected at the Moose (Elan) and Beehive (Ruche) vents located on the southern part of the vent field (Figure 5). Both consist in large edifices covered with shrimp swarms and expelling hot-black fluids. In terms of mineralogy, the Beehive site is enriched in Zn and present immature facies. Chalcopyrite, isocubanite, pyrite and sphalerite are the dominant minerals with the presence of some pyrrhotite, marcasite and amorphous silica. Deep-sea reference water sample was taken at ~50 m and ~75 m of the Beehive and Moose vents, respectively, at 18 m altitude.

### 2.5 Transatlantic Geotraverse (TAG)

The TAG hydrothermal vent field is located at 26°08'N on a 40 km-long ridge segment that is bordered to the north and the south by the Kane FZ and the Atlantis FZ, respectively (Figure 1). The TAG segment is characterised by an asymmetrical rift valley resulting of different spreading rates to the east (12.1 mm/y) and to the west (8.7 mm/y) (Canales *et al*., 2007; deMartin *et al*., 2007; Kleinrock and Humphris, 1996; Tivey *et al*., 2003).

The TAG hydrothermal vent field was first discovered by Rona and collaborators (1986) and has been active for the past ~140 000 y (Lalou *et al*., 1995). A detailed description of the vent field can be found in Humphris *et al.* (2015). The location of the TAG hydrothermal system is quite unique being on the hanging wall of an active detachment fault (Canales *et al*., 2007; deMartin *et al*., 2007; Tivey *et al*., 2003). It lies at 3600 m depth, 2.4 km to the east of the ridge axis and adjacent to the eastern wall of the valley (Lalou *et al*., 1993). High-resolution bathymetric data and imagery revealed that the active mound is 50 m-high and consists of two quasi-concentric platforms (Humphris and Kleinrock, 1996; Pontbriand and Sohn, 2014). The outer mound is ~200 m in diameter, whereas the inner one is only half its diameter and corresponds to the main currently active hydrothermal area. Focused, high-temperature activity mainly occurs at the summit of a 12 m tall conical structure and consists in a cluster of black smoker chimneys. However, a new active area was discovered during the

BICOSE cruise (2014) in the depression of the inner caldera, south-east of the active mound and comprised in tiny recently formed black smokers surrounded by juvenile shrimp lying on the floor (Figure 6). The active mound is hosted on a basalt crust of about 100,000 years old but consists in a massive sulphide deposit made of pyrite and pyrite breccia overlying pyrite, anhydrite and pyrite-silica breccia (Humphris *et al*., 2015). The stockwork zone consists of sulphide veins within altered basalt and is restricted to an 80-m-diameter central zone beneath the mound. Hydrothermal circulation is likely related to a deep gabbroic inclusion at the foot of the detachment fault (deMartin *et al*., 2007).

The sampling strategy aimed at collecting fluids from a variety of smokers to best constrain the geochemistry of the site (Figure 6). Both the summit (Marge Chimney) and the flank of the active mound were sampled as well as the newly discovered area (New Black Smoker). Reference water samples were taken on the outer mound rim at > 100 m to the southeast of the active area.

## 3 Sampling, sample preparation and analytical procedures

Sampling was achieved at all sites by the Remote Operated Vehicle (ROV) Victor 6000 during the BIOBAZ (Lallier, 2013) and BICOSE (Cambon, 2014) cruises conducted by Ifremer in 2013 and 2014. Samples of volumes up to 750 mL were collected in titanium air-tight syringes equipped with autonomous temperature sensors (S2T 6000-DH, nke instrumentation) and that were modified after the model described in Von Damm *et al.* (1985) to improve air-tightness and chemical inertness. The bottom pressure is compensated by volume adjustment which enables recovery of nearly 100% of gases. The inner cylinder is coated by a µm thick Teflon coating to avoid metal catalysed reactions within the sampler. Fluid samples were taken after flushing the dead volume of the syringes in the hydrothermal fluid and at the nose of smokers to minimise dilution and possible contamination by seawater

mixing. Reference deep seawater samples were taken at each hydrothermal field, in areas exempt of hydrothermal activity, in open waters, having the submersible moving forward and as much as possible to the opposite direction of the local current. Duplicate syringes were taken at each sampled vent, one for the study of gases and elements, the other one for organic geochemistry analyses. As soon as the fluids were recovered, pH, $H_2S$ and $Cl^-$ concentrations were measured to evaluate the quality of the sample. Total gases were immediately extracted, then analysed on-line, and aliquots of gas were conditioned for further stable isotopes measurements. The gas-free fluid was conditioned for major and minor elements analyses. The duplicate sample was not extracted for gases and directly prepared for organic compounds analyses.

### 3.1 Gases geochemistry

Total gas was extracted as described in Charlou and Donval (1993). Preliminary major gases ($CO_2$, $H_2$, $CH_4$, and $N_2$) concentrations were obtained on board by using a portable chromatograph (*Microsensor Technology Instruments Inc.*) that was on line with the gas extractor. Extracted gases were conditioned on board in stainless steel pressure-tight flasks and stored until analyses. Gases were separated by Gas-Chromatography (Agilent GC 7890A, *Agilent Technologies*) and quantitatively analysed by triple detection using mass (MS 5975C, *Agilent technologies*), flame ionisation (FID) and thermal conductivity (TCD) detectors. Aliquots of the total extracted gas were stored both in vacuum tight tubes (*Labco, Ltd.*) and copper tubes to be sent for further carbon isotope analyses (*Isolab b. v., Netherlands*) and He isotopes analyses (*CEA, Saclay, France*), respectively. Note that these same methods were used for samples collected in 1995, 2005 and 2008.

316 **3.2 Inorganic geochemistry**

Immediately after sample recovery from the submersible, (i) pH was measured using a
318 combined glass electrode (*ecotrode plus, Metrohm*) ; (ii) $Cl^-$ was measured by potentiometry using $AgNO_3$ (0.05 M) as titrating solution and $H_2S$ was measured, in NaOH (2M) buffered
320 aliquots, using $HgCl_2$ (0.01 M); (iii) Aliquots for silica determination were immediately diluted 100- to 200-fold and analysed by a silico-molybdate automatic colorimetric method
322 (Grasshoff, 1970; Mullin and Riley, 1955) ; the remaining of the sample was stored in nalgene bottles. Back on land, the entire volume of fluid samples was acidified and filtered
324 using Supor® 200 polyethersulfone membrane filters, 47 mm diameter, 0.2 µm pore size, resulting to separation of particles from the soluble fraction. Nalgene bottles were heated in
326 an HCl solution to remove all material adsorbed on the surface; this fraction was combined to the dissolved fraction. Filters were digested in a solution of $HNO_3$ resulting in the particulate
328 fraction. Major and minor elements compositions in both fractions were determined by high-resolution inductively coupled plasma mass spectrometry (HR-ICPMS) Element XR operated
330 at Ifremer. Indium solution was used as an internal standard and mixed on-line at a final concentration of 5 ppb to correct for instrument sensitivity changes. Solutions were
332 introduced into the plasma torch using a quartz spray chamber system equipped with a microconcentric PFA nebulizer operating at a flow rate of about 100 $\mu l.min^{-1}$. For each
334 element, ICPMS sensitivity was calibrated using matrix matched standard solutions, both commercial (IAPSO and NASS6) and personal, corresponding to seawater matrices.

336 Endmember concentrations were calculated via least-squares regression of an individual conservative chemical species as a function of Mg, weighted to pass through bottom seawater
338 composition and extrapolated to 0 $mmol.kg^{-1}$ of Mg. Sampled fluid compositions were thus assumed to reflect two-component mixing of a zero-Mg 'endmember' fluid with bottom
340 seawater. This is based on the hypothesis that hydrothermal fluids undergo near quantitative

removal of Mg and $SO_4$ during fluid-rock reaction with basalt and gabbro at high
342 temperatures (>300°C) and low water/rock ratio (e.g., Mottl and Holland, 1978; Von Damm *et al*., 1985), although this has been recently debated for the Rainbow hydrothermal vent field
344 (Seyfried Jr *et al*., 2011).

### 3.3 Organic geochemistry

346 Total Organic Carbon (TOC) was measured using a multi 3100 N/C (Analytik Jena AG, Germany) that was calibrated on a 0-20 ppm range with standard solutions of KHP
348 (potassium hydrogen phthalate). Unfiltered samples were acidified online with HCl and then purged with $O_2$ to remove inorganic carbon (IC). A Total Inorganic Carbon (TIC) control
350 analysis was performed to check the remaining level of TIC was well below the level of TOC and then followed by three TOC measurements on each sample. At the beginning of each
352 analytical sequence the machine was rinsed with Milli-Q® water (MQ water) until the level of organic carbon was below limit of quantification (usually 3 times) and then a 10 ppm TOC
354 standard (KHP) was injected until the value was correct (usually 3 times). Then samples were analysed and a MQ water control was inserted every 5 samples and a 10 ppm standard
356 solution was run in the middle and at the end of the sequence.

Acetate and formate concentrations were determined after centrifugation (5 min,
358 15000 g) and dilution (1/10 in deionised water) of samples. Analyses were performed using a Dionex ICS-2000 Reagent-Free Ion Chromatography System equipped with an AS50
360 autosampler (*Dionex Camberley UK*). Chromatographic separation was conducted using two Ionpac AS15 columns in series at 30°C and the determination of species was carried out using
362 an Anion Self-Regenerating Suppressor (*ASRS 300 4-mm*) unit in combination with a DS6 heated conductivity cell (35°C). The gradient program was as follows: 6 $mmol.L^{-1}$ KOH (43
364 min), increase 27 $mmol.L^{-1}$ KOH $min^{-1}$ to 60 $mmol.L^{-1}$ (39 min), decrease 54 $mmol.L^{-1}$ KOH $min^{-1}$ to 6 $mmol.L^{-1}$ (5 min).

366 Semi Volatile Organic Compounds (SVOCs) were extracted using Stir Bar Sorptive Extraction (SBSE). Any compound with a log Ko/w > 2.5 is recovered with a rate > 50 %
368 (Baltussen *et al*., 1999). The method was improved after Konn *et al.* (2012). The entire, unfiltered, content of the titanium syringe was transferred into a precombusted glass bottle
370 and six 90 mL-aliquots of the sample were poured into 100 mL precombusted glass vials. 10 mL of MeOH was added to avoid adsorption of the compounds onto the wall of the vials.
372 Internal standards (IS) were added to the solutions to enable quantification. Extraction was performed in sealed vials with ultra-inert septum crimps, at 300 rpm and using 48 µL PDMS
374 Twisters® (Gerstel GmbH). We focused on a selection of chemical groups that had previously been described as hydrothermally derived (Konn *et al*., 2009). To that respect,
376 pairs of aliquots were dedicated to separate analysis of *n*-alkanes, n-FAs and BTEXs + PAHs. Extraction kinetics were experimentally studied and showed that chemical equilibrium was
378 reached after 5h of extraction for n-alkanes, 4h for BTEXs and PAHs, and 14h for *n*-FAs (Konn, unpublished results). Twisters® were then removed, rinsed with MQ water, dried and
380 stored at +4°C until analyses by Thermal Desorption – Gas Chromatography – Mass Spectrometry (TD-GC-MS) (Konn *et al*., 2012). Compounds were separated by GC on a 30
382 m long HP5-ms capillary column (0.25mm ID, 0.25 µm film) and analytical parameters were adjusted for each group of compounds (Table 1).

384 For each batch of conditioned Twisters®, one was spared, stored at +4 °C and analysed in the same run as the other Twisters®. This dry blank aimed at detecting any
386 contamination that could have occurred during conditioning, storage and transport. MQ water samples were prepared and extracted on board as regular hydrothermal samples to check if
388 any contaminations occurred during the sample preparation step. Deep seawater was also collected, processed and analysed using the same titanium syringes and according to the same
390 protocols as for hydrothermal fluid samples; and thus constitute the reference blank sample.

Calibration was achieved using a commercial standard solution of BTEXs and custom standard solutions of C9-C20 *n*-alkanes, of C6-C18 n-FAs, and of PAHs containing Naphthalene (N), Acenaphtene (A), Fluorene (F), Phenanthrene (Ph), Anthracene (An), Fluoranthene (Fl), Pyrene (Py) (*LGC Standards, LGC Ltd.*). Respectively, deuterated *n*-alkanes ($C_{10}D_{22}$ and $C_{14}D_{34}$), methyl esters ($C_9H_{18}O_2$ and $C_{15}H_{30}O_2$) and deuterated PAHs (Naphthalene-D8, Biphenyl-D8 and Phenanthrene-D10) were used as IS. Calibration curves (Concentration (analyte) / Concentration (IS) vs area (analyte) / area (IS)) were obtained using at least five concentration levels covering the whole range of concentrations observed in natural fluids. Each level was replicated 3 times. Calibration model equations were obtained on maximum one order of magnitude for each individual compound. Although the correlation coefficient of the linear regressions was satisfactory for all compounds, the significance and lack of fit of the model were checked by statistical tests before validation. A series of Student, Barlett, Chi-square and Fisher tests was run for each individual compound using the Lumière software. The best fitting model was then chosen for each case and confidence intervals were calculated.

# 4 Results

## 4.1 Elements and gases

In 2013 and 2014, the Menez Gwen, Lucky Strike, Rainbow, Snake Pit and TAG hydrothermal vent fields were revisited and resampled both for monitoring element and gas concentrations and acquiring new parameters. Although data have been previously published for most species, some vent fields had hardly ever been revisited since their discovery. Elements and gases concentration data for each sample can be found in the supplementary material (Konn *et al.*, submitted to data in brief, 2021). Endmember compositions of the fluids of the studied vent fields are presented in Table 2 and a time series of endmembers can

be found in Table 3 as for elements and in Table 4 as for gases. In general, our results fall within the range of the analytical error when compared to previously published values which constitutes a precious piece of information regarding time scale evolution of hydrothermal vent fields. Nonetheless, some variations were observed and detailed by individual sites below.

At Menez Gwen, maximum measured temperature in 2013 was 300 °C which is 20 degrees higher than the last record (1994). We also measured higher concentrations of Mn (98.5 µM vs 65.6 µM) and Li (321 µM vs 203-278 µM) compared to 1994 data. Unlike Ba concentration was lower (10.3 µM vs 27 µM). Finally, B had never been reported at Menez Gwen and reached 445 µM.

At Lucky Strike, our Cl value (415mM) seemed to follow a decreasing slow trend over the 20 year-period of sampling. However, the Li concentration had slightly increased in 2013, while between 1993 and 2008 concentrations remained stable. Fe, Cu and Zn concentrations appeared to be very different at Tour Eiffel and at Montségur over the 1993-2005 period, yet, we did not observed this discrepancy in 2013 with a common endmember value of 429 µM, 13.6 µM, and 22.9 µM, respectively.

In the Rainbow fluid samples, Cl, Na and K were slightly lower in 2013 compared to the last 20 years of sampling whereas Sr, B and Fe showed a slight increase. More striking were both the significant increase of Li by ~100 µM and the Ba content that was divided by a factor of two.

In 2014, at Snake Pit, Si (17 mM) seemed to have decreased alongside with a temperature increase (357 °C) compared to 10 years earlier. Fe has been constantly increasing over the past 30 years and was ~ 64% higher in 2014 than in 1986. Zn, Cu, Li and K concentrations were also higher in 2014 compared to the 1986-1990 time period. Previous gas data were rather sporadic while a more comprehensive data set was obtained in 2014. Notably C and H

440 stable isotopes measurements were achieved and values obtained were $\delta D(H_2)$ = -315/-346 ‰, $\delta C(CO_2)$ = -3 ‰, $\delta C(CH_4)$ = +8.9/-7.4 ‰ in Beehive/Moose samples. Significant changes
442 have occurred in the Snake Pit fluid gas composition since 1988-1995 and compositions appear notably different at Moose and Beehive.

444 Small changes in the fluid element chemistry were observed in 2014 at TAG. The pH was lower, Fe was clearly increased in our samples and Li was almost twice as high in 2014 as in
446 the past. In terms of gas concentrations measured in 2014, $H_2$, $CO_2$ and He seemed to have dropped since 1993 whereas $H_2S$ and $CH_4$ concentrations have remained similar.

448 **4.2 Organics**

TOC was measured in 2014 in TAG and Snake Pit fluids and were in the 1.5-15.4 ppm
450 and 1.8-17.3 ppm, respectively. Formate and acetate concentrations were in the 1.0-2.4 µM and 4.5-8.1 µM ranges, respectively at Snake Pit. Similar values were obtained at TAG with
452 formate 1.4-1.9 µM and acetate 2.3-6.3 µM.

In addition, concentrations of chosen series of n-alkanes, n-FAs, BTEXs and PAHs were
454 measured at all visited vent fields both in hot fluids and background seawater. Such a large organic dataset had never been reported for the Atlantic. Individual compounds
456 concentrations are summarised in Table 5 and results are presented in Figure 7, Figure 8 and Figure 9. Note that the whole dataset has been submitted to data in brief (Konn *et al*., 458 submitted). Concentrations of *n*-alkanes and *n*-FAs were in the 0.1-12 ppb range in all samples, with the exception of Menez Gwen fluids that exhibited higher concentrations of *n*-
460 FAs reaching 24 ppb. Usually, BTEXs and PAHs concentrations were much lower not exceeding the sub-ppb level.

462 Extractable SVOCs were not detected in the dry control experiment. Unlike, the MQ water control experiment revealed the presence of *n*-alkanes (Table 5). The MQ system used
464 during the BIOBAZ cruise was not equipped with a UV light to remove the majority of the

TOC, so we assume that MQ water contained significant amount of TOC. Nevertheless, even with a controlled TOC rate, purifying water systems achieve TOC < 2-3 ppb which is significant compared to the concentration of most analysed organic compounds in hydrothermal fluids. Such a system was used in the BICOSE cruise and consistently concentrations were lower in the MQ water control. MQ water was not added to samples but only use for rinsing, so the contribution should be minimum and taken into account with the reference water samples. One exception was the presence of extremely large peaks of undecane in every single sample and blank analysis. This could be attributed to MeOH contamination. Unfortunately, our analyses indicated that our batch was contaminated, considering that our samples contained ~6 µM of undecane (C11). Decane was also high and had similar concentrations in all the Menez Gwen, Lucky Strike and Rainbow series of samples and blanks, strongly suggesting contamination from one unidentified source in the sample preparation. Therefore, we have to preclude the concentrations of decane (C10) from the fluids of these particular systems. Conversely, decane was much lower in the blank series of the Snake Pit and TAG and revealed a clear enrichment of decane at both sites. In any case, concentration of individual compounds in fluids should be compared to the reference deep seawater sample which should include all possible contaminants of the sampling, sample preparation and analytical procedures.

Generally BTEXs concentrations in fluids were very low and similar to the reference MQ- and deep-sea-waters. At such low concentrations, the analytical error is significant; as a result our data may only show that mono-aromatic compounds are present both in hydrothermal hot fluids and deep seawater. Similarly, most *n*-alkanes concentrations were associated with an analytical error that removes the results from further consideration. However, fluids were enriched in C12, C17, C18, and C20 at Menez Gwen; in C12 only at Lucky Strike; in C9, C10, C12, C15 and C17 at Rainbow; in C9, C10, C12, C13 and C17 at

490 Snake Pit; in C9 and C10 mainly at TAG. Unlike, *n*-FAs and PAHs background seawater concentrations were generally very low or below limit of quantification (LOQ) and were
492 consistently measured well above those levels in all samples at all sites. Nonetheless, for certain compounds the analytical error was too high to clearly conclude on their presence or
494 absence. Therefore, only organic molecules showing concentrations above local background levels (after analytical error correction) will be further discussed.

496 # 5 Discussion

## 5.1 Inorganic geochemistry: updates and temporal variability

498 Fluid geochemistry has been studied and used to try to unravel subsurface geochemical processes. Tectonics, geophysical and petrological data are very helpful to understand the
500 overall functioning of hydrothermal systems, whereas fluid geochemistry has proven to be the best tool to investigate the chemical reactions at the seawater/rock interface. It could also
502 potentially allow us to investigate fluid geochemical reactions deeper into the oceanic crust, provided that the fluids penetrate far enough. Concentrations in major and minor elements as
504 well as gases in hot hydrothermal fluids are mainly the result of water/rock reactions, equilibrium with rock assemblages, phase separation, and magmatic input (German and Von
506 Damm, 2004).

Key locations in hydrothermal vents are the recharge zone where seawater penetrates into
508 the crust, the so called "reaction zone" close to the heat source and the discharge zone where fluids are expelled. It is generally agreed that schematically water/rock reactions will occur at
510 any time and place during the complete circulation cycle including downflow (from recharge to reaction zone) and upflow (from reaction to discharge zone). However, reaction kinetics
512 are faster at high temperature so it is generally assumed that most reactions will occur in the "reaction zone". Yet, kinetic barrier may be overcome at lower temperature if the residence

514 time is long enough in the case of complex plumbing systems (e.g. Shock, 1992b; Horita and Berndt, 1999; Foustoukos and Seyfried, 2004). Phase separation has been proposed to 516 account for most of the observed chlorinities usually postulating that it occurs in the reaction zone and that the reacting fluid has the chlorinity of seawater (e.g. Von Damm, 1995). Yet, if 518 pressure and temperature conditions are met anywhere else during circulation it is likely possible that the fluid could experience several phase separations and starting from a modified 520 Cl concentration which may explain the difficulty to understand some data. The final concentration of the elements in the fluids is largely influenced by initial composition of the 522 reacting rocks and the mobility of the elements. Finally, if a magmatic body is present and if fluids circulate down to the roof of it, gases and magmatic fluids may enter the circulation in 524 the reaction zone (German and Von Damm, 2004 and references therein).

In this section we will present the current knowledge of hydrothermal processes proposed 526 to occur at the 5 studied sites and discuss whether our extended data set on fluid geochemistry supports or challenges current hypothesis.

528 *5.1.1 Menez Gwen*

It has been proposed previously that vent fluid composition at Menez Gwen was largely 530 controlled by phase separation occurring at ~600 mbsf with a good contribution of both water/E-MORB reactions and magmatic volatiles input ($CO_2$, $CH_4$ and He) (Charlou *et al.*, 532 2000; Douville *et al.*, 1999). The estimated depth of phase separation and thus the reaction zone was related to shallow hydrothermal circulation driven by a near-surface magmatic 534 body. At this depth, interaction with highly altered basalts was consistent and best explained the low metals, Li, Sr and $H_2S$ concentrations as well as the relatively high pH and Ca 536 content. The high Ca/Na was assigned to albitization. Precipitation of sulphides in the subsurface due to the relatively low temperature at the Menez Gwen vent field was also 538 inferred to contribute to the low metals and $H_2S$ concentrations observed.

But, in 2013, the maximum measured temperature was 300 °C which is 20 degrees higher than previously recorded. This new recorded temperature place the Menez Gwen system even closer to the 2-phases boundary curve and means that the fluids are boiling just beneath the surface of the mound. As sphalerite precipitates at temperature lower than ~250 °C, this slight temperature increase may account for the higher Zn observed in the fluids. Mn concentrations were also significantly higher (98.5 µM) than in 1994 and could be also due to a temperature elevation. The water/rock equilibrium response of Mn is far more sluggish than Zn which could indicate that the temperature increase has been going on for several years (Seewald and Seyfried, 1990).

Besides, the observed Li elevation in 2013 (321 µM vs 203-278 µM) likely signs interaction with relatively fresh basalts and might thus point to an eruptive event in the meantime consistent with the temperature elevation and the fairly fast eruptive rate of the system (Parson *et al*., 2000). Consistently, Cu, Ni and Fe concentrations should have been higher but have probably already been leach in a volatile phase during the emplacement of the system Marques *et al*. (2011). Unlike Ba concentration was lower (10.3 µM vs 27 µM) but should be taken carefully as Ba is really sensitive to barite precipitation. B had not been reported earlier and reached 445 µM in our samples which is in the range of other unsedimented basalts systems (von Damm, 1995).

The B/Cl ratio indicates a clear enrichment of the fluid which is most probably indicating water/rock reactions in the upflow zone (Butterfield *et al*., 1990). Alternatively, low-temperature serpentinisation is also capable of leaching B and this would support the hypothesis of the mantle-derived $CH_4$ through serpentinisation (Charlou *et al*., 2000; Mevel, 2003).

Our results show that the variations that seem to have occurred in the fluid composition at Menez Gwen are likely due to an external eruptive event and thus we believe the

564 hydrothermal activity can be considered to have been rather stable in the past 20 years. Hence, the observed variations do not disrupt the earlier conclusions on the overall
566 functioning of the Menez Gwen hydrothermal circulation and fluids inorganic geochemistry.

*5.1.2 Lucky Strike*

568 Over the 20 year-long sampling period, most elements variations fall within the error of the analytical methods (Table 3). Our results suggest that hydrothermal activity and processes
570 at the southerneast part of the Lucky Strike vent field represented by Tour Eiffel and Montségur (US4) seem to be very stable and consistent with discussions and conclusions
572 drawn by our predecessors (Charlou *et al*., 2000; Pester *et al*., 2012; Von Damm *et al*., 1998). Phase separation primarily controls the chlorinity and thus most of the metals concentrations
574 at Lucky Strike and has been proposed to occur at subcritical conditions at > 300 bar and 360-380 °C (Von Damm *et al*., 1998; Charlou *et al*., 2000). Nonetheless, the influence of the
576 Azores hotspot is clear at Lucky Strike. Enrichment in Ba, K, Cs and Rb indeed characterises water reaction with E-MORBs whereas high pH and Ca along with low Li, Sr and metals
578 indicate reactions with highly altered and relatively oxic basalts. Albitization was also shown to occur based on the low Sr/Ca and high Ca/Na ratios. A shallow heat source was inferred
580 (Fouquet *et al*., 1995).

Geochemistry of the fluids at Lucky Strike has shown to be highly geographically
582 variable at the hydrothermal field scale with almost as many endmembers as vents number. Major differences are observed between the northwest and the southeast areas and have been
584 attributed to 2 different fluid sources (Charlou *et al*., 2000; Pester *et al*., 2012; Von Damm *et al*., 1998). Unlike the emission of distinct fluids within each zone has been attributed to
586 variable contribution of phase separation, mixing processes and conductive cooling. The identification of an AMC right beneath the Lucky Strike vent field together with a fault
588 network as well as recent intrusion of a dike demonstrated a mixed tectonic and volcanic

control on hydrothermal activity (Dziak *et al*., 2004). Besides those major and conventional controlling factors, other aspects may influence hydrothermal fluids composition at Lucky Strike: (i) two hydrothermal cells have been identified with different circulation patterns (Crawford *et al*., 2013); (ii) both phases related to phase separation may be venting either as individual phases or as mix of different proportions (Pester *et al*., 2012); (iii) various parameters including temperature of exiting fluids may be affected by tidal cycles (Barreyre *et al*., 2014).

Our results seem to follow a slight decreasing trend of the Cl content over the 20 years of sampling which could be related to a change in the depth of the reaction zone or the AMC so that phase separation produce a lower salinity phase. Conversely, Ca together with Sr (so that the low Sr/Ca is conserved) seems to show a slight increasing trend consistent with the Na depletion and increased albitization rate. This is likely due to interaction with fresh rocks that could have been injected during the diking event. Alternatively, a possible constant input of fresh basalts at depth has been postulated due to replenishment of the magmatic heat source (Pester *et al*., 2012). Reaction of water with these fresh rocks rather than with altered rocks is consistent with new estimates of the reaction zone (410-480 bar and 430-475 °C) as well as the depth of the penetration of the faults and of the AMC roof (Pester *et al*., 2012; Singh *et al*., 2006). Consistently, Li concentration has increased in our samples whereas it had been stable over the 1993-2008 intervals.

Fe, Cu and Zn concentrations appeared to be very different at Tour Eiffel and at Montségur over the 1993-2005 period, yet, we did not observed this discrepancy in 2013 with a common endmember value of 429 µM, 13.6 µM, and 22.9 µM, respectively. These metals easily precipitate to sulphides so that slight difference in the fluid path and plumbing system could explain such lack of consistency among results. Also, it has been proposed elsewhere that re-equilibration of metals would take place during upflow thanks to a longer residence

614 time and lead to the low metal concentrations (Pester *et al*., 2012). In addition, Rouxel and coworkers (2004) demonstrated that subsurface reservoirs may exist at Lucky Strike and
616 sporadically mix with the endmember fluid source adding a supplemental parameter to the final composition of the Lucky Strike fluids.

618 *5.1.3 Rainbow*

Over the 1997-2008 intervals, the chemical composition of the Rainbow hot fluids have
620 been described as stable and characterised by consistent low $H_2S$, Si but elevated $CH_4$, $H_2$, Cl and metals (Table 3). Notably, Rainbow has by far the highest concentration of Fe of all vent
622 fields of the MAR. These features have usually been explained by phase separation at ~305bar and ~410 °C (e.g. Bischoff and Pitzer, 1989). Unlike elevated concentrations of $H_2$
624 and $CH_4$ in this brine phase have been attributed to serpentinisation reactions (Charlou *et al*., 2007; Mevel, 2003). Our results agree well with previous reported values although, Cl, Na
626 and K have slightly decreased whereas Sr, B and Fe show a slight increase (Table 3) (Charlou *et al*., 2002b; Douville *et al*., 2002; Seyfried Jr *et al*., 2011). More striking is the significant
628 increase of Li of ~100µM which we could not assign to any specific process and will need more investigation in future expeditions. Ba contents was divided by a factor of 2 but will not
630 be discussed further as concentration is really sensitive to precipitation of barite.

Besides, new physical data challenge earlier conclusions. The presence of magmatic
632 sills, distributed throughout the massif much deeper than previously thought (~2–10 km i.e., 430-1230 bar) is particularly questioning the phase separation process and the Cl enrichment
634 origin which is still under debate (Seyfried Jr *et al*., 2011). To that respect, Cannat and colleagues (2007) have suggested that the complex tectonics associated with ridge segment
636 end location might allow recharge of fluid through ultramafic rocks where hydration at low-temperature may contribute to Cl increase prior to attainment of maximum hydrothermal
638 grade. This is supported by the low B concentration reported in 2008 and confirmed in this

work. High amount of metal intake would occur deeper and at higher temperature and possibly controlled by equilibrium with tremolite (secondary mineral assemblage) that appeared to better fit the field data and which is consistent with the observed gabbroic intrusions. Thus, a model of hydrothermal circulation has been proposed elsewhere (Andreani *et al*., 2014).

### *5.1.4 Snake Pit*

Stability of the fluid geochemistry had been reported for the 1986-1990 intervals. Our 2014 dataset reflects a hydrothermal endmember that is largely in agreement with values reported in other studies conducted at Snake Pit (Campbell *et al*., 1988; Edmond *et al*., 1995) and which brought to the following conclusions : (i) fluids mostly interact with altered basalts at T~150 °C and shallow depth; (ii) conductive cooling occurs on the flank (Moose vent); (iii) major element chemistry is controlled by thermodynamic equilibria with mineral assemblages representative of altered basalts; (iv) the low Rb concentration is due to the Rb depleted MORB reported in the MARK area.

Nevertheless, our results diverged in some ways (Table 3). Si (17 mM) seems to have decreased alongside with a temperature increase (357 °C), which would indicate a reaction zone in the water column (275 bar), considering the fluid has been in equilibrium with quartz (Von Damm *et al*., 1991). At 350 bar, minimum temperature to reach 17 mM of silica in fluids is ~400 °C. A possible explanation is that fluids have equilibrated with quartz at T > 400 °C at greater depth and experienced subsequent conductive cooling. Fe has been constantly increasing over the past 30 years and is ~ 64% higher in 2014 than in 1986. Fe response to temperature is rapid. Since exit temperature variation is quite subtle, this may suggest that temperature deeper in the system has increased. This is consistent with higher Zn, Cu, Li and K. As the Rb and B concentrations have not changed over the years they should still witness low-temperature basalt alteration as proposed earlier (Edmond *et al*.,

1995). In that case, this means that this interaction has to take place in the recharge zone prior to reaching the deep and hot reaction zone. There exist one outstanding matter, if the fluid reaches T > 400 °C and P > 350 bar, phase separation should occur which is not shown by chlorinity data (e.g. Bischoff and Pitzer, 1989).

*5.1.5 TAG*

The TAG hydrothermal vent field was sampled in 1986, then 1990 and in May-June 1993 by an Alvin expedition, in August 1994 by a Japan-US expedition with Shinkai 6500, and in February-March 1995 by a US-UK group with Alvin. Although it had been revisited in 2005 during the EXOMAR cruise, results were not published and thus a period of 20 years has elapsed until the BICOSE cruise and the present new results. Black smokers vent fluid chemistry at TAG has remained similar over 12 years (1986-1998) and shown a single endmember reflecting seawater reaction with basaltic rocks (Table 3) (Chiba *et al*., 2001). Despite profound changes of the site topography in the 1986-1990 intervals, the ODP drilling experiment in 1995, and heatflow variations, the fluid chemistry variations are more subtle except for an increase in $CH_4$ and $CO_2$ reported after drilling (Charlou *et al*., 1996; Edmond *et al*., 1995; Edmonds *et al*., 1996). Our results show some variations but concentrations remain in the same order of magnitude as in the past 30 years.

Despite this apparent stability, understanding the TAG fluid geochemistry appears challenging and small changes in the 2014 fluid chemistry brings even more confusion in understanding the overall system. Water / rock reactions were proposed to occur at moderate temperature (~150 °C) along the recharge path in the crust and then followed by low-temperature remobilisation in altered rocks (Edmond *et al*., 1995). Consistently, Li was almost twice as high in 2013 as in the past, showing extensive leaching of Li which is favoured at T ≤ 150 °C. Also, evidence for seawater entrainment within the mound was clear according to the Mg content of very pure fluids that has been observed elsewhere and in our

study (11 mM of Mg in the 362 °C and pH 2.8 sample) (Table 3). Finally, Edmond and colleagues (1995) came up with the model that fluid composition at TAG was best explained by a 3-component mixing of a brine phase, the associated vapor phase and a partially reacted seawater phase.

According to more recent petrological data, these reasonings seem to present contradictions. Massive seawater entrainment within the mound to at least 120 mbsf was confirmed and fluid inclusions analyses revealed T > 337 °C in the shallow part of the mound and ~390 °C in the stockwork so that low-temperature reactions are unlikely (Humphris *et al*., 2015). Instead conductive heating of the entrained seawater would occur. This is consistent with the shallow reaction zone inferred but not with the low-temperature and the phase separation. Indeed, for phase separation to occur at 390 °C, pressure of ~270 bar is required; respectively at 370 bar, T of ~430 °C is needed, meaning that the Cl content has to be attributed to other processes (e.g. Bischoff and Pitzer, 1989). Leaching of Cl from mineral phases could be an option and has been discussed for the Rainbow system (Seyfried Jr *et al*., 2011). Another contradiction comes from geophysical data that did not reveal the presence of mid-crustal magma bodies beneath the hydrothermal field (Canales *et al*., 2007). Hence, it has been inferred and modelled that hydrothermal fluids must penetrate to great depths (>7 km) to extract heat out of a gabbroic intrusion at the root zone of the detachment fault and flow up along the detachment fault until they rise straight through the highly cracked hanging wall (deMartin *et al*., 2007; Humphris *et al*., 2015; Zhao *et al*., 2012). This is still under debate and the heat source remains quite enigmatic at TAG. In any case, from a chemical perspective, the composition of the fluid would argue against deep down processes.

Fe was clearly increased in our samples likely reflecting remobilization of Fe from pyrrhotite even though the temperature does not show such a clear increase. Inconsistently, pH decreased which should argue for iron sulphurs precipitation and Zn remobilisation

714 (Edmond *et al*., 1995). We propose that less precipitation occurs because of limited S. Alternatively, possible change in the water/rock ratio was suggested in 1994 and could
716 explain some of the complex data (Gamo *et al*., 1996).

### 5.2 Gases

718 New gas data were obtained in 2014 for the TAG and Snake Pit hot fluids. Unfortunately, gas could not be analysed in 2013 at the Menez Gwen, Lucky Strike and
720 Rainbow fluid samples, nevertheless, we discuss some older unpublished but still more recent gas data for those sites (Table 4).

722 No additional data were published on the gas content of the Menez Gwen hot fluids since the DIVA cruise in 1994, yet samples were collected and analysed in 1997 and 2001. Results
724 are presented in Table 4 and show that the Menez Gwen vent field has stable concentration of $H_2S$, $N_2$, $CH_4$ and $CO_2$.

726 Additional results from 1997 confirm that the gases concentrations in fluids of Lucky Strike have been stable over the years. Note that the dramatic elevation in $CO_2$ observed in
728 2008 has been discussed in detail by Pester and collaborators (2012) who invoked replenishment of the magmatic heat source and a possible recent magmatic event. This is an
730 additional line of evidence that $CH_4$ and $CO_2$ have a magmatic origin as proposed earlier although a serpentinisation contribution to the $CH_4$ amount should not be excluded (Charlou
732 *et al*., 2000; Pester *et al*., 2012).

The dataset for Rainbow, completed by results from 2005, covers the 1997-2008 time
734 period and shows also relative stability of the gas concentration (Table 4). $CH_4$ and $H_2$ were somewhat lower in 2005 and 2008 (EXOMAR) that we assume was due to a different sample
736 storage protocol during those cruises because of technical constraints. Indeed, similar concentrations as in 2001 and earlier have been reported elsewhere in 2008 (KNOXX08).
738 Rainbow fluids are characterised by high concentration of $CH_4$ and $H_2$ which have usually

been associated with serpentinisation reactions. Yet, recent results and models published elsewhere suggest that pH and redox conditions are better constrained by the magnetite - chlorite - talc mineral assemblage rather than by serpentine (Seyfried Jr *et al*., 2011). The debate on the abiogenic origin of gases at Rainbow (and other fields) is in constant evolution. The most recent genetic diagrams bring additional lines of evidence supporting the abiogenic origin of hydrocarbon gases at Rainbow (Figure 10) (Milkov and Etiope, 2018). The $\delta^{13}C$ vs 1/n (n is the carbon number) shows an inverse correlation at Rainbow both using the 2005 and 2008 results which also argues in favour of abiotic processes (Sherwood Lollar *et al*., 2006).

It may be notable that novel measurements of temperature-sensitive "clumped" isotopologues for $CH_4$ at the Rainbow vent fields indicate that the $CH_4$ formed and/or equilibrated at a common, uniformly high temperature, averaging 310 ± ~50 °C (Wang *et al*., 2018). Such conclusions also stand for other vent fields with totally different settings and chemistry which implies that $CH_4$, and possibly other organic molecules, in many hydrothermal fluids may come from other sources especially hydrothermal leaching of fluid inclusions as originally suggested by Welhan and Craig (1983) and supported by the recent finding of Ménez and collaborators (Ménez *et al*., 2018)

Unlike element chemistry, significant changes have occurred in the Snake Pit fluid gas composition since 1988-1995 and compositions appear significantly different at Moose and Beehive in 2014 (Table 4). The He isotopic ratio is still consistent with MORB interaction as already mentioned by Jean-Baptiste and colleagues (Jean-Baptiste *et al*., 1991). We report here the first data on isotopic composition of gases obtained in 2014. $CH_4$ was highly depleted in $^{13}C$ which together with the isotopic composition of $CO_2$ strongly support the abiogenic origin suspected by the same authors (Figure 10). Unlike, $\delta^{13}C$ ($CO_2$) value fall right between the magmatic $CO_2$ (-5 to -6 ‰) and the carbonates (0 ‰) values, indicating either a mix origin or fractionation processes. As $CO_2$ levels in the fluid were similar to that

764 of seawater we may argue that magmatic degassing was very limited if not absent at Snake Pit.

766 The ODP drilling at TAG in 1994 produced a small increase in $CH_4$ and $CO_2$ as reported in a study carried out before and after the drilling (Charlou *et al*., 1996) (Table 4). Besides of 768 this, since 1993, $H_2$, $CO_2$ and He seem to have dropped concomitantly whereas $H_2S$ and $CH_4$ concentrations have remained similar. To the best of our knowledge, isotopic data have not 770 been reported for the TAG gases therefore it is difficult to discuss processes and possible relation with concentration changes. Our data suggest that some changes occurred at depth as 772 $H_2$, $CO_2$ and $^3He$ inputs are more related to deep sources whereas $CH_4$ and $H_2S$ would be more locally produced, maybe from microbes, through more stable processes. Instead, $H_2$ is 774 widely used among bacteria, archaea and, to a lesser extent, eukaryotes from a wide range of environments (e.g. Peters *et al*., 2015, Greening *et al*., 2016). $H_2$ oxidation can be coupled 776 with the reduction of numerous electron acceptors, such as $CO_2$ or $HCO_3^-$ from carbonate minerals, $SO_4^{2-}$, $NO_3^-$, and $Fe^{3+}$ from iron oxides, as well as strong oxidants such as $O_2$ (e.g. 778 Adam and Perner, 2018).

Altogether, more variability was observed in the gas compositions over the years versus 780 the elemental composition.

## 5.3 Organic geochemistry: composition and origin

782 *5.3.1 Total Organic Carbon (TOC)*

Few data exist for TOC because most scientists separately measure the dissolved or 784 particulate fractions of organic matter. In the present study, TOC was only measured at TAG and Snake Pit (Table 5). Background deep seawater concentrations of dissolved organic 786 carbon (DOC) reported elsewhere were in the 0.43-0.55 ppm range (Lang *et al*., 2010; Hawkes *et al*., 2013; Longnecker *et al*., 2018). Local background at Snake Pit was a little 788 lower with 0.19 ppm TOC. Unlike, the deep seawater reference sample exhibited 5.74 ppm

TOC in the TAG area which may be due to some plume contribution and indicates that a large part of the organic carbon occurred in the particulate fraction in the water column. Vent fluids concentrations were in the 0.2-15 ppm range. The carbon equivalent concentration of all the quantified compounds (namely formate, acetate, *n*-alkanes and n-FAs for TAG and Snake Pit) represented as little as 0.1 % and up to 8% of the TOC. This leaves a large part of the TOC to be allocated. One reason is that only extractable and chosen organic compounds were quantified. Moreover, the calculated concentration should be regarded as minimum estimates of in-situ concentration for several reasons: (i) samples were processed at room temperature at which solubility of organic compounds is lower; (ii) it is very likely that a portion of the OM is adsorbed on small particles in the fluids which are not taken into account using our extraction and analytical techniques. However, since *in-situ* measurement techniques are currently under development, these values are the best estimates we can obtain. Similar unsolved carbon budget was reported at Lost City where a third of the DOC is still not accounted for to date (McCollom *et al*., 2015).

As for comparison, a comprehensive investigation of TOC in various substrates at Lost City revealed that TOC concentration in the fluids were in the 400-1500 ppm range and of which the DOC accounted for only 1.2 ppm (Bradley *et al*., 2009; Lang *et al*., 2010; Lang *et al*., 2018). This suggests that most of the organic carbon in the fluids would occur as particles including colloids, organic-metal complexes and adsorbed on small mineral particles. Besides, hydrothermal chimneys contained one order of magnitude more TOC (0.10-0.44 %) which is as high as TOC reported in hydrothermal sediments of the Western Pacific (0.1-2.5%) (Yamanaka and Sakata, 2004). By contrast, serpentinites presented similar concentration to fluids of ~85-1015 ppm. This may indicate that organics could be leached from the serpentinites and then deposited in the chimney wall (Delacour *et al*., 2008). Serpentinites and chimneys (both diffusor and sulphide) collected at the Rainbow vent field

814 during an earlier expedition exhibited similar concentrations to the Lost City chimneys (0.01-0.3%) although the fluid carbon content was much lower (~6 ppm) than at Lost City (Konn, 816 2008, PhD thesis work, *unpublished results*). This suggests that at Rainbow most of the organic carbon may deposit on the chimney walls possibly by a simple physical adsorption 818 process.

DOC and particulate organic carbon (POC) were measured in the buoyant plume over the 820 9°N hydrothermal field on the EPR. The DOC was ~2-10 % of the POC (i.e. 1-5 µM DOC) and the sum of the two represented 40-48 µM of carbon (i.e. ~0.5 ppm) (Bennett et al., 2011). 822 Concentration of DOC in associated hot fluids with T = 365 °C were ~14 µM (i.e., 0.17 ppm) while the diffused fluids contributed with 46 µM (i.e. 0.55 ppm) (Longnecker *et al*., 2018). 824 This could indicate that most of the DOC is exported as such in the water column with a small fraction converted in POC within the plume.

826 *5.3.2 Volatile Fatty Acids (VFAs)*

Formate and acetate were only measured at TAG and Snake Pit (Table 5). Formate and 828 acetate were not detected in bottom seawater whereas their concentrations reached ~1-3 µM at both sites which is orders of magnitude lower than concentrations reported for the alkaline 830 Lost City hydrothermal vent field (146 µM) and the Von Damm vent field at Mid-Cayman rise (88 µM) both located on the MAR (Lang *et al*., 2010; McDermott *et al*., 2015). Our 832 results are closer to concentrations measured in the Pacific (1-16 µM) but still fall in the lower range (Konn *et al*., 2018). The major difference of TAG and Snake Pit vs the other sites 834 resides in the $H_2$ concentrations. $H_2$ concentrations exceed 10 mM at Lost City, Von Damm and Kulo Lasi creating favourable conditions for abiotic synthesis of organic compounds 836 including formate (Shock, 1992; Shock and Schulte, 1998). At Lost City two sources of formate have actually been suspected. One is abiotic conversion of mantle $CO_2$ at depth 838 according to reaction (1) that proceeds rapidly at T > 175 °C and the second one is microbial

conversion of seawater $CO_2$ in shallow subsurface (Lang *et al*., 2010; Lang *et al*., 2018). Different processes have been suggested to explain formate concentrations at Von Damm hydrothermal vent field both in hot and diffused fluids. Leaching of fluid inclusions would be the source of formate in hot fluids whereas rapid conversion of seawater $CO_2$ in the diffusion areas would explain the higher concentration in the mixed fluids (McDermott *et al*., 2015).

$$HCO_3^- + H_2 \rightarrow HCOO^- + H_2O \qquad (1)$$

The fugacity of hydrogen $f(H_2)$ at Snake Pit implies that (i) the redox state is buffered by the fayalite-magnetite-quartz (FMQ) assemblage which is less but still favourable for abiotic synthesis ; (ii) at 357 °C kinetic inhibition of $CH_4$ is possible and organic compounds including formate may be in metastable equilibrium in the fluids. Yet, at 350-400 °C, 450-500 bar, formate should dominate over acetate in solutions buffered by the FMQ assemblage and higher concentrations of acetate could only be obtained at Snake Pit at ~250 °C and 400 bar i.e., in the very shallow subsurface (Shock, 1990; Shock, 1992). Both formate and acetate concentrations correlate to Mg concentrations in the Snake Pit fluids indicating subsurface and somewhat distant reaction zones and consistent with a common origin for both species. Furthermore, underlying rocks contain Cu and Fe but no Zn which indicates that temperature in the shallow subsurface coincides with the 250-300 °C range (Fouquet *et al*., 1993). Finally, both low-temperature/shallow and high-temperature/deep water/rock interactions have been suggested to control major and minor element chemistry at Snake Pit (section 5.1.4). To that respect, we argue that abiotic $CO_2$ conversion of formate and acetate could occur in the shallow subsurface at Snake Pit and to account for the overall geochemistry of the fluids; and that subsequent mixing with a hot deeply-sourced fluid, which would not let the time for the sluggish conversion of VFAs to $CH_4$ to happen, must occur.

Alternatively, the recent findings of Ménez and collaborators (2018) show that serpentine fluid inclusions should be considered as potential shallow reservoir and sources of organic

compounds. This hypothesis could be particularly considered at Snake Pit as serpentinites occur in relatively large amount in the vicinity of the field (Alt and Shanks, 2003). However, since formate is usually the dominant species in fluid inclusions over other organic acids including acetate, this contribution is rather unlikely in our samples (Zeng and Liu, 2000).

Unlike, $f(H_2)$ at TAG indicates that (i) the redox state is buffered by the pyrite-pyrhotite-magnetite (PPM) assemblage which is rather unfavourable for abiotic synthesis (Shock, 1990; Shock, 1992). Furthermore, none of the VFAs or TOC concentrations correlated with Mg concentration also suggesting that abiotic synthesis is unlikely at TAG. However, local thermal degradation of organic matter is very consistent with the higher acetate to formate concentrations, the massive seawater entrainment in the hot (T ~340-390 °C) TAG mound, and near surface processes as shown for metals (Humphris *et al*., 2015). Altogether our results indicate that abiotic synthesis of formate and acetate is unlikely at the TAG hydrothermal field and that both compounds have a thermogenic origin.

Independently of its origin, formate and acetate have microbiological implications as certain microorganisms present in chimneys, aquifers or plumes can efficiently utilise these compounds, which may have further implications resulting of the role of these microorganisms in terms of biology, chemistry and even mineralogy (Bennett *et al*., 2011; Windman *et al*., 2007). Especially, methanogens can produce $CH_4$ out of acetate and formate (Brazelton *et al*., 2011; Ferry, 2010; Takai *et al.*, 2004). At the Lost City vent field, sulfate reducers have been shown to live on formate which has implications for the sulfur cycle and thus metal deposition (Lang *et al*., 2018). Metal transport and deposition is also influenced by complexation and to that respect formate and acetate represent better ligands than $Cl^-$ as demonstrated for Cu and Fe (Lai *et al*., 2018; Liu *et al*., 2001; Palmer and Hyde, 1993) and may thus help resolve inconsistencies sometimes observed between Cl and metal concentrations. Organic-metal complexation is also of great importance for the plume

biogeochemistry because in this form metal become bioavailable for organisms and are stabilized for long distance transportation (Bennett *et al*., 2008). Complexation of Al by acetate has also been shown to increase the solubility of albite at T=100 °C, P=350 bar and 3 < pH < 6 where $(Al\text{-}CH_3COO)^{2+}$ and $(Al\text{-}C_2O_4)^{+}$ dominates (Franklin *et al*., 1994). Finally, the presence of formate is of great importance as it represents in some cases a more efficient starting material than $CO_2$ for abiotic synthesis of larger and semi-volatile organic compounds (McCollom *et al*., 2010).

### *5.3.3 Semi-Volatile Organic Compounds (SVOCs)*

The occurrence of hydrothermally derived SVOCs in hydrothermal fluids has often been discussed and reported both experimentally and in the field but to the best of our knowledge only two studies have reported on quantitative data (Konn *et al*., 2018; McCollom *et al*., 2015). In 2018, Konn and collaborators reported on fluids from the Fatu Kapa vent field in the Pacific and both composition and concentrations were in good agreement with the present study results. As a difference, McCollom and collaborators (2015) found mainly C8:0 to C12:0 n-FAs in fluid samples from the Lost City hydrothermal vent field with concentrations for individual n-FAs in the 46-111 ppb which is far higher than our values of 0.2-21 ppb. Besides, only PAHs of the phenanthrene series and possibly aliphatic compounds and n-alkanes (C>23) were identified as hydrothermally derived in their fluid samples from Rainbow and Lucky Strike. Our analyses, however, revealed the presence of organic compounds at concentrations as low as 0.04 ppb and up to 12 ppb in all samples of all the studied sites. While we used different sampling, sample preparation and analytical technics, it is possible that lower limits of detection enabled actual detection and quantification of organic molecules in the hydrothermal fluid samples collected in 2013 and 2014.

912 **5.3.3.1 Linear fatty acids (n-FA)**

Both vents at Lucky Strike were enriched in only the even carbon numbered series
914 although Tour Eiffel samples contained nonanoic acid as an exception. Similar preferential occurrence was reported in massive sulphides of the MAR, hydrothermal mussels, and in the
916 Lost City fluids (Ben-Mlih *et al*., 1992; Blumenberg *et al*., 2007; McCollom *et al*., 2015). The presence of only even carbon-numbered n-FAs indicates a biological source because all
918 known abiotic processes are unselective (e.g., McCollom *et al*, 2015). So at Lucky Strike, *n*-FAs with C<14 are likely originating from microbial production and directly incorporated to
920 the fluids whereas C16:0 and C18:0 which are typical components of cell membranes and ubiquitous to all organisms would originate from dead cells and subsequent entrainment in
922 hydrothermal circulation. A biological origin of the organic acids is also very likely at the Rainbow vent field where fluids were mainly enriched in the high molecular weight C16:0
924 and C18:0 *n*-FAs with possible minor amounts of C17:0.

Unlike, we suggest an abiotic origin of a portion of the n-FAs at the Menez Gwen vent
926 field. Indeed, at the exception of C11:0 which was not detected, the fluids contained the entire series of *n*-FAs in similar amounts. This distribution resemble that of Fischer Tropsch
928 Type (FTT) reactions leading to roughly equal amounts of odd and even carbon numbered long chained n-FAs (McCollom and Seewald, 2007). However, concentrations of C16:0 and
930 C18:0 were about 5 times higher which argues for an additional cellular source of *n*-FAs.

Fluids from the Snake Pit and TAG vent fields also contained the entire series but were
932 generally enriched in even carbon numbered n-FAs. Such even to odd carbon preference has been reported in sediments and associated with thermal degradation of OM (Aizenshtat *et al*.,
934 1973; Volkman *et al*., 1980; Yamanaka and Sakata, 2004). Consistently, at the Marge vent in the TAG field, only the purest sample contained n-FAs, which constitutes a strong line of
936 evidence that these compounds are derived from deep subsurface reactions and namely OM

degradation. Yet, at Snake Pit, the organic acids distribution seemed to show some inconsistencies with the sole input from OM degradation. Thereby fluids from the Beehive vent contained an additional large amount of C9:0 whereas the Moose fluids did not contain any C18:0. This suggests additional processes contributions to account for the observed n-FAs distribution in the Snake Pit fluids. Notably, abiotic sources of nonanoic acid derived from $CO_2$ and $H_2$ (Shock and Canovas, 2010), nonane (Schulte and Shock, 1993) or undecane (Seewald, 2001) are possible and such processes may also contribute to the large amount of C9:0 observed at Lucky Strike. Finally, both the shallow and low-temperature reaction zone and the absence of phase separation processes inferred at Snake Pit are particular features that could contribute to the distribution pattern of n-FAs in the fluids (see discussion 5.1.4).

In general, one should keep in mind that the final distribution observed reflects an ensemble of reactions and not only the result of abiotic, thermogenic or biologic syntheses. Especially, adsorption on minerals, dissolution equilibria, or chemical rearrangements most likely affect final distributions. Physical parameters such as temperature should also be considered. To that respect a temperature-dependant pattern seem to emerge from the comparison of the Azores vent fields (Menez Gwen, Lucky Strike and Rainbow). At the low temperature (Menez Gwen), all organic acids would persist in the fluids and as temperature increases (Lucky Strike) odd carbon numbered compounds would be first degraded and then in the > 350 °C fluids (Rainbow) only heavier compounds production and persistence would occur. Finally, recent studies of insoluble carbonaceous matter from subseafloor serpentinites have found that they contain a large component of aliphatic compounds up to C12 associated with carboxylate functional groups (Pasini *et al*., 2013). Reaction constants and equilibria in these substrates are likely to result in their own distribution patterns yet, these compounds may be leached during hydrothermal circulation and thus add another component to the final distribution of *n*-FAs in hydrothermal fluids.

962 **5.3.3.2 *n*-alkanes**

Generally, C10 and C12 were the dominant *n*-alkanes in all fluid samples with 964 concentration up to 2 orders of magnitude higher than their homologs. Concentration ranges were similar among all samples. These results are in good agreement with concentration and 966 distribution reported in the Pacific at the Fatu Kapa vent field (Konn *et al*., 2018).

Our Rainbow fluid samples appeared enriched in C9, C10, C12, C15 and C17 which is, 968 to some extent, consistent with the presence of C8 to >C23 *n*-alkanes reported in previous works (Konn *et al*., 2012; Konn *et al*., 2009; McCollom *et al*., 2015). McCollom *et al*. (2015) 970 argued for a thermal origin of >C23 *n*-alkanes in agreement with the OM thermally derived n-alkanes found in the chimneys (Simoneit *et al*., 2004). Conversely, Konn *et al*. argued for a 972 more likely abiogenic origin of the <C20 *n*-alkanes on the basis of theoretical and experimental work (Konn *et al*., 2009). Indeed, the redox conditions at the Rainbow 974 hydrothermal vent field should be thermodynamically favourable for the kinetic inhibition of $CH_4$ and thus the persistence of *n*-alkanes in metastable equilibria in the fluids (Shock, 1992) 976 (Figure 11). Consistently, the abiogenic origin of $CH_4$ and possibly derived from FTT reactions is strongly supported by gases isotopes data (see section 5.2). On the other hand, 978 high-temperature OM degradation is usually associated with absence of *n*-alkanes (Kawka and Simoneit, 1994; Konn *et al*., 2011; Simoneit, 1988). And finally, *n*-alkanes are not 980 typical products of biological or microbial activity (e.g., Engel *et al*., 2013; McCollom *et al*., 2015). Similarly, the purest sample of the Beehive vent at Snake Pit was clearly enriched in 982 C9, C10, C12, C13 and C17 whereas at the Moose vent only a subtle enrichment in C10, C12 and C17 was observed. Redox conditions set by $f(H_2)$ at Snake Pit would also point to an 984 abiogenic origin of n-alkanes and supported by the abiogenic origin of $CH_4$ (see section 5.2, Figure 11). In addition, the purest samples at both Beehive and Moose vents were strongly

depleted in C14 and C15 compared to local background indicating that hydrocarbons equilibria are controlled in the subsurface where abiotic reactions are favoured.

However, in experimental FTT reactions, products characteristically exhibited an increase from C9 to C12 and then a log-linear decrease in abundance with increasing carbon number (McCollom *et al*., 2010; McCollom and Seewald, 2006) which is rather different than the distribution observed in our samples. This means that other or additional processes have to be considered. First of all, abiotic reactions other than FTT should be considered in super-critical seawater where unconventional reactions are favoured (Akiya and Savage, 2002; Deguchi and Tsujii, 2007). Alternatively, *n*-alkanes are typically associated with low-temperature OM degradation and found in sedimentary basins (Rapp, 1991), oil fields (Kissin, 1987; Vishnoi *et al*., 1987), sediment covered-hydrothermal vent fields (Simoneit *et al*., 1992; Simoneit *et al*., 1988) or hydrothermal solids (Simoneit, 1988) but also show a different distribution to what we observed in the MAR fluid samples. Yet, although all the studied vent fields are sediment free, macro- and micro-fauna is relatively abundant and constitute a source of OM that may be entrained in the hydrothermal circulation at low-temperature recharge zones. Low-temperature OM degradation could thus occur in these zones but further reactions and re-equilibration must occur before venting in order to change the distribution of the n-alkanes. We argue that both abiotic reactions and low-temperature OM degradation may occur at Rainbow and Snake Pit. Besides, the partition coefficient and the solubility of *n*-alkanes in the various substrates may account for a great part to the difficulties in assigning the observed distribution.

The redox conditions at Menez Gwen, Lucky Strike and TAG suggest that abiotic synthesis of n-alkanes is unlikely (Figure 11). The Menez Gwen hot fluids clearly contained C10, C12, C17, C18 and possibly C20 whereas at Lucky Strike both sampled vents were clearly enriched in only C12. Enrichment and concentrations were generally lower at the

TAG vent field. However, despite some differences, *n*-alkanes concentrations and distribution were similar to that of Rainbow and Snake Pit. This indicates that, on the one hand, similar processes including low-temperature OM degradation may control the *n*-alkane distribution at Menez Gwen, Lucky Strike and TAG; and on the other hand that if abiotic reactions occur at Rainbow and Snake Pit, they are probably overprinted by other processes including low-temperature OM degradation. An interesting feature about TAG is that unlike other *n*-alkanes, C9 and C10 were clearly enriched by 2 to 10 times in the 2 mixed fluids having similar pH (~5.45) and Mg (~40.5 mM) contents (Marge (b) and New BS, Table 5). Note that the TOC seemed to follow the same trend which cannot either be accounted by local deep seawater input. Local and fast reactions may be favoured under the particular conditions in these mixed fluids and result in the production of lighter alkanes.

In any case, our results indicate that several concomitant processes must occur to generate the *n*-alkanes distribution observed in our MAR hot hydrothermal fluid samples. Yet, we may argue that, considering the similar distribution despite the great diversity of the studied hydrothermal systems (pressure, temperature, host-rocks, etc…), *n*-alkanes chemistry must be mainly controlled by processes common to all vents and overprinting other minor processes.

#### 5.3.3.3 Polyaromatic hydrocarbons (PAHs)

PAHs could not be analysed in the Snake Pit and TAG samples for technical reasons. PAHs were detected in the fluid samples from the Menez Gwen, Lucky Strike and Rainbow vent fields at concentrations in the 0.05-0.6 ppb range. Their concentrations are much lower than that of aliphatic compounds. This is in good agreement with the trace amount of the phenanthrene series reported in the fluids from the Lucky Strike and Rainbow vent fields (McCollom *et al*., 2015). Generally, acenaphthene and fluoranthene were either not detected or were present at low levels but with a strong uncertainty due to a large analytical error.

Naphthalene, phenanthrene, pyrene were the most abundant PAHs in all samples, possibly because they are the most stable of the measured PAHs series. Fluorene was present but at low concentrations. Anthracene was only detected in the Menez Gwen fluids and with a significant concentration. PAHs were already reported in similar concentration in hot fluids of the Fatu Kapa vent field in the Western Pacific, however, the distribution was different (Konn *et al*., 2018). Naphthalene was the most abundant with concentrations 5 to 10 times higher than the rest of the series, then Phenanthrene and then Fluorene. Besides, the occurrence was unsure for acenaphtene, fluoranthene and pyrene considering the analytical error. In addition, picomoles of aromatic compounds were also found in hot hydrothermal fluids (T=365 °C) at 9 °N on the EPR (Longnecker *et al*., 2018)

PAHs are characteristic products of high-temperature OM degradation and especially with increasing temperature (Kawka and Simoneit, 1990; Konn *et al*., 2011; Simoneit, 1992). All the studied sites exhibited T > 300 °C, suggesting that the presence of PAHs in the fluids could be attributed to high-temperature processes. PAHs can also be generated at lower temperature but need longer reaction times. Low-temperature alteration of OM in distal and recharge zones may indeed occur as discussed in section 5.3.3.2. Moreover at the Lucky Strike vent field long residence time of the fluids in the subsurface has been inferred (Pester *et al*., 2012). Hence, the presence of PAHs in the fluids is likely related to both high- and low-temperature processes. Indeed, if only one process was controlling the PAHs concentration and distribution, then we should observe a correlation with the endmember temperature. It is also likely that other physico-chemical processes modify the final distribution of PAHs in the fluids. Finally, the recent findings of Menez and collaborators (2018) show that serpentine fluid inclusions should be considered as potential shallow reservoir and sources of aromatic compounds. To that respect, some varieties of smectite, including saponite, were shown to promote abiotic synthesis of (poly)aromatic hydrocarbons under hydrothermal conditions

(that is, 300 °C, 100 MPa) (Golding and Glikson, 2010). This hypothesis could be particularly considered at the ultramafic hosted Rainbow vent field.

### 5.4 Organic compounds: implications for biogeochemical cycles

Organics can form complexes with metals as well as rare earth elements (Gerringa *et al*., 2015; Hawkes *et al*., 2013; Lecumberri-Sanchez *et al*., 2018), which greatly improves their dispersion in the ocean and prevents them from precipitation as sulphides or oxyhydroxydes (Bennett *et al*., 2008; Sander and Koschinsky, 2011). Fatty acids are especially efficient ligands and play a major role in making metals bioavailable and in transporting them both through the upper crust (Brugger *et al*., 2016 and references therein) and through the water column in the plume (Bennett *et al*., 2011; Greenwood *et al*., 2013; Liu *et al*., 2001; Palmer and Hyde, 1993). Acetate has notably been shown to be a better ligand to Cu in hydrothermal fluids (Lai *et al*., 2018). In addition, fatty acids have been shown to be involved in growth / dissolution processes of some minerals (Franklin *et al*., 1994; Gautier *et al*., 2016; Gautier *et al*., 2015). For these reasons, they are of particular importance in ore forming processes. Hydrocarbons which are weaker ligands would react with sulphates to generate bisulfide ($HS^-$), which in turn would easily react with metal chlorides to form metal sulphides according to mass balance equations (6) and (7).

(6) $3SO_4^{2-} + 3H^+ + 4\ R\text{-}CH_3 \rightarrow 4\ R\text{-}CO_2H + HS^- + 4\ H_2O$

(7) $HS^- + MeCl_2^+ \rightarrow MeS + H^+ + 2Cl^-$

Where R is a carbonated chain, either aliphatic or aromatic and represents OM (Machel *et al*., 1995). To that respect hydrocarbons are likely to be involved in depositional processes of metals. Notably associations of aliphatic and aromatic hydrocarbons with mineral deposits have also been observed on the EPR (Simoneit *et al*., 1990) and in sulphide sedimentary deposits on land (Greenwood *et al*., 2013).

The other way around, the formation of organic-metal complexes enhances the organic matter stability improving as well its bioavailability for the micro- and macro-fauna at the local and regional scales (Adhikari *et al*., 2019). Utilisation of organic compounds by microbial populations as their electron donors instead of $H_2$ or $CH_4$ is indeed possible (Fones *et al*., 2019; Ménez, 2020 for a review). It is for example well established that VFAs constitute a significant food source for some microorganisms and thus help sustaining hydrothermal ecosystems (Ferry, 2010; Kim *et al*., 2010; Lang *et al*., 2018; Windman *et al*., 2007). Also, some bacteria have proven to be capable of using naphthalene (Galushko *et al*., 1999) and other PAHs for their living (Trias *et al*., 2017). Besides, it was found that up to 8% of the C in the deep-sea shrimp, *Rimicaris hybisae*, diet was not microbial (Streit *et al*., 2015) and that tubeworms could use hydrocarbons in their metabolism (Bennett *et al*., 2015).

## 6 Concluding remarks

The study of major and minor elements suggested a recent eruptive event at Menez Gwen which, we believe, likely affected some geochemical parameters temporarily but does not challenge the overall hydrothermal stability of the system and the general understanding of the system (i.e., a control by phase separation, interaction with E-MORBs and highly altered basalts, a magmatic volatile input and a possible contribution of low-temperature serpentinisation.

For the southern Lucky Strike, most of our results fall within the range of the analytical error and support a geochemical control by both volcanic and tectonic processes as well as phase separation and the Azores hot spot influence. Only Cl and Li exhibited significant different values which could be consistent with a change in the depth of the reaction zone as suggested elsewhere (Pester *et al*., 2012). Unlike, Fe, Cu and Zn seemed to bring more confusion in the understanding of the processes and will need more investigation.

The Rainbow fluid chemistry has always been described as stable and controlled by both serpentinisation and phase separation. Yet, new geophysical data call to challenge some of these hypotheses. Consistently, the interpretation of our results was somewhat confusing and suggested that some processes still remain unravelled at Rainbow. Notably, we could not explain the significant increase in Li.

Our results may suggest that temperature has increased deeper in the system at Snake Pit and that an additional low-temperature alteration contribution likely occur in the recharge zone which is in addition supported by organic geochemistry data. The gas isotopic data confirm the suspected abiogenic origin of $CH_4$ at Snake Pit and point to both carbonate and magma as $CO_2$ sources.

Both element and gas data seem to show more inconsistencies at TAG. We believe that the overall apparent stability of the fluids (same order of magnitude) may be largely controlled by deep down processes, but that smaller temporal and spatial scale variations control another significant part of the chemistry as suggested elsewhere for the Lucky Strike hydrothermal vent field (Barreyre *et al*., 2014). To that respect a dedicated study of the TAG hydrothermal plume was carried out during the BICOSE 2 and HERMINE cruises (Mastin, 2020).

Such an extended dataset on quantitative organic geochemistry is the first one to be presented for the MAR region. TOC was highly enriched in some fluids but a large part remains to be allocated as the total equivalent carbon of the studied SVOCs was far to balance the budget. Formate, acetate and *n*-FAs concentrations appeared far lower than at $H_2$-rich hydrothermal vent field as theoretically expected. In addition, formate and acetate data support some of the hypothesis formulated based on mineral geochemistry. At Snake Pit, formate and acetate must originate from abiotic conversion of $CO_2$ in the shallow subsurface and thus imply subsequent mixing with a deeper-rooted fluid. At TAG, formate and acetate

must be thermogenic probably through entrainment of large amount of OM-rich seawater within the hot mound. Although some discrepancies can be noted, our results for SVOCs were generally consistent with other studies. *n*-FAs, *n*-alkanes and mono- and poly-aromatic hydrocarbons were measured at all sites. Overall, the distribution patterns were difficult to interpret and most likely reflect a high level of mixing between sources and reactions. n-FAs may be biogenic at Lucky Strike, and Rainbow, abiogenic at Menez Gwen, thermogenic at TAG and of various sources at Snake Pit. *n*-Alkanes probably originate from low-temperature OM degradation at all sites which argues that a low-temperature fluid component may exist. Yet a small abiogenic contribution is possible at Snake Pit and Rainbow. Conversely, the presence of PAHs at Rainbow, Menez Gwen and Lucky Strike implies another high-temperature component and possibly a contribution of serpentine fluid inclusion at Rainbow.

## Acknowledgement

The authors are grateful to chief scientists M.A. Cambon (BICOSE cruise: Cambon, 2014) and F. Lallier (BIOBAZ cruise: Lallier, 2013). Many thanks go to the ship crew; and the ship captains for running these two cruises with skills and professionalism. We are also rewarding to the engineers who processed the bathymetric data on board. Last we would like to thank warmly H. Ondreas and C. Cathalot for their constructive discussions as well as X. Middleton for having kindly checked grammar and language use.

# Figures and Tables

**Figure 1: Location map of the sampled vent fields on the Mid-Atlantic Ridge. Menez Gwen (Menez Gwen) – 37°N50', Lucky Stricke (Lucky Strike) - 37°N17' and Rainbow (Rainbow) - 36°N14' were visited in 2013 during the BIOBAZ cruise. Transatlantic Geotraverse (TAG) – 26°08' and Snake Pit (Snake Pit) – 23°N22' were visited in 2014 during the BICOSE cruise.**

**Figure 2: Left: bathymetric map of the Menez Gwen (37°N50') hydrothermal vent field with samples locations taken in 2013 during the BIOBAZ cruise (red disks). Right: Picture of a typical sampled vent showing translucent fluids.**

**Figure 3: Top left: bathymetric map of the Lucky Strike (37°N17') hydrothermal vent field with location of the main known vents (stars). Bottom right: bathymetric map showing sampled vents during the BIOBAZ cruise in 2013 (red disks). Top right and bottom left: pictures of sampled chimneys.**

**Figure 4: Top right: bathymetric map of the Rainbow ridge showing the location of the Rainbow (36°N14') hydrothermal vent field. Bottom left: bathymetric map showing the main active areas at Rainbow (stars) and locations (red disks) of samples collected in 2013 during the BIOBAZ cruise. Top left and bottom right: pictures of sampled chimneys.**

**Figure 5: Left: Bathymetric map of the Snake Pit area showing the vent field location. Middle right: bathymetric map showing the two main active areas at Snake Pit (stars) and locations (red disks) of fluid samples collected in 2014 during the BICOSE cruise. Top right and bottom right: pictures of sampled chimneys.**

**Figure 6: Bathymetric map of the TAG active mound showing locations of hydrothermal fluid samples (red disks) collected during the BICOSE cruise in 2014. Pictures show sampled chimneys in the flank of active mound (top right), summit of active mound (top left) and new black smoker area (bottom left).**

**Figure 7: Full bars represent n-alkanes concentrations (µg.$L^{-1}$) in individual fluid samples collected in 2013 at the Menez Gwen, Lucky Strike and Rainbow hydrothermal vent fields and in 2014 at the, Snake Pit and TAG hydrothermal vent fields. Horizontal axis labels correspond to the carbon number of the compounds (ex : C9 for nonane). Concentrations in the reference deep seawater sample taken at each site are represented by the empty bars.**

**Figure 8: Full bars represent n-fatty acids concentrations (µg.$L^{-1}$) in individual fluid samples collected in 2013 at the Menez Gwen, Lucky Strike and Rainbow hydrothermal vent fields and in 2014 at the, Snake Pit and TAG hydrothermal vent fields. Horizontal axis labels correspond to the carbon number of the compounds and the number of insaturation (ex : C9:0 for nonanoic acid). Concentrations in the reference deep seawater sample taken at each site are represented by the empty bars.**

**Figure 9: Full bars represent mono- (Top) and poly-aromatic (Bottom) hydrocarbons concentrations (µg.L$^{-1}$) in individual fluid samples collected in 2013 at the Menez Gwen, Lucky Strike and Rainbow hydrothermal vent fields. Horizontal axis labels abbreviations are Me = methyl, Et = ethyl, Pr = propyl, Bu = butyl, Bz = benzene, Xy = xylene, Sty = styrene, i=iso, n=linear. Concentrations in the reference deep seawater sample taken at each site are represented by the empty bars.**

**Figure 10: Genetic diagram of $\delta^{13}C$-$C_1$ versus $\delta^{13}C$-$CO_2$ showing revised genetic fields after Milkov *et al*., 2018. Acronyms: CR – CO2 reduction, F – methyl-type fermentation, SM – secondary microbial, EMT – early mature thermogenic gas, OA – oil-associated thermogenic gas, LMT – late mature thermogenic gas. Symbols show hot fluid endmember composition: star Rainbow; triangle = Lucky Strike; diamond full = beehive (Snake Pit), diamond empty = moose (Snake Pit)**

**Figure 11: Modified after Shock *et al*., 1992. Plot of log$fH_2$ against temperature. Solid curves show values of log$fH_2$ buffered by the FMQ (fayalite-magnetite-quartz), PPM (pyrite-pyrrhotite-magnetite), HM (hematite-magnetite) mineral assemblages as function of temperature. Dashed curves correspond to contours of log ($fCO_2$/$fCH_4$) equal to 2, 0 and -2 as function of temperature. Dotted vertical line at 500 °C separates range of temperature where stable equilibrium in the C-H-O system is attained in submarine hydrothermal system (T > 500 °C), from that at which $CO_2$ reduction to $CH_4$ is kinetically inhibited, and where metastable equilibrium states between $CO_2$ and aqueous organic compounds may prevail. Stippled area corresponds to the region where synthesis of aqueous organic compounds in metastable states may be most easily detected. Plain light red area bordered by semi-dashed line represents the extended stippled area in the hypothetical (HYP) buffering more representative of ultramafic-hosted vent fields (Konn *et al*., 2009). T/$fH_2$ conditions in hot fluids are shown for Menez Gwen (circle), Lucky Strike (triangle), Rainbow (star), Snake Pit - Beehive (full diamond), Snake Pit – Moose (empty diamond) and TAG (square).**

**Table 1: Gas chromatography analytical conditions used for each group of compounds.**

**Table 2: Endmembers composition and significant ratios of fluids from the Menez Gwen, Lucky Strike, Rainbow, Snake Pit and TAG hydrothermal vent fields. Values were obtained by least square regression to Mg=0 except for TAG where significant concentrations of Mg remain in pure fluids. However extrapolation to Mg=0 is also presented in the table for comparison reasons. [1] measured value. *calculated value.**

**Table 3: Time series of the concentration in major and minor elements in hydrothermal endmember fluids at Menez Gwen, Lucky Strike, Rainbow, Snake Pit and TAG hydrothermal vent fields. Concentrations obtained after extrapolation to Mg=0 for TAG are reported for comparison reasons. Red arrows remind significant events that occurred in the time line: "ODP" for drilling of the TAG mound during the ocean drilling program cruise leg 158 in 1994 and "Diking" for the dike intrusion at Lucky Strike in 2001.**

**Table 4: Time series of gases composition and gas stable isotopes in endmember fluids of the Menez Gwen, Lucky Strike, Rainbow, Snake Pit and TAG hydrothermal vent fields. Endmembers were obtained using linear regression vs. Mg concentration. Lucky Strikes exhibits several endmembers depending on the vent, therefore ranges of values**

**are presented. When linear regression was not possible, measured values in the purest fluid sample are reported instead and appear in bold.**

**Table 5: Organic compounds concentration in fluid samples from the Menez Gwen, Lucky Strike, Rainbow, Snake Pit and TAG hydrothermal vent fields. Rt is the chromatographic retention time. The first line corresponds to the sample name used on the location maps. BB are samples collected in 2013 during the BIOBAZ cruise and BIC are samples collected in 20104 during the BICOSE cruise. For an easy read the MQ water control data appear in grey, the background seawater samples (REF) data are presented in bold and regular fluid samples are written in normal font. Acronyms signification: N.A. for not analysed, N.D. for not detected, TOC for total organic carbon, Total eq. C for total equivalent carbon.**

## References


Adhikari, D. *et al*., 2019. Formation and redox reactivity of ferrihydrite-organic carbon-calcium co-precipitates. Geochimica et Cosmochimica Acta, 244: 86-98.

Aizenshtat, Z., Baedecker, M.J., Kaplan, I.R., 1973. Distribution and diagenesis of organic compounds in JOIDES sediment from Gulf of Mexico and western Atlantic. Geochimica et Cosmochimica Acta, 37(8): 1881.

Akiya, N., Savage, P.E., 2002. Roles of water for chemical reactions in high-temperature water. Chem Rev, 102(8): 2725-50.

Alt, J.C., Shanks, W.C., 2003. Serpentinization of abyssal peridotites from the MARK area, Mid-Atlantic Ridge: Sulfur geochemistry and reaction modeling. Geochimica Et Cosmochimica Acta, 67(4): 641-653.

Amon, R.M.W., 2016. CARBON CYCLE Ocean dissolved organics matter. Nature Geoscience, 9(12): 864-865.

Andreani, M. *et al*., 2014. Tectonic structure, lithology, and hydrothermal signature of the Rainbow massif (Mid-Atlantic Ridge 36°14′N). Geochemistry, Geophysics, Geosystems, 15(9): 3543-3571.

Auzende, J.-M. *et al*., 1994. Observation of sections of oceanic crust and mantle cropping out on the southern wall of Kane FZ (N. Atlantic). Terra Nova, 6(2): 143-148.

Baltussen, E., Sandra, P., David, F., Cramers, C., 1999. Stir bar sorptive extraction (SBSE), a novel extraction technique for aqueous samples: Theory and principles. Journal of Microcolumn Separations, 11(10): 737-747.

Barreyre, T. *et al*., 2014. Temporal variability and tidal modulation of hydrothermal exit-fluid temperatures at the Lucky Strike deep-sea vent field, Mid-Atlantic Ridge. Journal of Geophysical Research-Solid Earth, 119(4): 2543-2566.

Beaulieu, S.E., Szafranski, K., 2020. InterRidge Global Database of Active Submarine Hydrothermal Vent Fields: Version 3.4. World Wide Web electronic publication available from http://vents-data.interridge.org Accessed 2021-02-21.

Ben-Mlih, F., Marty, J.C., Fiala-Medioni, A., 1992. Fatty acid composition in deep hydrothermal vent symbiotic bivalves. J Lipid Res, 33(12): 1797-806.

Bennett, S.A. *et al*., 2008. The distribution and stabilisation of dissolved Fe in deep-sea hydrothermal plumes. Earth and Planetary Science Letters, 270(3-4): 157-167.

Bennett, S.A. *et al*., 2011. Dissolved and particulate organic carbon in hydrothermal plumes from the East Pacific Rise, 9 degrees 50 ' N. Deep-Sea Research Part I-Oceanographic Research Papers, 58(9): 922-931.

Bennett, S.A., Van Dover, C., Breier, J.A., Coleman, M., 2015. Effect of depth and vent fluid composition on the carbon sources at two neighboring deep-sea hydrothermal vent fields (Mid-Cayman Rise). Deep-Sea Research Part I-Oceanographic Research Papers, 104(0): 122-133.

Bischoff, J.L., Pitzer, K.S., 1989. Liquid-vapor relations for the system NaCl-H 2 O; summary of the P-T-x surface from 300 degrees to 500 degrees C. Am J Sci, 289(3): 217-248.

Blumenberg, M., Seifert, R., Petersen, S., Michaelis, W., 2007. Biosignatures present in a hydrothermal massive sulfide from the Mid-Atlantic Ridge. Geobiology, 5(4): 435-450.

Bradley, A.S., Hayes, J.M., Summons, R.E., 2009. Extraordinary $^{13}C$ enrichment of diether lipids at the Lost City Hydrothermal Field indicates a carbon-limited ecosystem. Geochimica et Cosmochimica Acta, 73(1): 102-118.

1292 Brazelton, W.J., Mehta, M.P., Kelley, D.S., Baross, J.A., 2011. Physiological differentiation within a single-species biofilm fueled by serpentinization. MBio, 2(4).
1294 Breier, J.A. *et al*., 2012. Sulfur, sulfides, oxides and organic matter aggregated in submarine hydrothermal plumes at 9°50′N East Pacific Rise. Geochimica et Cosmochimica Acta, 1296 88(0): 216-236.
Brugger, J. *et al*., 2016. A review of the coordination chemistry of hydrothermal systems, or 1298 do coordination changes make ore deposits? Chemical Geology, 447: 219-253.
Butterfield, D.A., Massoth, G.J., Mcduff, R.E., Lupton, J.E., Lilley, M.D., 1990. 1300 Geochemistry of Hydrothermal Fluids from Axial Seamount Hydrothermal Emissions Study Vent Field, Juan-De-Fuca Ridge - Subseafloor Boiling and Subsequent Fluid-1302 Rock Interaction. Journal of Geophysical Research-Solid Earth and Planets, 95(B8): 12895-12921.
1304 Cambon, M-A, 2014. BICOSE cruise, Pourquoi pas ? R/V. Sismer. https://doi.org/10.17600/14000100
1306 Campbell, A.C. *et al*., 1988. Chemistry of Hot Springs on the Mid-Atlantic Ridge. Nature, 335(6190): 514-519.
1308 Canales, J.P., Dunn, R.A., Arai, R., Sohn, R.A., 2017. Seismic imaging of magma sills beneath an ultramafic-hosted hydrothermal system. Geology, 45(5): 451-454.
1310 Canales, J.P., Sohn, R.A., deMartin, B.J., 2007. Crustal structure of the Trans-Atlantic Geotraverse (TAG) segment (Mid-Atlantic Ridge, 26°10′N): Implications for the 1312 nature of hydrothermal circulation and detachment faulting at slow spreading ridges. Geochemistry, Geophysics, Geosystems, 8(8).
1314 Cannat, M. *et al*., 1995. Thin crust, ultramafic exposures, and rugged faulting patterns at the Mid-Atlantic Ridge (22°–24°N). Geology, 23(1): 49-52.
1316 Cannat, M. *et al*., 2007. Geological Context of Ultramafic-Hosted Hydrothermal Vent Fields in the 13-15°N Region of the Mid Atlantic Ridge : Preliminary Results of the 1318 Serpentine Cruise. Eos Trans. AGU, 88(52): T51F-02.
Cannat, M. *et al*., 2011. MoMar-Demo at Lucky Strike. A near-real time multidisciplinary 1320 observatory of hydrothermal processes and ecosystems at the Mid-Atlantic Ridge, pp. OS22A-05.
1322 Charlou, J. *et al*., 2007. High Hydrogen and abiotic hydrocarbons from new ultramafic hydrothermal sites between 12°N and 15°N on the Mid Atlantic Ridge- Results of the 1324 Serpentine cruise (March 2007), Eos Trans. AGU, pp. Fall Meet. Suppl., Abstract T51F-04.
1326 Charlou, J.L., Donval, J.P., 1993. Hydrothermal Methane Venting Between 12°N and 26°N Along the Mid-Atlantic Ridge. J. Geophys. Res., 98(B6): 9625-9642.
1328 Charlou, J.L. *et al*., 2000. Compared geochemical signatures and the evolution of Menez Gwen (37°50′N) and Lucky Strike (37°17′N) hydrothermal fluids, south of the Azores 1330 Triple Junction on the Mid-Atlantic Ridge. Chemical Geology, 171(1): 49-75.
Charlou, J.L., Donval, J.P., Fouquet, Y., Jean-Baptiste, P., Holm, N., 2002a. Geochemistry of 1332 high H2 and CH4 vent fluids issuing from ultramafic rocks at the Rainbow hydrothermal field (36 Deg14'N, MAR). Chemical Geology, 191(4): 345-359.
1334 Charlou, J.L., Donval, J.P., Fouquet, Y., Jean-Baptiste, P., Holm, N., 2002b. Geochemistry of high H2 and CH4 vent fluids issuing from ultramafic rocks at the Rainbow 1336 hydrothermal field (36°14′N, MAR). Chemical Geology, 191(4): 345-359.
Charlou, J.L., Donval, J.P., JeanBaptiste, P., Dapoigny, A., 1996. Gases and helium isotopes 1338 in high temperature solutions sampled before and after ODP Leg 158 drilling at TAG hydrothermal field (26 degrees N, MAR). Geophysical Research Letters, 23(23): 1340 3491-3494.

Charlou, J.L. *et al*., 1998. Intense CH4 plumes generated by serpentinization of ultramafic rocks at the intersection of the 15 Deg20'N fracture zone and the Mid-Atlantic Ridge. Geochimica et Cosmochimica Acta, 62(13): 2323-2333.

Chavagnac, V. *et al*., 2018. Spatial Variations in Vent Chemistry at the Lucky Strike Hydrothermal Field, Mid-Atlantic Ridge (37°N): Updates for Subseafloor Flow Geometry From the Newly Discovered Capelinhos Vent. Geochemistry, Geophysics, Geosystems, 19(11): 4444-4458.

Chiba, H., Masuda, H., Lee, S.-Y., Fujioka, K., 2001. Chemistry of hydrothermal fluids at the TAG Active Mound, MAR 26°N, in 1998. Geophysical Research Letters, 28(15): 2919-2922.

Corliss, J.B. *et al*., 1979. Submarine Thermal Springs on the Galápagos Rift. Science, 203(4385): 1073-1083.

Crawford, W.C. *et al*., 2013. Hydrothermal seismicity beneath the summit of Lucky Strike volcano, Mid-Atlantic Ridge. Earth and Planetary Science Letters, 373(0): 118-128.

Deguchi, S., Tsujii, K., 2007. Supercritical water: a fascinating medium for soft matter. Soft Matter, 3(7): 797-803.

Delacour, A., Fruh-Green, G.L., Bernasconi, S.M., Schaeffer, P., Kelley, D.S., 2008. Carbon geochemistry of serpentinites in the Lost City hydrothermal system (30 degrees N, MAR). Geochimica Et Cosmochimica Acta, 72(15): 3681-3702.

deMartin, B.J., Sohn, R.A., Canales, J.P., Humphris, S.E., 2007. Kinematics and geometry of active detachment faulting beneath the Trans-Atlantic Geotraverse (TAG) hydrothermal field on the Mid-Atlantic Ridge. Geology, 35(8): 711-714.

Douville, E. *et al*., 1999. Yttrium and rare earth elements in fluids from various deep-sea hydrothermal systems. Geochimica et Cosmochimica Acta, 63(5): 627-643.

Douville, E. *et al*., 2002. The rainbow vent fluids (36 degrees 14 ' N, MAR): the influence of ultramafic rocks and phase separation on trace metal content in Mid-Atlantic Ridge hydrothermal fluids. Chemical Geology, 184(1-2): 37-48.

Dziak, R.P. *et al*., 2004. Evidence of a recent magma dike intrusion at the slow spreading Lucky Strike segment, Mid-Atlantic Ridge. Journal of Geophysical Research-Solid Earth, 109(B12): B12102.

Edmond, J.M. *et al*., 1995. Time series studies of vent fluids from the TAG and MARK sites (1986, 1990) Mid-Atlantic Ridge: a new solution chemistry model and a mechanism for Cu/Zn zonation in massive sulphide orebodies. Geological Society, London, Special Publications, 87(1): 77-86.

Edmond, J.M. *et al*., 1979. Ridge Crest Hydrothermal Activity and the Balances of the Major and Minor Elements in the Ocean - Galapagos Data. Earth and Planetary Science Letters, 46(1): 1-18.

Edmonds, H.N. *et al*., 1996. Continuation of the hydrothermal fluid chemistry time series at TAG, and the effects of ODP drilling. Geophysical Research Letters, 23(23): 3487-3489.

Engel, M.H., Macko, S.A., 2013. Organic geochemistry: principles and applications, 11. Springer Science & Business Media.

Escartin, J. *et al*., 2015. Hydrothermal activity along the slow-spreading Lucky Strike ridge segment (Mid-Atlantic Ridge): Distribution, heatflux, and geological controls. Earth and Planetary Science Letters, 431: 173-185.

Ferry, J.G., 2010. The chemical biology of methanogenesis. Planetary and Space Science, 58(14-15): 1775-1783.

Fitzsimmons, J.N. *et al*., 2017. Iron persistence in a distal hydrothermal plume supported by dissolved-particulate exchange. Nature Geoscience, 10(3): 195-U150.

Fones, E.M. *et al*., 2019. Physiological adaptations to serpentinization in the Samail Ophiolite, Oman. The ISME Journal, 13(7): 1750-1762.

Fouquet, Y. *et al*., 1998. FLORES diving cruise with the Nautile near the Azores - Firts dives on the Rainbow field: hydrothermal seawater/mantle interaction. InterRidge News, 7(1): 24-28.

Fouquet, Y. *et al*., 1994. A detailed Study of the Lucky Strike Hydrothermal Site and Discovery of a New Hydrothermal Site: Menez Gwen; Preliminary Results of the DIVA1 Cruise (5-29 May, 1994). InterRidge News, 3(2): 14-17.

Fouquet, Y. *et al*., 1995. Atlantic lava lakes and hot vents. Nature, 377(6546): 201-201.

Fouquet, Y. *et al*., 1993. Tectonic setting and mineralogical and geochemical zonation in the Snake Pit sulfide deposit (Mid-Atlantic Ridge at 23 degrees N). Economic Geology, 88(8): 2018-2036.

Foustoukos, D.I., Seyfried, W.E., Jr., 2004. Hydrocarbons in hydrothermal vent fluids: the role of chromium-bearing catalysts. Science, 304(5673): 1002-5.

Franklin, S.P., Hajash, A., Dewers, T.A., Tieh, T.T., 1994. The Role of Carboxylic-Acids in Albite and Quartz Dissolution - an Experimental-Study under Diagenetic Conditions. Geochimica Et Cosmochimica Acta, 58(20): 4259-4279.

Galushko, A., Minz, D., Schink, B., Widdel, F., 1999. Anaerobic degradation of naphthalene by a pure culture of a novel type of marine sulphate-reducing bacterium. Environ Microbiol, 1(5): 415-20.

Gamo, T. *et al*., 1996. Chemical characteristics of hydrothermal fluids from the TAG mound of the Mid-Atlantic Ridge in August 1994: Implications for spatial and temporal variability of hydrothermal activity. Geophysical Research Letters, 23(23): 3483-3486.

Gautier, Q., Benezeth, P., Schott, J., 2016. Magnesite growth inhibition by organic ligands: An experimental study at 100, 120 and 146 degrees C. Geochimica Et Cosmochimica Acta, 181: 101-125.

Gautier, Q., Berninger, U.N., Schott, J., Jordan, G., 2015. Influence of organic ligands on magnesite growth: A hydrothermal atomic force microscopy study. Geochimica Et Cosmochimica Acta, 155(0): 68-85.

Gente, P., Mével, C., Auzende, J.M., Karson, J.A., Fouquet, Y., 1991. An example of a recent accretion on the Mid-Atlantic Ridge: the Snake Pit neovolcanic ridge (MARK area, 23°22′N). Tectonophysics, 190(1): 1-29.

German, C.R., Von Damm, K.L., 2004. Hydrothermal Processes. Treatise on Geochemistry, 6(6): 181-222.

Gerringa, L.J.A., Rijkenberg, M.J.A., Schoemann, V., Laan, P., de Baar, H.J.W., 2015. Organic complexation of iron in the West Atlantic Ocean. Marine Chemistry, 177(0): 434-446.

Golding, S.D., Glikson, M., 2010. Earliest life on Earth: habitats, environments and methods of detection. Springer Science & Business Media.

Grasshoff, K., 1970. A simultaneous multiple channel system for nutrient analysis in seawater with analog and digital data record. Advances in Automated Analysis; Mediad Inc, New York 135-145.

Greenwood, P.F. *et al*., 2013. Organic geochemistry and mineralogy. I. Characterisation of organic matter associated with metal deposits. Ore Geology Reviews, 50(0): 1-27.

Hawkes, J.A., Connelly, D.P., Gledhill, M., Achterberg, E.P., 2013. The stabilisation and transportation of dissolved iron from high temperature hydrothermal vent systems. Earth and Planetary Science Letters, 375(0): 280-290.

Hawkes, J.A., Hansen, C.T., Goldhammer, T., Bach, W., Dittmar, T., 2016. Molecular alteration of marine dissolved organic matter under experimental hydrothermal conditions. Geochimica Et Cosmochimica Acta, 175: 68-85.

Hawkes, J.A. *et al*., 2015. Efficient removal of recalcitrant deep-ocean dissolved organic matter during hydrothermal circulation. Nature Geoscience, 8(11): 856-+.

Homoky, W.B., 2017. Deep ocean iron balance. Nature Geoscience, 10(3): 162-163.

Horita, J., Berndt, M.E., 1999. Abiogenic CH4 formation and isotopic fractionation under hydrothermal conditions. Science, 285(5430): 1055-7.

Humphris, S.E., Fornari, D.J., Scheirer, D.S., German, C.R., Parson, L.M., 2002. Geotectonic setting of hydrothermal activity on the summit of Lucky Strike Seamount (37°17′N, Mid-Atlantic Ridge). Geochemistry, Geophysics, Geosystems, 3(8): 1-25.

Humphris, S.E., Kleinrock, M.C., 1996. Detailed morphology of the TAG active hydrothermal mound: Insights into its formation and growth. Geophysical Research Letters, 23(23): 3443-3446.

Humphris, S.E., Tivey, M.K., Tivey, M.A., 2015. The Trans-Atlantic Geotraverse hydrothermal field: A hydrothermal system on an active detachment fault. Deep-Sea Research Part Ii-Topical Studies in Oceanography, 121(0): 8-16.

Ildefonse, B. *et al*., 2007. Oceanic core complexes and crustal accretion at slow-spreading ridges. Geology, 35(7): 623-626.

Jean-Baptiste, P. *et al*., 1991. Helium and methane measurements in hydrothermal fluids from the mid-Atlantic ridge: The Snake Pit site at 23°N. Earth and Planetary Science Letters, 106(1-4): 17-28.

Karson, J.A., Brown, J.R., 1988. Geologic setting of the Snake Pit hydrothermal site: An active vent field on the Mid-Atlantic Ridge. Marine Geophysical Researches, 10(1): 91-107.

Kawka, O.E., Simoneit, B.R.T., 1990. Polycyclic Aromatic-Hydrocarbons in Hydrothermal Petroleums from the Guaymas Basin Spreading Center. Applied Geochemistry, 5(1-2): 17-27.

Kawka, O.E., Simoneit, B.R.T., 1994. Hydrothermal pyrolysis of organic matter in Guaymas Basin: I. Comparison of hydrocarbon distributions in subsurface sediments and seabed petroleums. Organic Geochemistry, 22(6): 947.

Kelley, D.S., Baross, J.A., Delaney, J.R., 2002. Volcanoes, fluids, and life at mid-ocean ridge spreading centers. Annual Review of Earth and Planetary Sciences, 30(1): 385-491.

Kim, Y.J. *et al*., 2010. Formate-driven growth coupled with $H_2$ production. Nature, 467(7313): 352-355.

Kissin, Y.V., 1987. Catagenesis and Composition of Petroleum - Origin of N-Alkanes and Isoalkanes in Petroleum Crudes. Geochimica Et Cosmochimica Acta, 51(9): 2445-2457.

Kleinrock, M.C., Humphris, S.E., 1996. Structural asymmetry of the TAG rift valley: Evidence from a near-bottom survey for episodic spreading. Geophysical Research Letters, 23(23): 3439-3442.

Kong, L. *et al*., 1985. Bare rock drill sites, ODP legs 106 and 109: Evidence for hydrothermal activity at 23" N on the Mid Atlantic Ridge. Eos, 66: 46.

Konn, C., Charlou, J.-L., Donval, J.-P., Holm, N., 2012. Characterisation of dissolved organic compounds in hydrothermal fluids by stir bar sorptive extraction - gas chomatography - mass spectrometry. Case study: the Rainbow field (36degreesN, Mid-Atlantic Ridge). Geochemical Transactions, 13(1): 8.

Konn, C. *et al*., 2009. Hydrocarbons and oxidized organic compounds in hydrothermal fluids from Rainbow and Lost City ultramafic-hosted vents. Chemical Geology, 258(3-4): 299-314.

Konn, C. *et al*., 2018. Organic, Gas, and Element Geochemistry of Hydrothermal Fluids of the Newly Discovered Extensive Hydrothermal Area in the Wallis and Futuna Region (SW Pacific). Geofluids, 2018: 25.

Konn, C., Testemale, D., Querellou, J., Holm, N.G., Charlou, J.L., 2011. New insight into the contributions of thermogenic processes and biogenic sources to the generation of organic compounds in hydrothermal fluids. Geobiology, 9(1): 79-93.

Lai, F., Liu, L., Cao, W., 2018. Complexation of copper in acetate-rich low-temperature hydrothermal fluids: Evidence from ab initio molecular dynamics simulations. Chemical Geology, 476: 100-118.

Lallier, F, 2013. BIOBAZ 2013 cruise, Pourquoi pas ? R/V. Sismer. https://doi.org/10.17600/13030030

Lalou, C. *et al*., 1993. New age data for Mid-Atlantic Ridge hydrothermal sites: TAG and Snakepit chronology revisited. Journal of Geophysical Research: Solid Earth, 98(B6): 9705-9713.

Lalou, C., Reyss, J.-L., Brichet, E., Rona, P.A., Thompson, G., 1995. Hydrothermal activity on a 105-year scale at a slow-spreading ridge, TAG hydrothermal field, Mid-Atlantic Ridge 26°N. Journal of Geophysical Research: Solid Earth, 100(B9): 17855-17862.

Lang, S.Q., Butterfield, D.A., Lilley, M.D., Johnson, H.P., Hedges, J.I., 2006. Dissolved organic carbon in ridge-axis and ridge-flank hydrothermal systems. Geochimica Et Cosmochimica Acta, 70(15): 3830-3842.

Lang, S.Q., Butterfield, D.A., Schulte, M., Kelley, D.S., Lilley, M.D., 2010. Elevated concentrations of formate, acetate and dissolved organic carbon found at the Lost City hydrothermal field. Geochimica Et Cosmochimica Acta, 74(3): 941-952.

Lang, S.Q. *et al*., 2018. Deeply-sourced formate fuels sulfate reducers but not methanogens at Lost City hydrothermal field. Scientific Reports, 8(1): 755.

Langmuir, C. *et al*., 1997. Hydrothermal vents near a mantle hot spot: the Lucky Strike vent field at 37°N on the Mid-Atlantic Ridge. Earth and Planetary Science Letters, 148(1): 69-91.

Lecumberri-Sanchez, P., Bouabdellah, M., Zemri, O., 2018. Transport of rare earth elements by hydrocarbon-bearing brines: Implications for ore deposition and the use of REEs as fluid source tracers. Chemical Geology, 479: 204-215.

Liu, W.H., McPhail, D.C., Brugger, J., 2001. An experimental study of copper(I)-chloride and copper(I)-acetate complexing in hydrothermal solutions between 50 degrees C and 250 degrees C and vapor-saturated pressure. Geochimica Et Cosmochimica Acta, 65(17): 2937-2948.

Longnecker, K., Sievert, S.M., Sylva, S.P., Seewald, J.S., Kujawinski, E.B., 2018. Dissolved organic carbon compounds in deep-sea hydrothermal vent fluids from the East Pacific Rise at 9°50′N. Organic Geochemistry, 125: 41-49.

Machel, H.G., Krouse, H.R., Sassen, R., 1995. Products and Distinguishing Criteria of Bacterial and Thermochemical Sulfate Reduction. Applied Geochemistry, 10(4): 373-389.

Marques, A.F.A., Scott, S.D., Guillong, M., 2011. Magmatic degassing of ore-metals at the Menez Gwen: Input from the Azores plume into an active Mid-Atlantic Ridge seafloor hydrothermal system. Earth and Planetary Science Letters, 310(1-2): 145-160.

Mastin, M., 2020. Étude tridimensionnelle du panache hydrothermal du site TAG - Identification des processus d'export et de vieillissement du panache. Master thesis. IUEM.

McCollom, T.M., 2013. Laboratory Simulations of Abiotic Hydrocarbon Formation in Earth's Deep Subsurface. Carbon in Earth, 75(1): 467-494.

McCollom, T.M., Lollar, B.S., Lacrampe-Couloume, G., Seewald, J.S., 2010. The influence of carbon source on abiotic organic synthesis and carbon isotope fractionation under hydrothermal conditions. Geochimica Et Cosmochimica Acta, 74(9): 2717-2740.

McCollom, T.M., Seewald, J.S., 2006. Carbon isotope composition of organic compounds produced by abiotic synthesis under hydrothermal conditions. Earth and Planetary Science Letters, 243(1-2): 74-84.

McCollom, T.M., Seewald, J.S., 2007. Abiotic synthesis of organic compounds in deep-sea hydrothermal environments. Chem Rev, 107(2): 382-401.

McCollom, T.M., Seewald, J.S., German, C.R., 2015. Investigation of extractable organic compounds in deep-sea hydrothermal vent fluids along the Mid-Atlantic Ridge. Geochimica Et Cosmochimica Acta, 156(0): 122-144.

McDermott, J.M., Seewald, J.S., German, C.R., Sylva, S.P., 2015. Pathways for abiotic organic synthesis at submarine hydrothermal fields. Proc Natl Acad Sci U S A, 112(25): 7668-72.

Ménez, B., 2020. Abiotic Hydrogen and Methane: Fuels for Life. ELEMENTS, 16(1): 39-46.

Ménez, B. *et al*., 2018. Abiotic synthesis of amino acids in the recesses of the oceanic lithosphere. Nature.

Mevel, C., 2003. Serpentinization of abyssal peridotites at mid-ocean ridges. Comptes Rendus Geoscience, 335(10-11): 825-852.

Milkov, A.V., Etiope, G., 2018. Revised genetic diagrams for natural gases based on a global dataset of >20,000 samples. Organic Geochemistry, 125: 109-120.

Mottl, M.J., Holland, H.D., 1978. Chemical exchange during hydrothermal alteration of basalt by seawater--I. Experimental results for major and minor components of seawater. Geochimica et Cosmochimica Acta, 42(8): 1103.

Mullin, J.B., Riley, J.P., 1955. The colorimetric determination of silicate with special reference to sea and natural waters. Analytica Chimica Acta, 12(0): 162-176.

Ondréas, H. *et al*., 2009. Recent volcanic events and the distribution of hydrothermal venting at the Lucky Strike hydrothermal field, Mid-Atlantic Ridge. Geochemistry, Geophysics, Geosystems, 10(2).

Ondréas, H., Fouquet, Y., Voisset, M., Radford-Knoery, J., 1997. Detailed Study of Three Contiguous Segments of the Mid-Atlantic Ridge, South of the Azores (37° N to 38°30′ N), Using Acoustic Imaging Coupled with Submersible Observations. Marine Geophysical Researches, 19(3): 231-255.

Palmer, D.A., Hyde, K.E., 1993. An Experimental-Determination of Ferrous Chloride and Acetate Complexation in Aqueous-Solutions to 300-Degrees-C. Geochimica Et Cosmochimica Acta, 57(7): 1393-1408.

Parson, L., Gracia, E., Coller, D., German, C., Needham, D., 2000. Second-order segmentation; the relationship between volcanism and tectonism at the MAR, 38 degrees N-35 degrees 40 ' N. Earth and Planetary Science Letters, 178(3-4): 231-251.

Pasini, V. *et al*., 2013. Low temperature hydrothermal oil and associated biological precursors in serpentinites from Mid-Ocean Ridge. Lithos, 178: 84-95.

Pester, N.J. *et al*., 2012. Subseafloor phase equilibria in high-temperature hydrothermal fluids of the Lucky Strike Seamount (Mid-Atlantic Ridge, 37°17′N). Geochimica et Cosmochimica Acta, 90(0): 303-322.

Pontbriand, C.W., Sohn, R.A., 2014. Microearthquake evidence for reaction-driven cracking within the Trans-Atlantic Geotraverse active hydrothermal deposit. Journal of Geophysical Research: Solid Earth, 119(2): 822-839.

Rapp, J.B., 1991. A Statistical Approach to the Interpretation of Aliphatic Hydrocarbon Distributions in Marine-Sediments. Chemical Geology, 93(1-2): 163-177.

Reeves, E.P., Fiebig, J., 2020. Abiotic Synthesis of Methane and Organic Compounds in Earth's Lithosphere. ELEMENTS, 16(1): 25-31.

Reeves, E.P., McDermott, J.M., Seewald, J.S., 2014. The origin of methanethiol in midocean ridge hydrothermal fluids. Proc Natl Acad Sci U S A, 111(15): 5474-9.

Rona, P., Klinkhammer, G., Nelsen, T., Trefry, J., Elderfield, H., 1986. Black smokers, massive sulphides and vent biota at the Mid-Atlantic Ridge. Nature, 321(6065): 33-37.

Rouxel, O., Fouquet, Y., Ludden, J.N., 2004. Subsurface processes at the lucky strike hydrothermal field, Mid-Atlantic ridge: evidence from sulfur, selenium, and iron isotopes 11Associate editor: S. Sheppard. Geochimica et Cosmochimica Acta, 68(10): 2295-2311.

Sander, S.G., Koschinsky, A., 2011. Metal flux from hydrothermal vents increased by organic complexation. Nature Geoscience, 4(3): 145-150.

Schulte, M.D., Shock, E.L., 1993. Aldehydes in hydrothermal solution: Standard partial molal thermodynamic properties and relative stabilities at high temperatures and pressures. Geochimica et Cosmochimica Acta, 57(16): 3835-3846.

Scott, R.B., Rona, P.A., McGregor, B.A., Scott, M.R., 1974. The TAG hydrothermal field. Nature, 251(5473): 301-302.

Seewald, J.S., 2001. Aqueous geochemistry of low molecular weight hydrocarbons at elevated temperatures and pressures: Constraints from mineral buffered laboratory experiments. Geochimica Et Cosmochimica Acta, 65(10): 1641-1664.

Seewald, J.S., Seyfried, W.E., 1990. The Effect of Temperature on Metal Mobility in Subseafloor Hydrothermal Systems - Constraints from Basalt Alteration Experiments. Earth and Planetary Science Letters, 101(2-4): 388-403.

Seward, T.M., Williams-Jones, A.E., Migdisov, A.A., 2014. The Chemistry of Metal Transport and Deposition by Ore-Forming Hydrothermal Fluids. In: Turekian, K.K. (Ed.), Treatise on Geochemistry. Elsevier, Oxford, pp. 29-57.

Seyfried Jr, W.E., Pester, N.J., Ding, K., Rough, M., 2011. Vent fluid chemistry of the Rainbow hydrothermal system (36°N, MAR): Phase equilibria and in situ pH controls on subseafloor alteration processes. Geochimica et Cosmochimica Acta, 75(6): 1574-1593.

Sherwood Lollar, B. *et al*., 2006. Unravelling abiogenic and biogenic sources of methane in the Earth's deep subsurface. Chemical Geology, 226(3-4): 328-339.

Shock, E., Canovas, P., 2010. The potential for abiotic organic synthesis and biosynthesis at seafloor hydrothermal systems. Blackwell Publishing Ltd, pp. 161-192.

Shock, E.L., 1990. Geochemical Constraints on the Origin of Organic-Compounds in Hydrothermal Systems. Origins of Life and Evolution of Biospheres, 20(3-4): 331-367.

Shock, E.L., 1992. Chapter 5 Chemical environments of submarine hydrothermal systems. Origins of Life and Evolution of Biospheres, 22(1): 67-107.

Shock, E.L., 1992b. Chapter 7 Hydrothermal organic synthesis experiments. Origins of Life and Evolution of Biospheres, 22(1): 135-146.

Shock, E.L., Schulte, M.D., 1998. Organic synthesis during fluid mixing in hydrothermal systems. Journal of Geophysical Research-Planets, 103(E12): 28513-28527.

Simoneit, B.R.T., 1988. Petroleum Generation in Submarine Hydrothermal Systems - an Update. Canadian Mineralogist, 26(3): 827-840.

Simoneit, B.R.T., 1992. Chapter 4 Aqueous organic geochemistry at high temperature/high pressure. Origins of Life and Evolution of Biospheres, 22(1): 43-65.

Simoneit, B.R.T., Brault, M., Saliot, A., 1990. Hydrocarbons Associated with Hydrothermal Minerals, Vent Waters and Talus on the East Pacific Rise and Mid-Atlantic Ridge. Applied Geochemistry, 5(1-2): 115-124.

Simoneit, B.R.T., Goodfellow, W.D., Franklin, J.M., 1992. Hydrothermal petroleum at the seafloor and organic matter alteration in sediments of Middle Valley, Northern Juan de Fuca Ridge. Applied Geochemistry, 7(3): 257.

Simoneit, B.R.T., Kawka, O.E., Brault, M., 1988. Origin of Gases and Condensates in the Guaymas Basin Hydrothermal System (Gulf of California). Chemical Geology, 71(1-3): 169-182.

Simoneit, B.R.T., Lein, A.Y., Peresypkin, V.I., Osipov, G.A., 2004. Composition and origin of hydrothermal petroleum and associated lipids in the sulfide deposits of the Rainbow field (Mid-Atlantic Ridge at 36[deg]N). Geochimica et Cosmochimica Acta, 68(10): 2275.

Singh, S.C. *et al*., 2006. Discovery of a magma chamber and faults beneath a Mid-Atlantic Ridge hydrothermal field. Nature, 442(7106): 1029-1032.

Streit, K., Bennett, S.A., Van Dover, C.L., Coleman, M., 2015. Sources of organic carbon for Rimicaris hybisae: Tracing individual fatty acids at two hydrothermal vent fields in the Mid-Cayman rise. Deep-Sea Research Part I-Oceanographic Research Papers, 100(0): 13-20.

Takai, K., Nealson, K.H., Horikoshi, K., 2004. Methanotorris formicicus sp. nov., a novel extremely thermophilic, methane-producing archaeon isolated from a black smoker chimney in the Central Indian Ridge. Int J Syst Evol Microbiol, 54(Pt 4): 1095-100.

Tivey, M.A., Schouten, H., Kleinrock, M.C., 2003. A near-bottom magnetic survey of the Mid-Atlantic Ridge axis at 26°N: Implications for the tectonic evolution of the TAG segment. Journal of Geophysical Research: Solid Earth, 108(B5).

Toner, B.M. *et al*., 2009. Preservation of iron(II) by carbon-rich matrices in a hydrothermal plume. Nature Geoscience, 2(3): 197-201.

Trias, R. *et al*., 2017. High reactivity of deep biota under anthropogenic CO2 injection into basalt. Nature Communications, 8(1): 1063.

Vishnoi, S.C., Bhagat, S.D., Kapoor, V.B., Chopra, S.K., Krishna, R., 1987. Simple Gas-Chromatographic Determination of the Distribution of Normal Alkanes in the Kerosene Fraction of Petroleum. Analyst, 112(1): 49-52.

Volkman, J.K., Johns, R.B., Gillan, F.T., Perry, G.J., Bavor, H.J., 1980. Microbial lipids of an intertidal sediment—I. Fatty acids and hydrocarbons. Geochimica et Cosmochimica Acta, 44(8): 1133-1143.

von Damm, K.L., 1995. Controls on the chemistry of temporal variability of seafloor hydrothermal fluids., Seafloor hydrothermal systems: physical, chemical, biological and geological interactions systems. American Geophysical Union, pp. 222-247.

Von Damm, K.L., Bischoff, J.L., Rosenbauer, R.J., 1991. Quartz solubility in hydrothermal seawater; an experimental study and equation describing quartz solubility for up to 0.5 M NaCl solutions. American Journal of Science, 291(10): 977-1007.

Von Damm, K.L., Bray, A.M., Buttermore, L.G., Oosting, S.E., 1998. The geochemical controls on vent fluids from the Lucky Strike vent field, Mid-Atlantic Ridge. Earth and Planetary Science Letters, 160(3-4): 521-536.

Von Damm, K.L. *et al*., 1985. Chemistry of submarine hydrothermal solutions at 21 °N, East Pacific Rise. Geochimica et Cosmochimica Acta, 49(11): 2197-2220.

Wang, D.T., Reeves, E.P., McDermott, J.M., Seewald, J.S., Ono, S., 2018. Clumped isotopologue constraints on the origin of methane at seafloor hot springs. Geochimica et Cosmochimica Acta, 223: 141-158.

Wanless, V.D. *et al*., 2015. Magmatic plumbing at Lucky Strike volcano based on olivine-hosted melt inclusion compositions. Geochemistry Geophysics Geosystems, 16(1): 126-147.

1686 Welhan, J.A., Craig, H., 1983. Methane, Hydrogen and Helium in Hydrothermal Fluids at 21°N on the East Pacific Rise. In: Rona, P., Boström, K., Laubier, L., Smith, K., Jr.
1688 (Eds.), Hydrothermal Processes at Seafloor Spreading Centers. NATO Conference Series. Springer US, pp. 391-409.
1690 Windman, T., Zolotova, N., Schwandner, F., Shock, E.L., 2007. Formate as an energy source for microbial metabolism in chemosynthetic zones of hydrothermal ecosystems.
1692 Astrobiology, 7(6): 873-90.
Yamanaka, T., Sakata, S., 2004. Abundance and distribution of fatty acids in hydrothermal
1694 vent sediments of the western Pacific Ocean. Organic Geochemistry, 35(5): 573-582.
Zeng, Y.S., Liu, J.Q., 2000. Short-chain carboxylates in fluid inclusions in minerals. Applied
1696 Geochemistry, 15(1): 13-25.
Zhao, M., Canales, J.P., Sohn, R.A., 2012. Three-dimensional seismic structure of a Mid-
1698 Atlantic Ridge segment characterized by active detachment faulting (Trans-Atlantic Geotraverse, 25°55′N-26°20′N). Geochemistry, Geophysics, Geosystems, 13(11).
1700

1702

**Table 1**

| | ***n-alkanes*** | ***BTEX & PAHs*** | ***n-fatty acids*** |
|---|---|---|---|
| ***oven*** | | | |
| *initial T (°C)* | 40 | 40 | 40 |
| *initial t (min)* | 1 | 1 | 1 |
| *ramp* | 40 to 320 °C at 12°C/min | 40 to 320 °C at 12°C/min | 40 to 320 °C at 20°C/min |
| *final T (°C)* | 320 | 320 | 320 |
| *final t (min)* | 2 | 2 | 2 |
| ***injector*** | | | |
| *T (°C)* | 250 | 250 | 325 |

**TABLE 2**

| *Field* | | ***IAPSO*** | ***TAG*** | ***TAG*** | ***Snake Pit*** | ***Menez Gwenn*** | ***Lucky Strike*** |
|---|---|---|---|---|---|---|---|
| Depth | | - | 3600 | 3600 | 3500 | 800 | 1700 |
| T max[1] | *°C* | - | 362 | 362 | 357 | 300 | 322 |
| pH min[1] | | - | 2.83 | 2.83 | 3.33 | 4.35 | 3.74 |
| NaCl* | *(wt%)* | 3.19 | 3.80 | 3.77 | 3.35 | 2.16 | 2.43 |
| Mg | *mM* | 53.2 | 0.0 | 2.9 | 0.0 | 0.0 | 0.0 |
| Cl | *mM* | 546 | 650 | 645 | 574 | 370 | 415 |
| Si | *mM* | 29.9 | 19.6 | 18.5 | 17.0 | n.m. | n.m. |
| Na | *mM* | 468 | 561 | 558 | 520 | 296 | 329 |
| SO4 | *mM* | 28.2 | 0 | 0 | 0 | 1.2 | 0.2 |
| Fe | *µM* | 0 | 6400 | 5892 | 3285 | 25 | 429 |
| Mn | *µM* | 0 | 650 | 598 | 465 | 99 | 236 |
| Cu | *µM* | 0.0 | 52.4 | 45.3 | 18.9 | 2.0 | 13.6 |
| Zn | *µM* | 1.8 | 30.4 | 27.7 | 63.4 | 15.1 | 22.9 |
| B | *µM* | 407 | 334 | 338 | 533 | 445 | 429 |
| Ba | *µM* | 0.7 | 10.5 | 10.0 | 7.4 | 10.3 | 43.7 |
| Br | *µM* | 839 | n.m. | n.m. | n.m. | 616.3 | 702.4 |
| Ca | *mM* | 11.1 | 30.3 | 28.2 | 11.3 | 30.8 | 36.8 |
| Cr | *µM* | 7.0 | n.l. | n.l. | n.l. | n.l. | n.l. |
| K | *mM* | 10.2 | 18.1 | 11.7 | 26.4 | 21.7 | 20.1 |
| Li | *µM* | 28 | 522 | 483 | 1185 | 321 | 376 |
| Rb | *µM* | 1.5 | 9.8 | 9.1 | 11.3 | 28.4 | 26.7 |
| Sr | *µM* | 96.3 | 99.9 | 97.7 | 52.1 | 104.8 | 86.5 |
| Na/K | | 45.88 | 31.00 | 47.59 | 19.73 | 13.60 | 16.39 |
| Si/Cl | | 0.055 | 0.030 | 0.029 | 0.030 | - | - |
| $SO_4$/Cl | | 0 | 0 | 0 | 0 | 0.003 | 0.001 |
| Na/Cl | | 8.6E-01 | 8.6E-01 | 8.6E-01 | 9.1E-01 | 8.0E-01 | 7.9E-01 |
| K/Cl | | 1.9E-02 | 2.8E-02 | 1.8E-02 | 4.6E-02 | 5.9E-02 | 4.8E-02 |
| Ca/Cl | | 2.0E-02 | 4.7E-02 | 4.4E-02 | 2.0E-02 | 8.3E-02 | 8.9E-02 |
| Br/Cl | *x10*$^{3}$ | - | - | - | - | 1.667 | 1.692 |

| | | | | | | | |
|---|---|---|---|---|---|---|---|
| Li/Cl | *x10*$^{3}$ | 5.2E-02 | 8.0E-01 | 7.5E-01 | 2.1E+00 | 8.7E-01 | 9.1E-01 |
| B/Cl | *x10*$^{3}$ | 7.5E-01 | 5.1E-01 | 5.2E-01 | 9.3E-01 | 1.2E+00 | 1.0E+00 |
| Ba/Cl | *x10*$^{3}$ | 1.3E-03 | 1.6E-02 | 1.6E-02 | 1.3E-02 | 2.8E-02 | 1.1E-01 |
| Rb/Cl | *x10*$^{3}$ | 2.7E-03 | 1.5E-02 | 1.4E-02 | 2.0E-02 | 7.7E-02 | 6.4E-02 |
| Sr/Cl | *x10*$^{3}$ | 1.8E-01 | 1.5E-01 | 1.5E-01 | 9.1E-02 | 2.8E-01 | 2.1E-01 |
| Fe/Cl | *x10*$^{3}$ | 0.00 | 9.85 | 9.14 | 5.72 | 6.9E-02 | 1.03 |
| Mn/Cl | *x10*$^{3}$ | 0.00 | 1.00 | 0.93 | 8.1E-01 | 2.7E-01 | 5.7E-01 |
| Cu/Cl | *x10*$^{3}$ | 2.1E-05 | 8.1E-02 | 7.0E-02 | 3.3E-02 | 5.4E-03 | 3.3E-02 |
| Zn/Cl | *x10*$^{3}$ | 3.3E-03 | 4.7E-02 | 4.3E-02 | 1.1E-01 | 4.1E-02 | 5.5E-02 |

[1]mesured

| *Vent field* | | | | | | | *Lucky Strike* | | | | | | |
|---|---|---|---|---|---|---|---|---|---|---|---|---|---|
| *Coordinates* | | | | | | | *37°17'N* | | | | | | |
| Depth | *m* | | | | | | 1700 | | | | | | |
| *Vent* | | | | *Tour Eiffel* | | | | | | *Montségur (US4)* | | | *TE+US4* |
| **Year** | | **1993** | **1994** | **1996** | **1997** | **2005** | **1993** | **1994** | **1996** | **1997** | **2008** | **2013** |
| T (max) | *°C* | 325 | 324 | 323 | - | 303 | 297 | 310 | 318 | - | 299 | 322 |
| pH (min) | | 4.07 | 3.7 | 4.32 | 3.4 | 3.8 | 4.06 | 3.7 | 3.88 | 3.8 | - | 3.74 |
| NaCl | *wt %* | 2.56 | 2.44 | 2.58 | 2.50 | 2.44 | 2.57 | 2.53 | 2.58 | 2.52 | 2.42 | 2.43 |
| Mg | *mM* | 0 | 0 | 0 | 0 | 0 | 0 | 0 | 0 | 0 | 0 | 0 |
| Cl | *mM* | 438 | 417 | 441 | 427 | 418 | 440 | 433 | 441 | 431 | 414 | 415 |
| Si | *mM* | 15.7 | 13.3 | 15.4 | 15.2 | | 16 | 16.1 | 15.2 | 15.7 | 14.7 | - |
| Na | *mM* | 386 | 347 | 346 | 348 | 326 | 385 | 357 | 339 | 349 | 332 | 329 |
| $SO_4$ | *mM* | 1.16 | - | 0.862 | - | - | 1.53 | - | 0.459 | - | - | 0.2 |
| Fe | *µM* | 623 | 624 | 595 | - | - | 252 | 282 | 467 | - | 321 | 429 |
| Mn | *µM* | 267 | 289 | 257 | - | - | 261 | 303 | 256 | - | 223 | 236 |
| Cu | *µM* | - | 26 | - | - | - | - | 7.6 | - | - | - | 13.6 |
| Zn | *µM* | - | 16.5 | - | - | - | - | 30 | - | - | - | 22.9 |
| B | *µM* | - | - | - | - | - | - | - | - | - | 430 | 429 |
| Ba | *µM* | - | 42.4 | - | - | - | - | 47.3 | - | - | 40 | 43.7 |
| Br | *µM* | - | 735 | - | 682 | - | - | 781 | - | 692 | 661 | 702 |
| Ca | *mM* | 29.8 | 32.3 | 33 | 33.8 | 35.2 | 30 | 33.2 | 33.4 | 33.9 | 33 | 36.8 |
| Cs | *nM* | - | 167 | - | - | - | - | - | - | - | - | - |
| K | *mM* | 20.7 | 21.6 | 22.2 | 23.6 | 17.9 | 20.6 | 21.9 | 22.7 | 22.7 | 20.1 | 20.1 |
| Li | *µM* | 303 | 286 | 358 | 306 | 257 | 292 | 287 | 339 | 297 | 288 | 376 |
| Rb | *µM* | - | 22.7 | - | 33.1 | - | - | 22.7 | - | 33.5 | 33 | 26.7 |
| Sr | *µM* | 77.3 | 76 | 74.9 | - | - | 77.1 | 77 | 72.1 | - | 78 | 86.5 |
| *Reference* | | *i* | *j* | *i* | *k* | *l* | *i* | *j* | *i* | *k* | *m* | *This work** |

Diking

Diking

| *Site* | | *Lucky Strike* | *Lucky Strike* | *Lucky Strike* | *Lucky Strike* | *Lucky Strike* | *Menez Gwen* | *Menez Gwen* | *Menez Gwen* | *Rainbow* | *Rainbow* | *Rainbow* | *Rainbow* | *Rainbow* |
|---|---|---|---|---|---|---|---|---|---|---|---|---|---|---|
| *Year* | | *1993* | *1994* | *1996* | *1997* | *2008* | *1994* | *1997* | *2001* | *1997* | *2001* | *2005* | *2008* | *2008* |
| Ref | | g | h | g | i | j | h | i | k | i | k | e | l, * | m |
| Cruise | | RV AtlantisII #A129-06 | DIVA1 | LUSTRE'96 | FLORES | KNOX18RR | DIVA1 | FLORES | IRIS | FLORES | IRIS | EXOMAR | MoMAR08 | KNOX18RR |
| **$H_2S$** | *mM* | 1.39-3.29 | 2.00-3.00 | 1.78-4.64 | 1.19-3.28 | 2.9-4 | 1.6 | 1.37 | 1.7 | 1.2 | 1.3 | 1.5 | | 2.9 |
| **$N_2$** | *mM* | n.m. | 0.5-1.84 | n.m. | 0.95-5.86 | - | 1.01 | 1.76 | 1.90 | nl | n.m. | n.m. | 2.3 | n.m. |
| **$^3He$** | *mM* | n.m. | 1.27E-9 to 9.94E-9 | n.m. | n.m. | - | n.m. | n.m. | n.m. | n.m. | n.m. | n.m. | n.m. | n.m. |
| **R/Ra** | | n.m. | 8.0-8.2 | n.m. | n.m. | - | n.m. | n.m. | n.m. | n.m. | n.m. | n.m. | n.m. | n.m. |
| **$H_2$** | *mM* | n.m. | 0.003-0.727 | n.m. | n.d. | 0.028-0.071 | 0.038 | n.d. | n.m. | 11.1 | 15.1 | 9.6 | 6.5 | 15.2 |
| **log $f H_2$** | | n.m. | (-0.22)-2.17 | n.m. | - | 0.75-1.16 | -1.42 | - | - | 1.05 | 1.18 | 0.98 | 0.81 | 1.18 |
| **$CH_4$** | *mM* | n.m. | 0.3-0.85 | n.m. | 0.531-0.915 | 0.75-1.06 | 1.7 | 2.20 | 1.57 | 1.76 | 2.26 | 1.31 | 1.00 | n.m. |
| **$CO_2$** | *mM* | n.m. | 19.6-39.9 | n.m. | 16.2-37.4 | 35-133 | 21.7 | 20.4 | 29.3 | 14.7 | 17.1 | 13.9 | 5.5 | 30 |
| **$C_2H_6$** | *µM* | n.m. | 53-179 | n.m. | n.d. | - | n.m. | n.d. | n.m. | n.m. | n.m. | 0.77 | 0.47 | n.m. |
| **$C_2H_4$** | *µM* | n.m. | 15-41 | n.m. | n.d. | - | n.m. | n.d. | n.m. | n.m. | n.m. | n.m. | n.m. | n.m. |
| **$C_3H_8$** | *µM* | n.m. | 7-155 | n.m. | n.d. | - | n.m. | n.d. | n.m. | n.m. | n.m. | 0.04 | 0.05 | n.m. |
| **$C_3H_6$** | *µM* | n.m. | 19 | n.m. | n.d. | - | n.m. | n.d. | n.m. | n.m. | n.m. | n.m. | n.m. | n.m. |
| **n-$C_4H_{10}$** | *µM* | n.m. | n.m. | n.m. | n.m. | - | n.m. | n.m. | n.m. | n.m. | n.m. | n.m. | n.m. | n.m. |
| **n-$C_5H_{12}$** | *µM* | n.m. | n.m. | n.m. | n.m. | - | n.m. | n.m. | n.m. | n.m. | n.m. | n.m. | n.m. | n.m. |
| **$\delta D$ ($H_2$)** | *‰* | n.m. | n.m. | n.m. | n.m. | - | n.m. | n.m. | n.m. | n.m. | n.m. | -379 | -337 | n.m. |
| **$\delta D$ ($CH_4$)** | *‰* | n.m. | n.m. | n.m. | n.m. | - | n.m. | n.m. | n.m. | n.m. | n.m. | -107 | -102 | n.m. |
| **$\delta^{13}C$ ($CO_2$)** | *‰* | n.m. | -7.2 to -10.6 | n.m. | n.m. | -3.9 to -5.6 | n.m. | n.m. | n.m. | n.m. | n.m. | -2.5 | -1.4 | n.m. |
| **$\delta^{13}C$ ($CH_4$)** | *‰* | n.m. | -12.7 to -13.7 | n.m. | n.m. | -12.5 to -14.7 | n.m. | n.m. | n.m. | n.m. | n.m. | -17.8 | -16.7 | n.m. |
| **$\delta^{13}C$ ($C_2H_6$)** | *‰* | n.m. | n.m. | n.m. | n.m. | - | n.m. | n.m. | n.m. | n.m. | n.m. | -13.4 | n.m. | n.m. |
| **$\delta^{13}C$ ($C_3H_8$)** | *‰* | n.m. | n.m. | n.m. | n.m. | - | n.m. | n.m. | n.m. | n.m. | n.m. | -13 | n.m. | n.m. |
| **$\delta^{13}C$ ($C_4H_{10}$)** | *‰* | n.m. | n.m. | n.m. | n.m. | - | n.m. | n.m. | n.m. | n.m. | n.m. | n.m. | n.m. | n.m. |

g LUSTRE'96 cruise (1996), published results in Von Damm et al., 1998.
h DIVA 1 cruise (1994), published results in Charlou et al., 1996, 2000 and Jean-Baptiste et al., 1998.
i FLORES cruise (1995), mostly unpublished results (Charlou pers. Com.). Preliminary results in Fouquet et al., 1998.
j KNOX18RR cruise (2008), published results in Pester et al., 2012.
k IRIS cruise (2001), results presented at AGU fall meeting 2001 (Charlou et al., 2001)
l MoMAR08 cruise, Charlou et al., unpublished results
m KNOX18RR cruise (2008), published results in Seyfried et al., 2011.
* these results are most likely underestimated as measurements were performed back on land.
nl non-linear results so taht the end-member could not be calculated

| | Rt | *Units* | BB-MQ | **BB-PL3-Ti4** | **BB-PL4-Ti4** | **BB-PL7-Ti4** | BB-PL3-TiG2 | BB-PL4-TiG2 | BB-PL10-TiG2 | BB-PL7-TiG2 | BB-PL8-TiG2 |
|---|---|---|---|---|---|---|---|---|---|---|---|
| | | | MQ water | **REF-MG** | **REF-LS** | **REF-Rbw** | White Flammes | Monségur | Tour Eiffel | IRIS 3 | USB -TAC |
| | min | | Control | **Menez Gwenn** | **Lucky Strike** | **Rainbow** | Menez Gwenn | Lucky Strike | Lucky Strike | Rainbow | Rainbow |
| pH | | | N.A. | **8.07** | **8.11** | **8.34** | 4.35 | 4.27 | 4.12 | 3.34 | 3.23 |
| Mg | | *mM* | N.A. | **N.A.** | **N.A.** | **N.A.** | N.A. | N.A. | N.A. | N.A. | N.A. |
| TOC | | *ppm* | N.A. | **N.A.** | **N.A.** | **N.A.** | N.A. | N.A. | N.A. | N.A. | N.A. |
| Formate | | *ppb* | N.A. | **N.A.** | **N.A.** | **N.A.** | N.A. | N.A. | N.A. | N.A. | N.A. |
| Acetate | | *ppb* | N.A. | **N.A.** | **N.A.** | **N.A.** | N.A. | N.A. | N.A. | N.A. | N.A. |
| ***Linear Alkanes*** | | | | | | | | | | | |
| Nonane | 4.68 | *ppb* | 0.59 +/- 0.36 | **0.52 +/- 0.36** | **0.70 +/- 0.36** | **0.30 +/- 0.36** | 0.62 +/- 0.36 | 0.96 +/- 0.37 | 0.67 +/- 0.36 | 1.14 +/- 0.37 | 1.08 +/- 0.37 |
| Decane | 5.911 | *ppb* | 52.71 +/- 2.04 | **52.85 +/- 2.04** | **57.57 +/- 2.22** | **30.17 +/- 1.19** | 64.14 +/- 2.47 | 59.18 +/- 2.28 | 52.28 +/- 2.02 | 56.79 +/- 2.19 | 54.08 +/- 2.09 |
| Undecane | 7.183 | *ppb* | | | | | METHANOL CONTAMINATION | | | | |
| Dodecane | 8.394 | *ppb* | 13.29 +/- 1.65 | **7.60 +/- 1.17** | **6.74 +/- 1.11** | **4.01 +/- 0.95** | 11.08 +/- 1.45 | 9.98 +/- 1.36 | 9.78 +/- 1.34 | 8.99 +/- 1.28 | 8.80 +/- 1.27 |
| Tridecane | 9.549 | *ppb* | 0.98 +/- 0.38 | **0.77 +/- 0.38** | **0.50 +/- 0.38** | **1.18 +/- 0.39** | 0.57 +/- 0.38 | 0.84 +/- 0.38 | 1.10 +/- 0.39 | 1.34 +/- 0.39 | 1.22 +/- 0.39 |
| Tetradecane | 10.641 | *ppb* | 0.61 +/- 0.37 | **0.55 +/- 0.38** | **0.60 +/- 0.38** | **0.66 +/- 0.37** | 0.57 +/- 0.38 | 0.58 +/- 0.38 | 0.59 +/- 0.38 | 0.59 +/- 0.38 | 0.87 +/- 0.36 |
| Pentadecane | 11.675 | *ppb* | 0.41 +/- 0.23 | **0.37 +/- 0.23** | **0.44 +/- 0.22** | **0.49 +/- 0.22** | 0.37 +/- 0.23 | 0.37 +/- 0.23 | 0.40 +/- 0.23 | 0.47 +/- 0.22 | 0.86 +/- 0.21 |
| Hexadecane | 12.65 | *ppb* | 0.19 +/- 0.51 | **N.Q.** | **0.13 +/- 0.51** | **0.20 +/- 0.52** | 0.37 +/- 0.52 | 0.26 +/- 0.52 | 0.21 +/- 0.51 | 0.40 +/- 0.52 | 0.57 +/- 0.52 |
| Heptadecane | 13.576 | *ppb* | 0.57 +/- 0.23 | **0.24 +/- 0.22** | **0.22 +/- 0.23** | **0.33 +/- 0.23** | 1.10 +/- 0.23 | 0.38 +/- 0.23 | 0.57 +/- 0.23 | 0.91 +/- 0.23 | 0.79 +/- 0.23 |
| Octadecane | 14.452 | *ppb* | 0.18 +/- 0.12 | **0.09 +/- 0.12** | **0.11 +/- 0.12** | **0.13 +/- 0.12** | 0.39 +/- 0.13 | 0.27 +/- 0.13 | 0.27 +/- 0.13 | 0.28 +/- 0.13 | 0.28 +/- 0.13 |
| Nonadecane | 15.295 | *ppb* | 0.93 +/- 0.95 | **0.36 +/- 0.93** | **0.44 +/- 0.92** | **0.61 +/- 0.93** | 1.54 +/- 1.00 | 0.95 +/- 0.96 | 1.01 +/- 0.96 | 1.24 +/- 0.97 | 1.21 +/- 0.98 |
| Eicosane | 16.104 | *ppb* | 0.71 +/- 0.87 | **0.27 +/- 0.86** | **0.30 +/- 0.86** | **0.47 +/- 0.87** | 2.07 +/- 0.98 | 1.20 +/- 0.90 | 0.71 +/- 0.87 | 1.04 +/- 0.89 | 0.98 +/- 0.89 |
| ***Linear Fatty Acids*** | | | | | | | | | | | |
| Nonanoic acid | 6.914 | *ppb* | N.D. | **N.D.** | **N.D.** | **N.D.** | 3.07 +/- 1.81 | N.D. | 3.85 +/- 2.49 | 1.40 +/- 2.35 | N.D. |
| Decanoic acid | 7.542 | *ppb* | N.D. | **N.Q.** | **N.D.** | **0.48 +/- 1.16** | 0.98 +/- 1.12 | 0.70 +/- 1.14 | 1.15 +/- 1.16 | 0.47 +/- 1.15 | N.Q. |
| Undecanoic acid | 8.178 | *ppb* | N.D. | **0.12 +/- 0.18** | **N.D.** | **0.13 +/- 0.14** | 0.16 +/- 0.14 | 0.17 +/- 0.18 | N.D. | 0.26 +/- 0.13 | N.D. |
| Dodecanoic acid | 8.773 | *ppb* | N.Q. | **0.95 +/- 0.35** | **1.35 +/- 0.36** | **1.78 +/- 0.37** | 4.32 +/- 0.51 | 2.22 +/- 0.39 | 3.07 +/- 0.43 | 1.00 +/- 0.35 | 1.02 +/- 0.35 |
| Tridecanoic acid | 9.31 | *ppb* | N.D. | **0.28 +/- 0.17** | **0.29 +/- 0.17** | **0.32 +/- 0.16** | 0.63 +/- 0.14 | 0.30 +/- 0.17 | 0.37 +/- 0.16 | 0.32 +/- 0.17 | 0.31 +/- 0.16 |
| Tetradecanoic acid | 9.859 | *ppb* | N.Q. | **1.46 +/- 0.24** | **1.82 +/- 0.24** | **1.95 +/- 0.24** | 5.13 +/- 0.34 | 2.07 +/- 0.24 | 2.44 +/- 0.24 | 2.04 +/- 0.24 | 2.32 +/- 0.24 |
| Pentadecanoic acid | 10.355 | *ppb* | N.D. | **0.77 +/- 0.64** | **0.76 +/- 0.65** | **0.85 +/- 0.64** | 3.26 +/- 0.63 | 1.06 +/- 0.62 | 1.26 +/- 0.61 | 1.36 +/- 0.60 | 1.57 +/- 0.60 |
| Hexadecanoic acid | 10.902 | *ppb* | N.D. | **2.14 +/- 0.87** | **2.04 +/- 0.86** | **2.11 +/- 0.86** | 22.61 +/- 2.50 | 5.88 +/- 1.04 | 6.80 +/- 1.10 | 7.35 +/- 1.13 | 8.50 +/- 1.22 |
| Heptadecanoic acid | 11.317 | *ppb* | N.D. | **N.D.** | **0.26 +/- 0.21** | **N.D.** | 3.46 +/- 1.89 | N.D. | N.D. | 0.64 +/- 0.25 | N.D. |
| Octadecanoic acid | 11.78 | *ppb* | N.D. | **1.27 +/- 1.39** | **1.64 +/- 1.63** | **1.48 +/- 1.47** | 23.93 +/- 5.29 | 7.99 +/- 2.26 | 11.47 +/- 2.86 | 11.97 +/- 2.95 | 9.11 +/- 2.46 |
| ***BTEXs*** | | | | | | | | | | | |
| Ethyl, Benzene | 4.344 | *ppb* | 0.10 +/- 0.13 | **0.09 +/- 0.11** | **0.12 +/- 0.13** | **0.09 +/- 0.12** | 0.13 +/- 0.12 | 0.10 +/- 0.11 | 0.17 +/- 0.10 | 0.18 +/- 0.11 | 0.17 +/- 0.10 |
| p-,m-Xylene | 4.443 | *ppb* | 0.23 +/- 0.04 | **0.16 +/- 0.04** | **0.25 +/- 0.04** | **0.21 +/- 0.04** | 0.27 +/- 0.04 | 0.20 +/- 0.04 | 0.32 +/- 0.04 | 0.29 +/- 0.04 | 0.26 +/- 0.04 |
| o-Xylene | 4.708 | *ppb* | 0.24 +/- 0.04 | **0.16 +/- 0.04** | **0.27 +/- 0.05** | **0.22 +/- 0.04** | 0.33 +/- 0.05 | 0.21 +/- 0.04 | 0.38 +/- 0.05 | 0.33 +/- 0.05 | 0.27 +/- 0.05 |
| Styrene | 4.831 | *ppb* | N.D. | **N.D.** | **N.D.** | **N.D.** | N.D. | N.D. | N.D. | N.D. | N.D. |
| isopropyl, Benzene | 5.006 | *ppb* | 0.08 +/- 0.04 | **0.08 +/- 0.04** | **0.08 +/- 0.04** | **0.09 +/- 0.04** | 0.07 +/- 0.04 | 0.07 +/- 0.04 | 0.09 +/- 0.04 | 0.08 +/- 0.04 | 0.08 +/- 0.04 |
| n-Propyl, Benzene | 5.468 | *ppb* | 0.04 +/- 0.03 | **0.04 +/- 0.03** | **0.04 +/- 0.03** | **0.04 +/- 0.03** | 0.05 +/- 0.03 | 0.04 +/- 0.03 | 0.05 +/- 0.03 | 0.05 +/- 0.03 | 0.04 +/- 0.03 |
| 1,2,4-triMethyl-Benzene | 5.572 | *ppb* | 0.12 +/- 0.03 | **0.10 +/- 0.03** | **0.11 +/- 0.03** | **0.11 +/- 0.03** | 0.13 +/- 0.03 | 0.11 +/- 0.03 | 0.15 +/- 0.03 | 0.15 +/- 0.03 | 0.14 +/- 0.03 |
| 1,3,5-triMethyl-Benzene | 5.95 | *ppb* | 0.05 +/- 0.05 | **0.04 +/- 0.04** | **0.08 +/- 0.05** | **0.07 +/- 0.05** | 0.06 +/- 0.05 | 0.08 +/- 0.05 | 0.12 +/- 0.05 | 0.14 +/- 0.05 | 0.12 +/- 0.05 |
| sec-Butyl-Benzene | 6.106 | *ppb* | 0.04 +/- 0.04 | **N.D.** | **N.D.** | **N.D.** | N.D. | N.D. | N.D. | N.D. | N.D. |
| 2,isopropyl, Toluene | 6.305 | *ppb* | 0.04 +/- 0.02 | **0.03 +/- 0.02** | **0.03 +/- 0.02** | **0.04 +/- 0.02** | 0.03 +/- 0.02 | 0.04 +/- 0.02 | 0.05 +/- 0.02 | 0.04 +/- 0.02 | 0.04 +/- 0.02 |
| n-Butyl, Benzene | 6.66 | *ppb* | 0.07 +/- 0.02 | **0.10 +/- 0.02** | **0.05 +/- 0.02** | **0.07 +/- 0.02** | 0.07 +/- 0.02 | 0.08 +/- 0.02 | 0.07 +/- 0.02 | 0.07 +/- 0.02 | 0.11 +/- 0.02 |
| ***PAHs*** | | | | | | | | | | | |
| Naphthalene | 8.351 | *ppb* | N.Q. | **N.Q.** | **N.Q.** | **N.Q.** | 0.56 +/- 0.10 | 0.37 +/- 0.08 | 0.39 +/- 0.08 | 0.25 +/- 0.07 | 0.23 +/- 0.07 |
| Acenaphtene | 11.796 | *ppb* | N.D. | **N.Q.** | **N.Q.** | **N.Q.** | 0.01 +/- 0.02 | N.Q. | 0.01 +/- 0.02 | 0.01 +/- 0.02 | 0.01 +/- 0.02 |
| Fluorene | 12.778 | *ppb* | N.D. | **N.D.** | **N.D.** | **N.D.** | 0.06 +/- 0.02 | 0.01 +/- 0.02 | N.Q. | 0.04 +/- 0.02 | 0.04 +/- 0.02 |
| Phenanthrene | 14.582 | *ppb* | 0.02 +/- 0.03 | **0.01 +/- 0.03** | **N.Q.** | **N.Q.** | 0.25 +/- 0.04 | 0.17 +/- 0.03 | 0.16 +/- 0.03 | 0.12 +/- 0.03 | 0.11 +/- 0.03 |
| Anthracene | 14.788 | *ppb* | N.D. | **N.D.** | **N.D.** | **N.D.** | 0.14 +/- 0.08 | N.D. | N.D. | N.D. | N.D. |
| Fluoranthene | 17.117 | *ppb* | N.Q. | **N.Q.** | **N.Q.** | **N.Q.** | 0.06 +/- 0.10 | 0.04 +/- 0.10 | N.Q. | N.Q. | N.Q. |

| | | | | | | | | | | | |
|---|---|---|---|---|---|---|---|---|---|---|---|
| Pyrene | 17.52 | *ppb* | 0.05 +/- 0.07 | **N.Q.** | **N.Q.** | **N.Q.** | 0.11 +/- 0.08 | 0.09 +/- 0.07 | 0.09 +/- 0.08 | 0.05 +/- 0.07 | 0.06 +/- 0.07 |
| Total eq. C (nM) | | | 5.1 | **5.0** | **5.3** | **3.3** | 10.2 | 6.7 | 6.8 | 6.9 | 6.5 |
| Total eq. C (ppb) | | | 61 | **60** | **64** | **40** | 122 | 80 | 81 | 83 | 78 |

| | Rt | Units | BIC-MQ | BIC-PL05-TiG2 | BIC-PL08-TiG2 | BIC-PL04-TiD1 | BIC-PL01-TiD1 | BIC-PL05-TiD1 | BIC-PL01-TiD3 | BIC-PL10-Ti1 | BIC-PL12-TiG3 | BIC-PL07-TiD3 | BIC-PL10-TiG3 | BIC-PL12-TiG1 |
|---|---|---|---|---|---|---|---|---|---|---|---|---|---|---|
| | | | MQ water | REF-SP | REF-TAG | Behive (a) | Behive (b) | Moose (a) | Moose (b) | Marge (a) | Marge (b) | Marge (c) | Active Mound | New BS |
| | min | | Control | Snake Pit | TAG | Snake Pit | Snake Pit | Snake Pit | Snake Pit | TAG | TAG | TAG | TAG | TAG |
| pH | | | N.A. | **N.A.** | **N.A.** | 4.2 | 4.82 | 4.1 | 5.8 | 2.83 | 5.47 | 5.88 | 3.85 | 5.37 |
| Mg | | *mM* | N.A. | **53.52** | **55.24** | 5.89 | 30.11 | 2.72 | 44.42 | 11.47 | 40.25 | 44.23 | 13.66 | 41.07 |
| | | | | | | | | | | | | | | |
| TOC | | *ppm* | N.D. | **0.19 +/- 0.03** | **5.74 +/- 0.05** | N.A. | 1.48 +/- 0.05 | 4.57 +/- 0.10 | 15.44 +/- 0.14 | 1.77 +/- 0.10 | 17.25 +/- 0.19 | 7.12 +/- 0.05 | 4.29 +/- 0.02 | 6.40 +/- 0.15 |
| Formate | | *ppb* | N.Q. | **N.Q.** | **N.Q.** | N.A. | 46 +/- 133 | 107 +/- 169 | N.Q. | 64 +/- 95 | N.Q. | N.Q. | N.Q. | 84 +/- 247 |
| Acetate | | *ppb* | N.Q. | **N.Q.** | **N.Q.** | N.A. | 410 +/- 267 | 476 +/- 420 | 265 +/- 52 | 374 +/- 109 | 322 +/- 57 | 134 +/- 18 | 192 +/- 68 | 292 +/- 48 |
| ***Linear Alkanes*** | | | | | | | | | | | | | | |
| Nonane | 4.68 | *ppb* | 0.44 +/- 0.36 | **0.40 +/- 0.36** | **0.49 +/- 0.36** | 2.17 +/- 0.41 | 0.74 +/- 0.36 | 0.78 +/- 0.36 | 0.89 +/- 0.51 | 1.16 +/- 0.37 | 2.01 +/- 0.40 | 0.74 +/- 0.51 | 0.46 +/- 0.36 | 1.37 +/- 0.38 |
| Decane | 5.911 | *ppb* | 7.64 +/- 0.42 | **6.98 +/- 0.41** | **8.01 +/- 0.43** | 51.50 +/- 1.99 | 6.59 +/- 0.40 | 12.04 +/- 0.55 | 6.88 +/- 0.40 | 7.94 +/- 0.43 | 111.9 +/- 4.29 | 8.69 +/- 0.55 | 9.48 +/- 0.48 | 42.20 +/- 1.64 |
| Undecane | 7.183 | *ppb* | | | | | | METHANOL CONTAMINATION | | | | | | |
| Dodecane | 8.394 | *ppb* | 2.04 +/- 0.37 | **1.74 +/- 0.36** | **1.51 +/- 0.35** | 7.88 +/- 0.77 | 1.50 +/- 0.35 | 2.56 +/- 0.39 | 2.25 +/- 0.38 | 2.26 +/- 0.38 | 2.39 +/- 0.38 | 2.42 +/- 0.50 | 2.27 +/- 0.38 | 2.29 +/- 0.38 |
| Tridecane | 9.549 | *ppb* | 0.24 +/- 0.37 | **0.31 +/- 0.37** | **0.35 +/- 0.37** | 1.54 +/- 0.40 | 0.50 +/- 0.37 | 0.86 +/- 0.38 | 0.47 +/- 0.37 | 1.10 +/- 0.39 | 0.83 +/- 0.38 | 0.64 +/- 0.53 | 0.54 +/- 0.38 | 0.56 +/- 0.38 |
| Tetradecane | 10.641 | *ppb* | 4.29 +/- 2.64 | **4.23 +/- 2.93** | **0.54 +/- 0.38** | 0.56 +/- 0.38 | 4.31 +/- 2.57 | 0.56 +/- 0.38 | 4.27 +/- 2.76 | 0.56 +/- 0.38 | 0.63 +/- 0.37 | 0.56 +/- 0.47 | 0.57 +/- 0.38 | 0.61 +/- 0.38 |
| Pentadecane | 11.675 | *ppb* | 1.11 +/- 0.51 | **1.00 +/- 0.61** | **0.35 +/- 0.23** | 0.39 +/- 0.23 | 1.18 +/- 0.47 | 0.42 +/- 0.23 | 1.07 +/- 0.54 | 0.40 +/- 0.23 | 0.61 +/- 0.22 | 0.44 +/- 0.28 | 0.41 +/- 0.23 | 0.53 +/- 0.22 |
| Hexadecane | 12.65 | *ppb* | 0.20 +/- 0.52 | **N.Q.** | **N.Q.** | 0.17 +/- 0.51 | 0.40 +/- 0.52 | 0.17 +/- 0.52 | 0.19 +/- 0.52 | 0.36 +/- 0.52 | 0.42 +/- 0.52 | 0.27 +/- 0.73 | 0.13 +/- 0.52 | 0.40 +/- 0.52 |
| Heptadecane | 13.576 | *ppb* | 0.28 +/- 0.22 | **0.13 +/- 0.22** | **0.15 +/- 0.23** | 0.55 +/- 0.23 | 0.44 +/- 0.23 | 0.57 +/- 0.23 | 0.19 +/- 0.23 | 1.78 +/- 0.25 | 0.44 +/- 0.23 | 0.46 +/- 0.32 | 0.29 +/- 0.23 | 0.48 +/- 0.23 |
| Octadecane | 14.452 | *ppb* | 0.11 +/- 0.12 | **0.06 +/- 0.12** | **0.08 +/- 0.12** | 0.19 +/- 0.12 | 0.27 +/- 0.13 | 0.16 +/- 0.12 | 0.15 +/- 0.12 | 0.96 +/- 0.18 | 0.29 +/- 0.13 | 0.19 +/- 0.17 | 0.12 +/- 0.12 | 0.23 +/- 0.13 |
| Nonadecane | 15.295 | *ppb* | 0.56 +/- 0.94 | **0.26 +/- 0.91** | **0.29 +/- 0.93** | 1.04 +/- 0.95 | 1.70 +/- 1.01 | 1.01 +/- 0.96 | 0.80 +/- 0.95 | 1.13 +/- 0.97 | 0.93 +/- 0.96 | 0.55 +/- 1.34 | 0.43 +/- 0.93 | 0.59 +/- 0.94 |
| Eicosane | 16.104 | *ppb* | 0.56 +/- 0.87 | **0.33 +/- 0.86** | **0.32 +/- 0.85** | 0.48 +/- 0.86 | 1.09 +/- 0.89 | 0.50 +/- 0.87 | 0.62 +/- 0.87 | 1.48 +/- 0.92 | 1.28 +/- 0.91 | 1.01 +/- 1.24 | 0.40 +/- 0.86 | 1.17 +/- 0.89 |
| ***Linear Fatty Acids*** | | | | | | | | | | | | | | |
| Nonanoic acid | 6.914 | *ppb* | N.D. | **N.Q.** | **1.05 +/- 1.73** | 3.07 +/- 1.86 | 5.10 +/- 2.03 | N.D. | N.D. | 4.44 +/- 1.95 | N.Q. | N.D. | 6.76 +/- 2.22 | 4.60 +/- 1.95 |
| Decanoic acid | 7.542 | *ppb* | N.D. | **N.D.** | **N.D.** | 1.01 +/- 1.15 | 1.54 +/- 1.15 | 0.86 +/- 1.13 | 0.78 +/- 1.15 | 1.40 +/- 1.15 | N.Q. | N.D. | 1.23 +/- 1.14 | 0.99 +/- 1.13 |
| Undecanoic acid | 8.178 | *ppb* | N.D. | **N.D.** | **N.D.** | 0.11 +/- 0.14 | 0.16 +/- 0.13 | 0.14 +/- 0.14 | 0.13 +/- 0.13 | 0.44 +/- 0.14 | N.D. | N.D. | 0.12 +/- 0.13 | 0.10 +/- 0.14 |
| Dodecanoic acid | 8.773 | *ppb* | N.D. | **0.73 +/- 0.22** | **0.29 +/- 0.20** | 1.90 +/- 0.32 | 1.26 +/- 0.26 | 1.44 +/- 0.28 | 0.95 +/- 0.24 | 1.96 +/- 0.33 | 0.37 +/- 0.21 | 0.20 +/- 0.21 | 1.19 +/- 0.26 | 3.38 +/- 0.45 |
| Tridecanoic acid | 9.31 | *ppb* | N.D. | **N.D.** | **0.21 +/- 0.21** | 0.31 +/- 0.16 | N.D. | 0.35 +/- 0.16 | 0.21 +/- 0.18 | 0.72 +/- 0.15 | 0.20 +/- 0.18 | 0.20 +/- 0.18 | 0.28 +/- 0.17 | 0.39 +/- 0.15 |
| Tetradecanoic acid | 9.859 | *ppb* | N.D. | **0.82 +/- 0.26** | **0.35 +/- 0.17** | 1.73 +/- 0.24 | 0.80 +/- 0.26 | 1.88 +/- 0.24 | 0.25 +/- 0.16 | 5.57 +/- 0.36 | 0.20 +/- 0.15 | 0.36 +/- 0.27 | N.Q. | 2.00 +/- 0.24 |
| Pentadecanoic acid | 10.355 | *ppb* | N.D. | **0.45 +/- 0.68** | **N.D.** | 0.83 +/- 0.64 | 0.55 +/- 0.67 | 1.23 +/- 0.61 | 0.45 +/- 0.82 | 2.63 +/- 0.60 | N.D. | N.D. | 0.61 +/- 0.67 | 0.70 +/- 0.65 |
| Hexadecanoic acid | 10.902 | *ppb* | N.D. | **0.63 +/- 0.99** | **N.D.** | 5.79 +/- 1.03 | 4.33 +/- 1.12 | 9.60 +/- 1.30 | 0.76 +/- 0.96 | 14.04 +/- 1.69 | N.D. | N.Q. | 1.79 +/- 0.90 | 3.38 +/- 0.97 |
| Heptadecanoic acid | 11.317 | *ppb* | N.D. | **N.D.** | **N.D.** | N.D. | N.D. | N.D. | N.D. | N.D. | N.D. | N.D. | N.D. | N.D. |
| Octadecanoic acid | 11.78 | *ppb* | N.D. | **N.Q.** | **N.D.** | 5.39 +/- 1.88 | 5.22 +/- 1.89 | N.D. | N.Q. | 11.40 +/- 2.84 | N.Q. | 1.12 +/- 1.57 | 1.96 +/- 1.52 | 1.66 +/- 1.50 |
| ***BTEXs*** | | | | | | | | | | | | | | |
| Ethyl, Benzene | 4.344 | *ppb* | N.A. | **N.A.** | **N.A.** | N.A. | N.A. | N.A. | N.A. | N.A. | N.A. | N.A. | N.A. | N.A. |
| p-,m-Xylene | 4.443 | *ppb* | N.A. | **N.A.** | **N.A.** | N.A. | N.A. | N.A. | N.A. | N.A. | N.A. | N.A. | N.A. | N.A. |
| o-Xylene | 4.708 | *ppb* | N.A. | **N.A.** | **N.A.** | N.A. | N.A. | N.A. | N.A. | N.A. | N.A. | N.A. | N.A. | N.A. |
| Styrene | 4.831 | *ppb* | N.A. | **N.A.** | **N.A.** | N.A. | N.A. | N.A. | N.A. | N.A. | N.A. | N.A. | N.A. | N.A. |
| isopropyl, Benzene | 5.006 | *ppb* | N.A. | **N.A.** | **N.A.** | N.A. | N.A. | N.A. | N.A. | N.A. | N.A. | N.A. | N.A. | N.A. |
| n-Propyl, Benzene | 5.468 | *ppb* | N.A. | **N.A.** | **N.A.** | N.A. | N.A. | N.A. | N.A. | N.A. | N.A. | N.A. | N.A. | N.A. |
| 1,2,4-triMethyl-Benzene | 5.572 | *ppb* | N.A. | **N.A.** | **N.A.** | N.A. | N.A. | N.A. | N.A. | N.A. | N.A. | N.A. | N.A. | N.A. |
| 1,3,5-triMethyl-Benzene | 5.95 | *ppb* | N.A. | **N.A.** | **N.A.** | N.A. | N.A. | N.A. | N.A. | N.A. | N.A. | N.A. | N.A. | N.A. |
| sec-Butyl-Benzene | 6.106 | *ppb* | N.A. | **N.A.** | **N.A.** | N.A. | N.A. | N.A. | N.A. | N.A. | N.A. | N.A. | N.A. | N.A. |
| 2,isopropyl, Toluene | 6.305 | *ppb* | N.A. | **N.A.** | **N.A.** | N.A. | N.A. | N.A. | N.A. | N.A. | N.A. | N.A. | N.A. | N.A. |
| n-Butyl, Benzene | 6.66 | *ppb* | N.A. | **N.A.** | **N.A.** | N.A. | N.A. | N.A. | N.A. | N.A. | N.A. | N.A. | N.A. | N.A. |
| ***PAHs*** | | | | | | | | | | | | | | |
| Naphthalene | 8.351 | *ppb* | N.A. | **N.A.** | **N.A.** | N.A. | N.A. | N.A. | N.A. | N.A. | N.A. | N.A. | N.A. | N.A. |
| Acenaphtene | 11.796 | *ppb* | N.A. | **N.A.** | **N.A.** | N.A. | N.A. | N.A. | N.A. | N.A. | N.A. | N.A. | N.A. | N.A. |
| Fluorene | 12.778 | *ppb* | N.A. | **N.A.** | **N.A.** | N.A. | N.A. | N.A. | N.A. | N.A. | N.A. | N.A. | N.A. | N.A. |
| Phenanthrene | 14.582 | *ppb* | N.A. | **N.A.** | **N.A.** | N.A. | N.A. | N.A. | N.A. | N.A. | N.A. | N.A. | N.A. | N.A. |
| Anthracene | 14.788 | *ppb* | N.A. | **N.A.** | **N.A.** | N.A. | N.A. | N.A. | N.A. | N.A. | N.A. | N.A. | N.A. | N.A. |
| Fluoranthene | 17.117 | *ppb* | N.A. | **N.A.** | **N.A.** | N.A. | N.A. | N.A. | N.A. | N.A. | N.A. | N.A. | N.A. | N.A. |
| Pyrene | 17.52 | *ppb* | N.A. | **N.A.** | **N.A.** | N.A. | N.A. | N.A. | N.A. | N.A. | N.A. | N.A. | N.A. | N.A. |

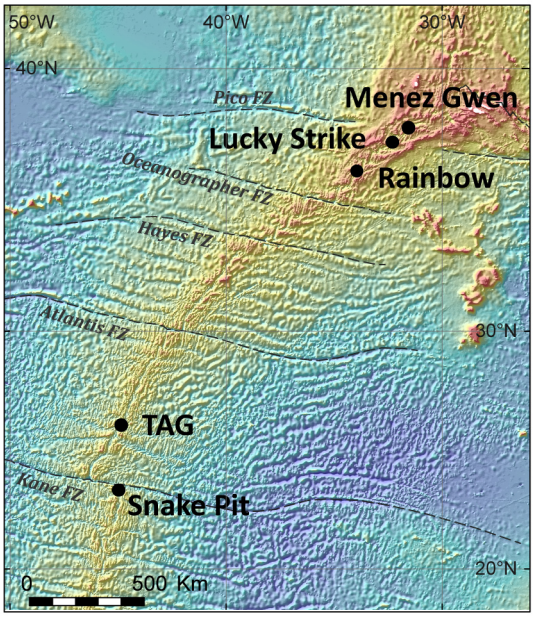

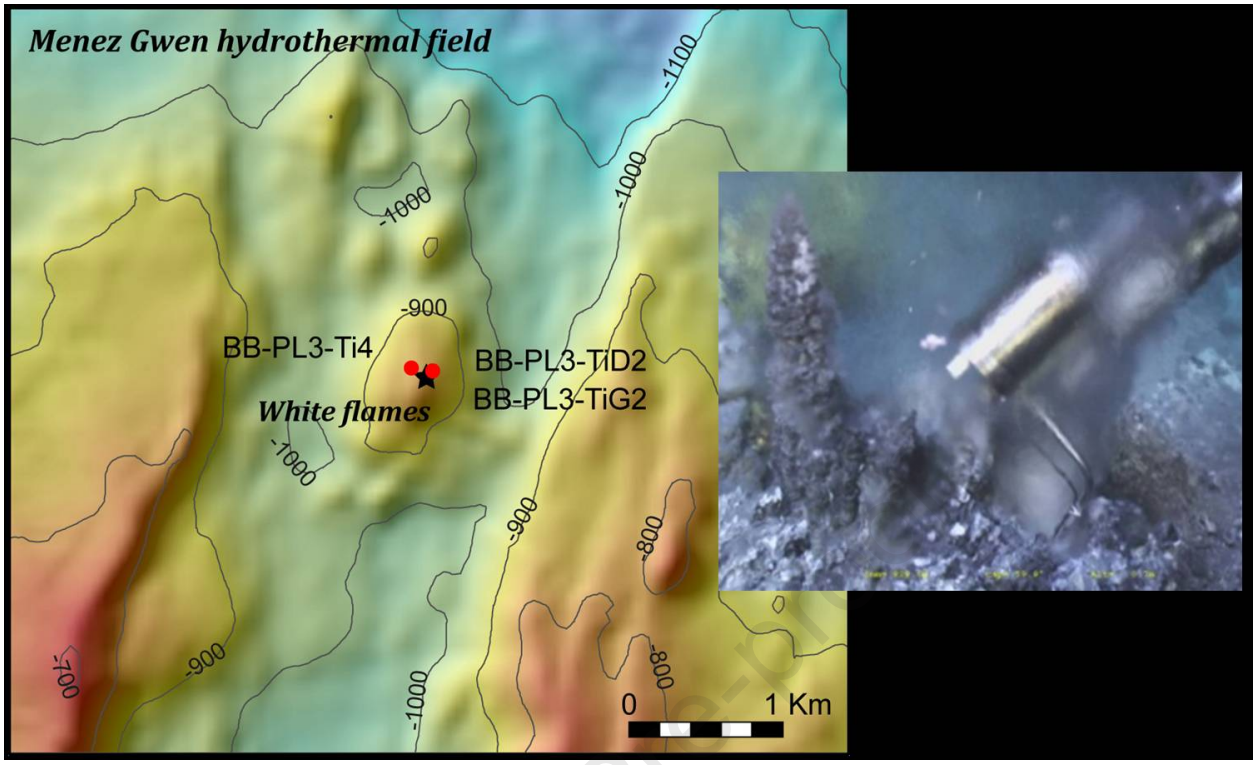

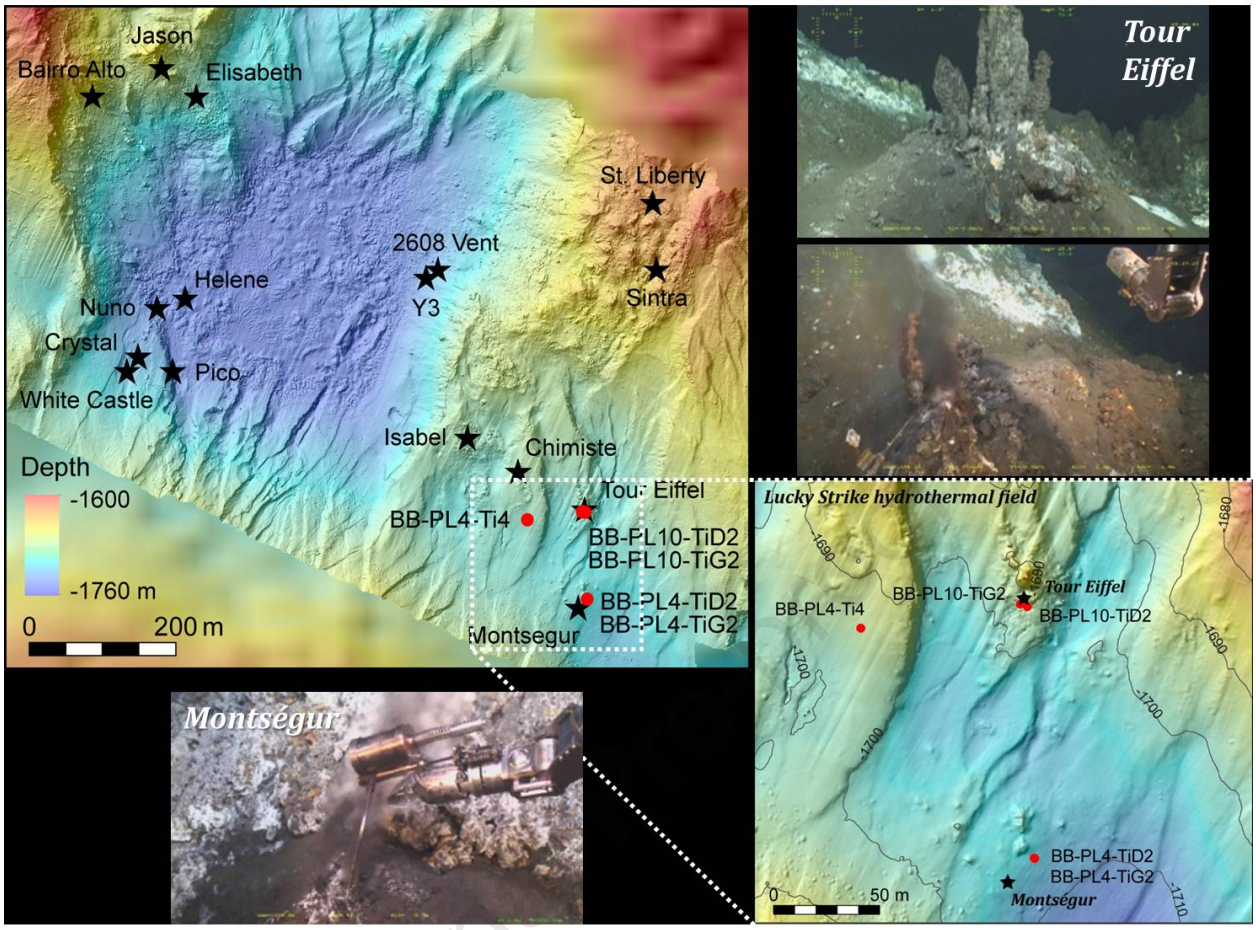
Jason
Bairro Alto
Elisabeth
St. Liberty
2608 Vent
Helene
Nuno
Y3
Sintra
Crystal
Pico
White Castle
Isabel
Chimiste
Depth
-1600
-1760 m
0
200 m
Tour Eiffel
BB-PL4-Ti4
BB-PL10-TiD2
BB-PL10-TiG2
BB-PL4-TiD2
BB-PL4-TiG2
Montsegur
Tour Eiffel
Lucky Strike hydrothermal field
BB-PL4-Ti4
BB-PL10-TiG2
Tour Eiffel
BB-PL10-TiD2
BB-PL4-TiD2
BB-PL4-TiG2
Montségur
0
50 m
Montségur

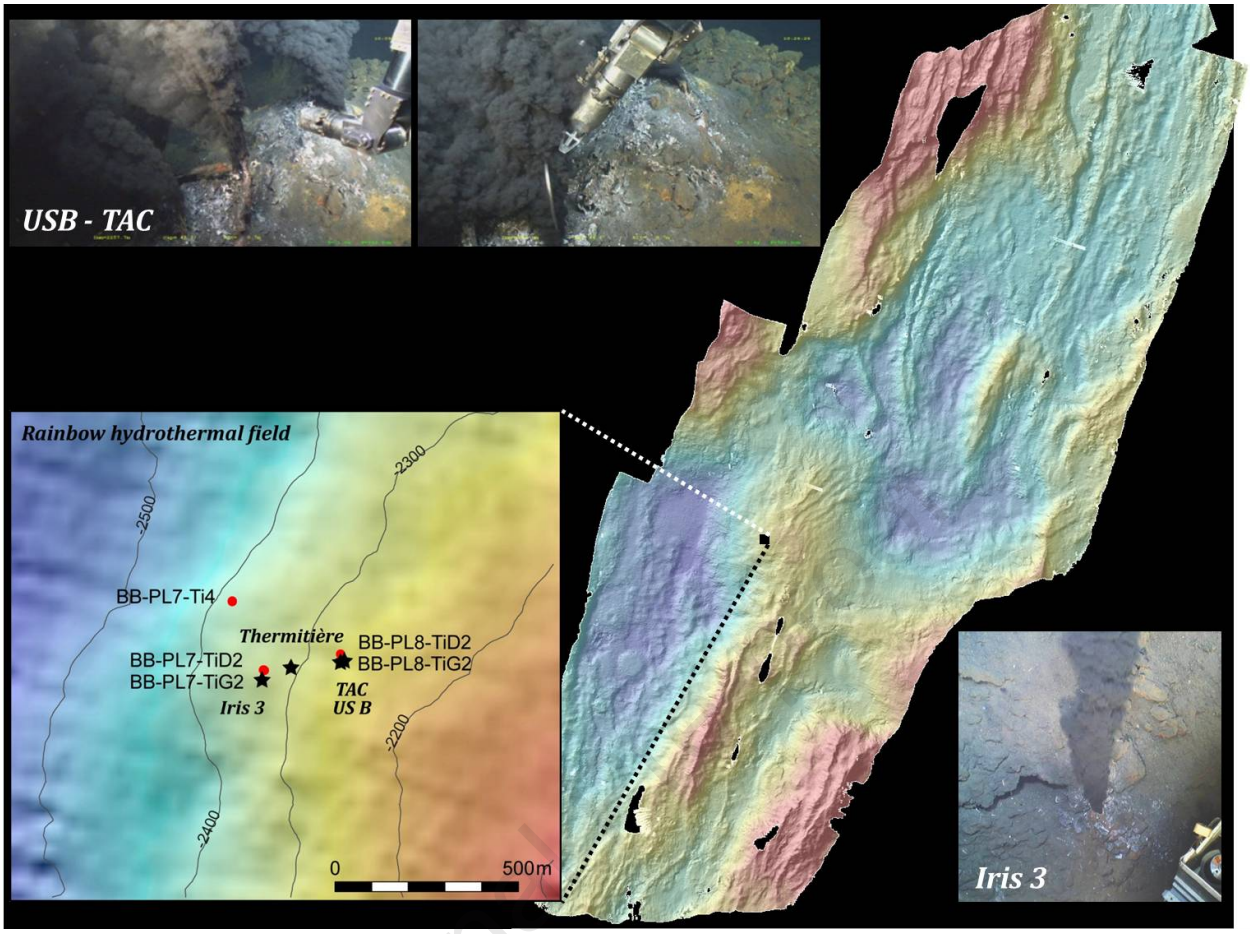
USB - TAC
Rainbow hydrothermal field
2300
2500
2400
2200
BB-PL7-Ti4
Thermitière
BB-PL8-TiD2
BB-PL8-TiG2
BB-PL7-TiD2
BB-PL7-TiG2
Iris 3
TAC
US B
0
500 m
Iris 3

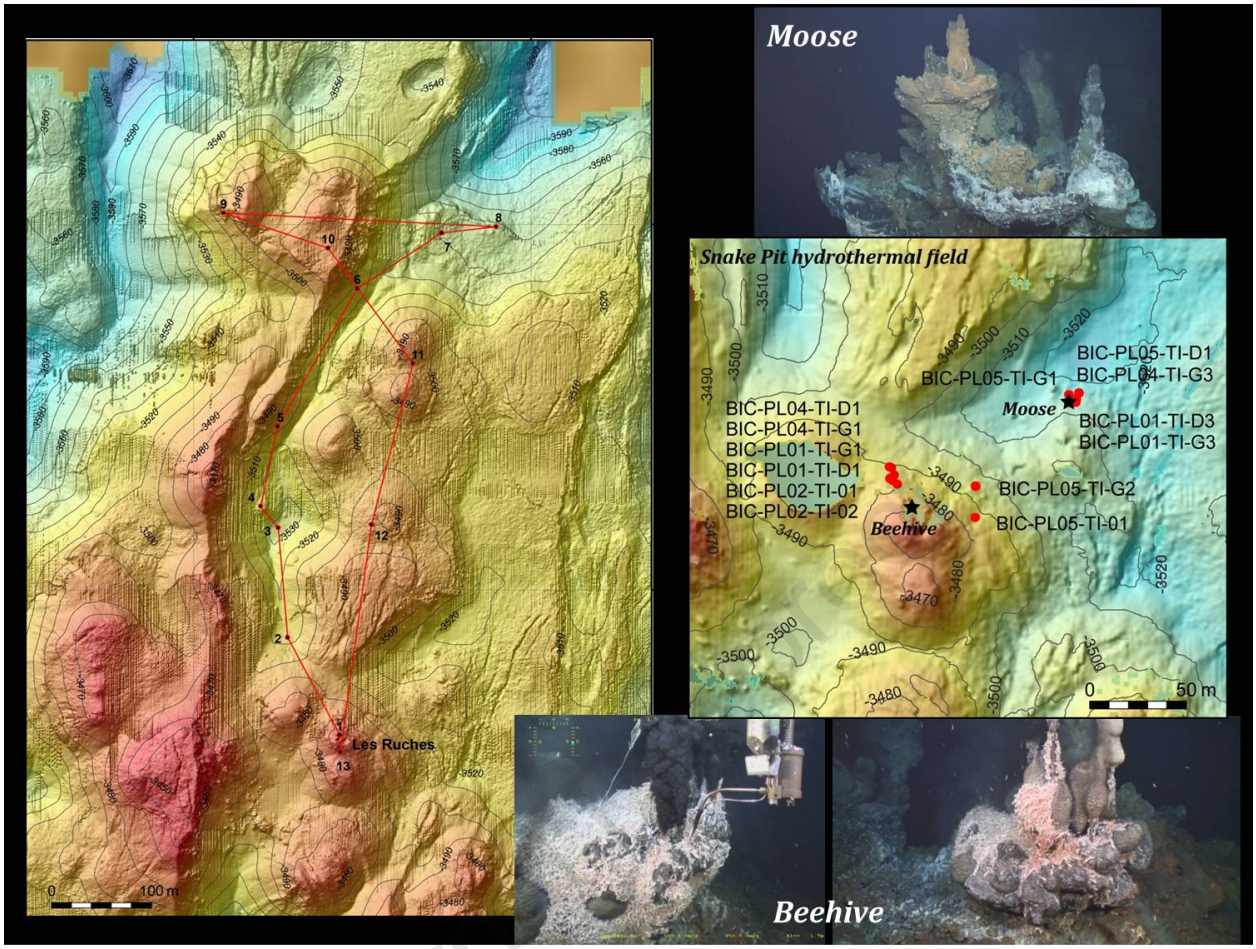

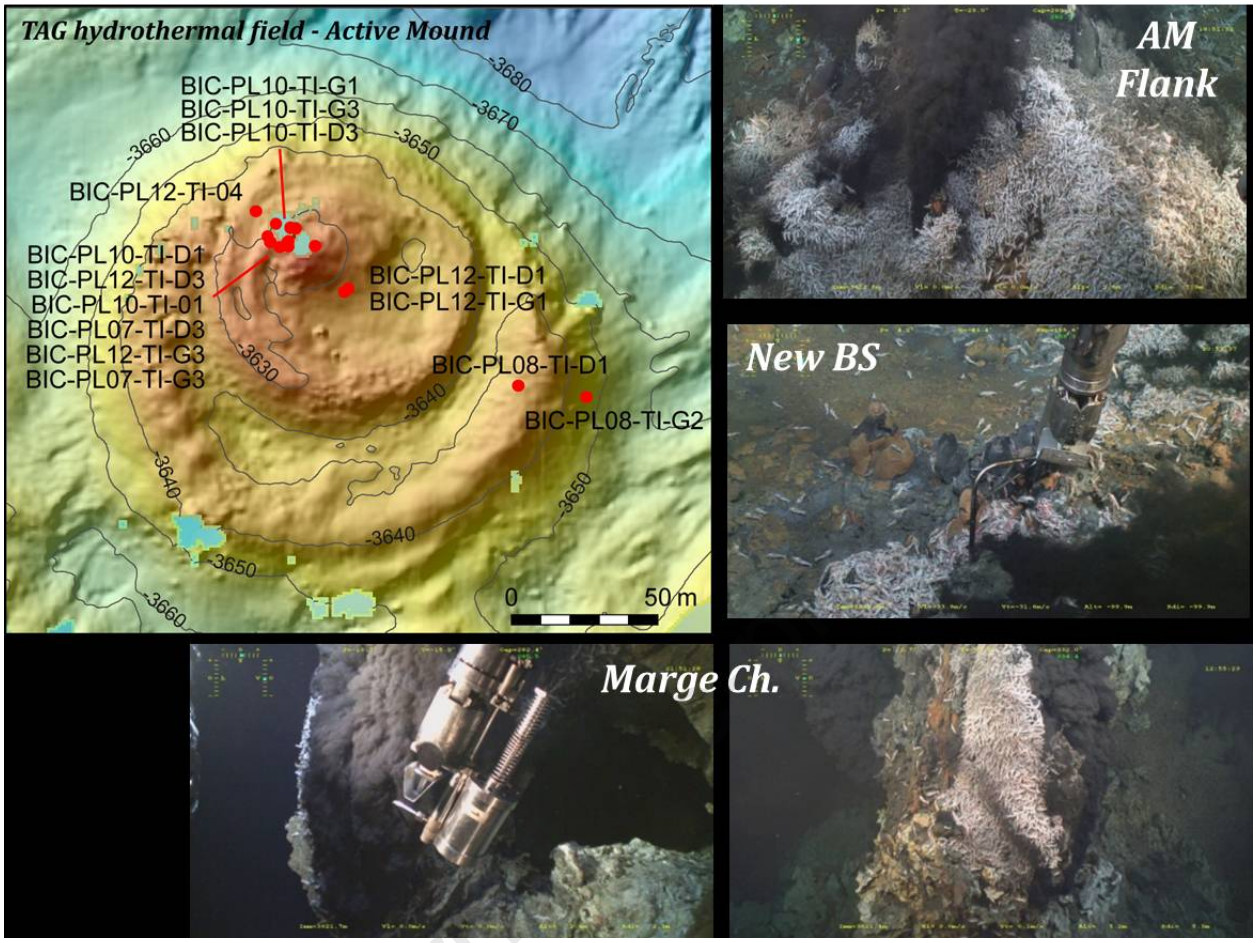
TAG hydrothermal field - Active Mound
BIC-PL10-TI-G1
BIC-PL10-TI-G3
BIC-PL10-TI-D3
BIC-PL12-TI-04
BIC-PL10-TI-D1
BIC-PL12-TI-D3
BIC-PL10-TI-01
BIC-PL07-TI-D3
BIC-PL12-TI-G3
BIC-PL07-TI-G3
BIC-PL12-TI-D1
BIC-PL12-TI-G1
BIC-PL08-TI-D1
BIC-PL08-TI-G2
-3680
-3670
-3660
-3650
-3630
-3640
-3650
-3640
-3650
-3660
0
50 m
AM
Flank
New BS
Marge Ch.

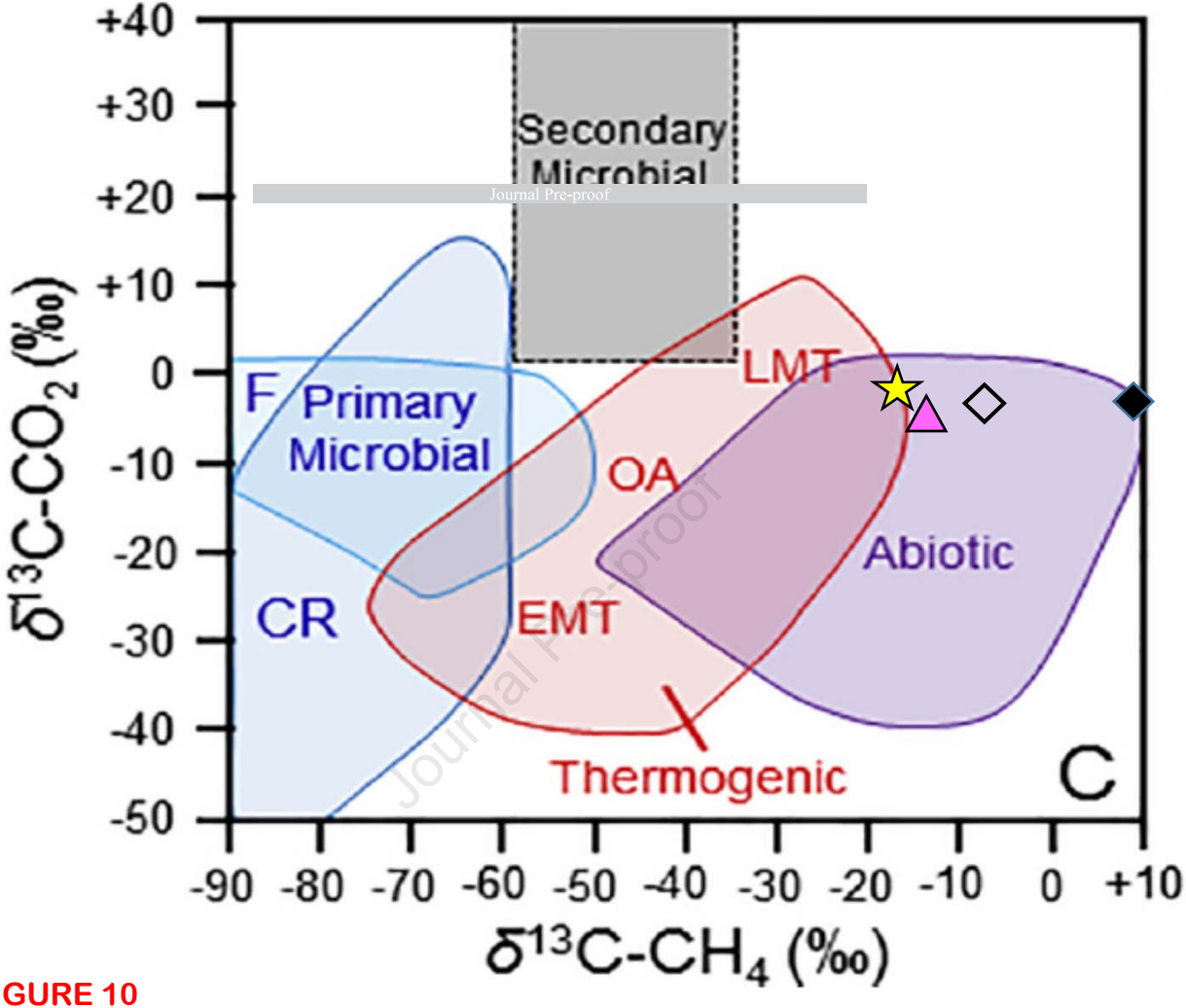
+40
+30
+20
+10
0
-10
-20
-30
-40
-50
Secondary Microbial
Journal Pre-proof
LMT
F
Primary Microbial
OA
Abiotic
CR
EMT
Thermogenic
C
-90 -80 -70 -60 -50 -40 -30 -20 -10 0 +10
δ13C-CO2 (‰)
δ13C-CH4 (‰)

FIGURE 10

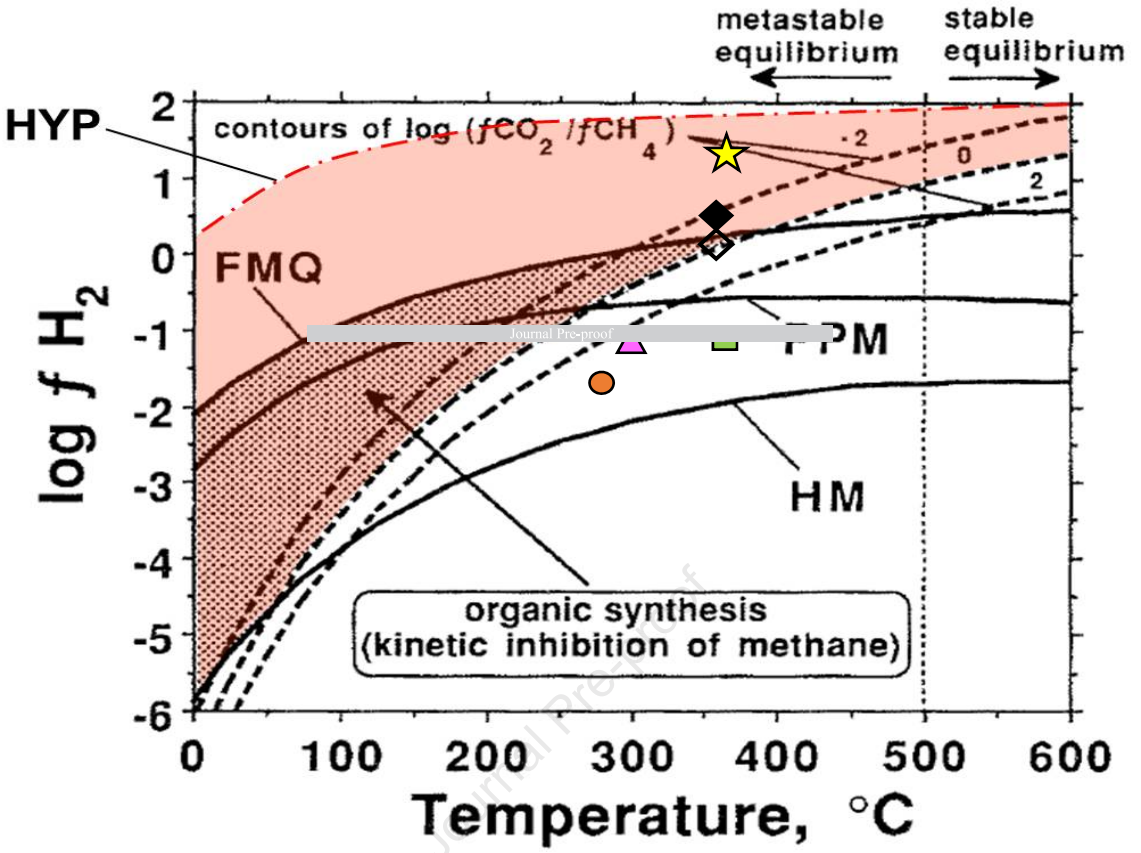

## Menez Gwen - linear alkanes

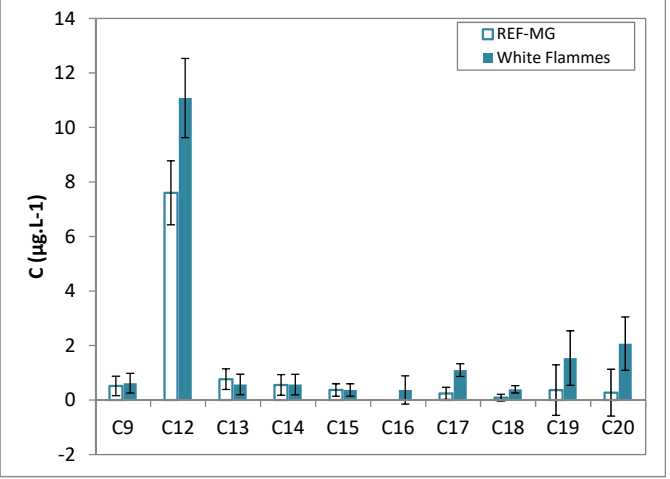


## Lucky Strike - linear alkanes

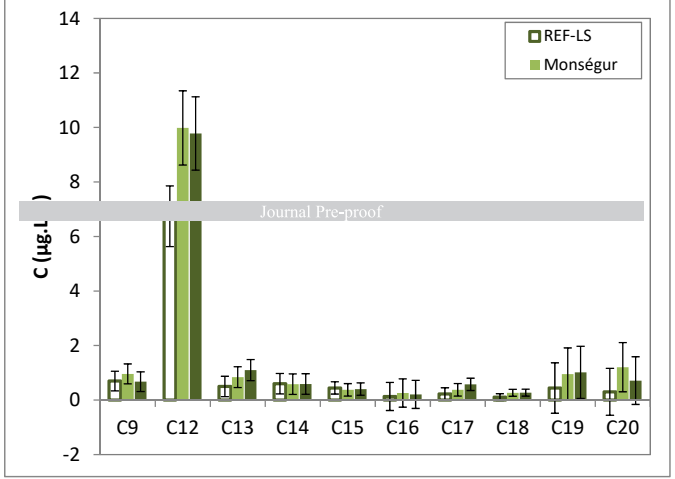




## Rainbow - linear alkanes

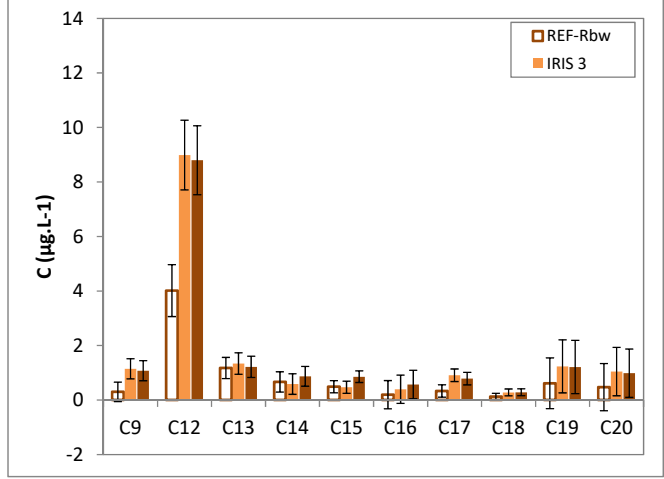


## Snake Pit - linear alkanes

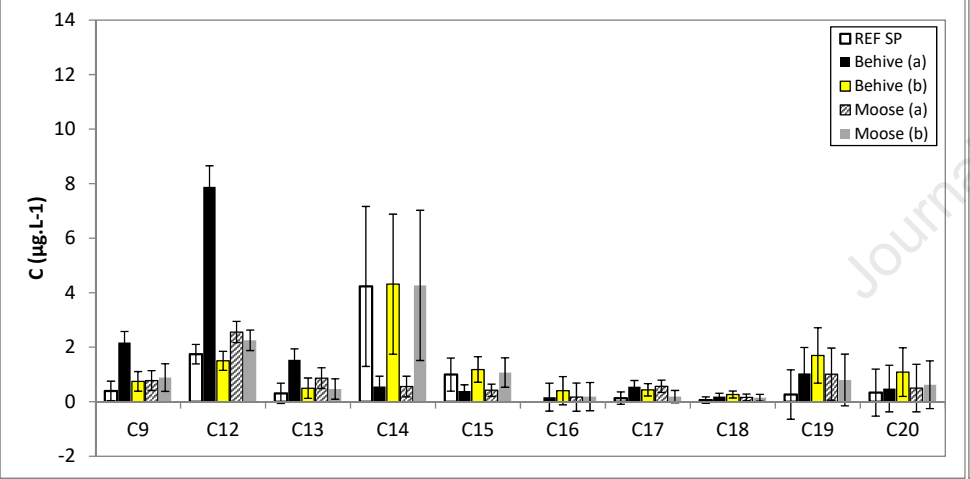


## TAG - linear alkanes

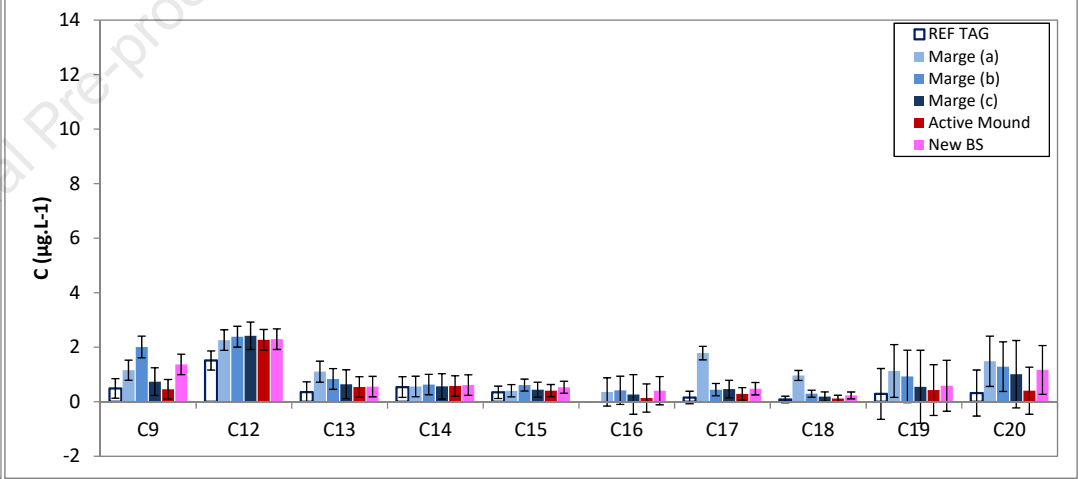

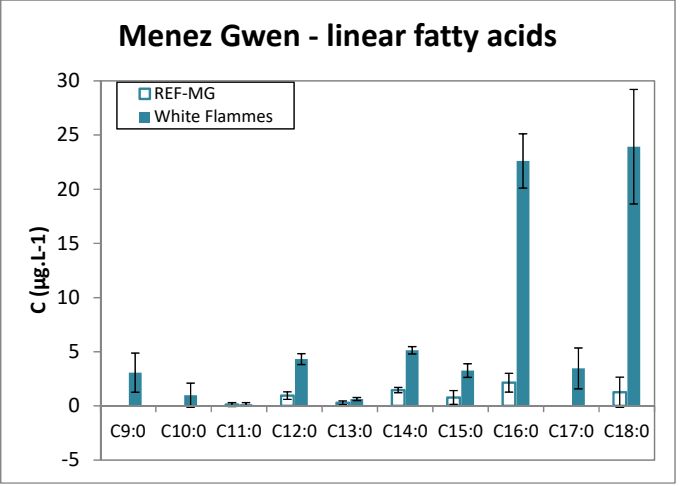


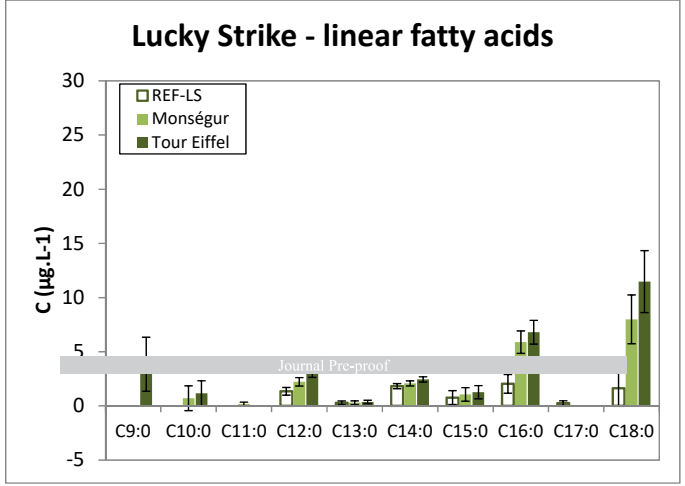


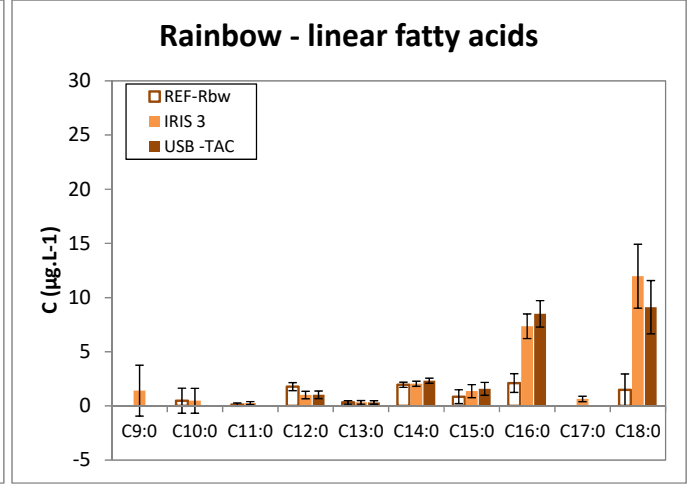


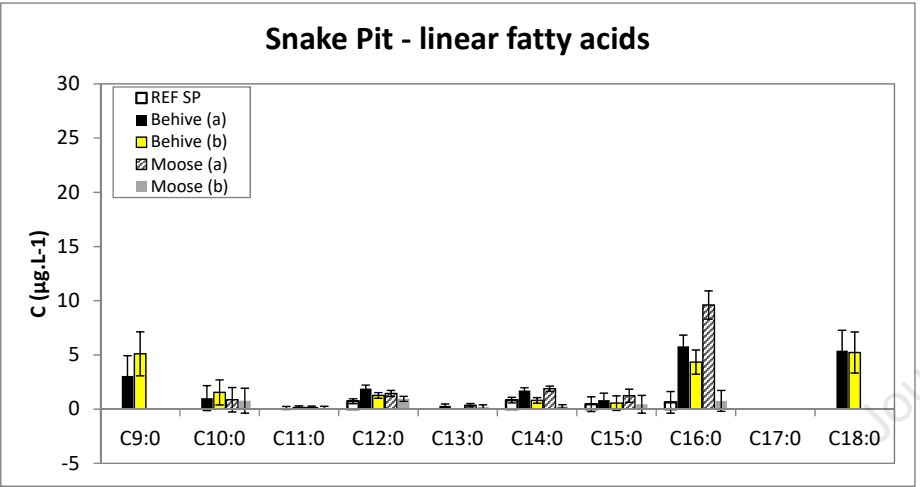


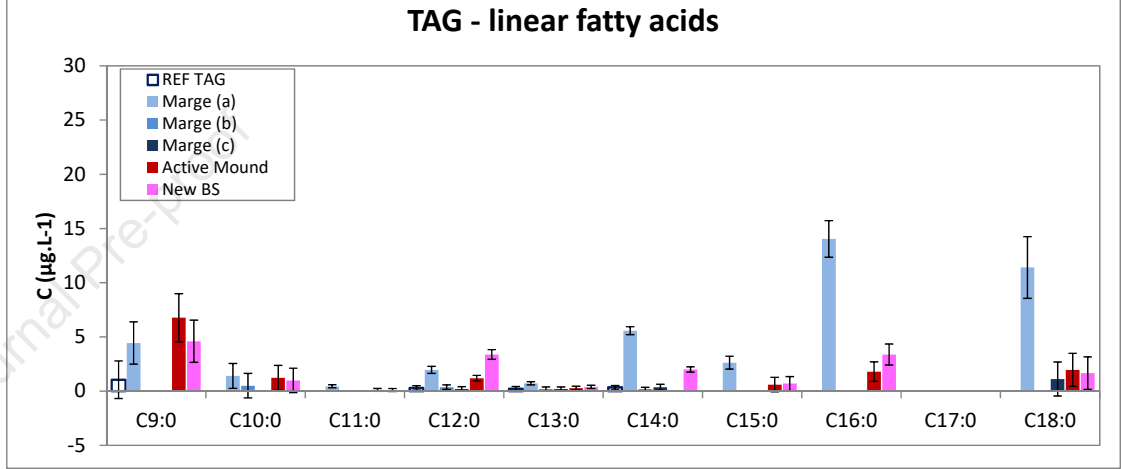

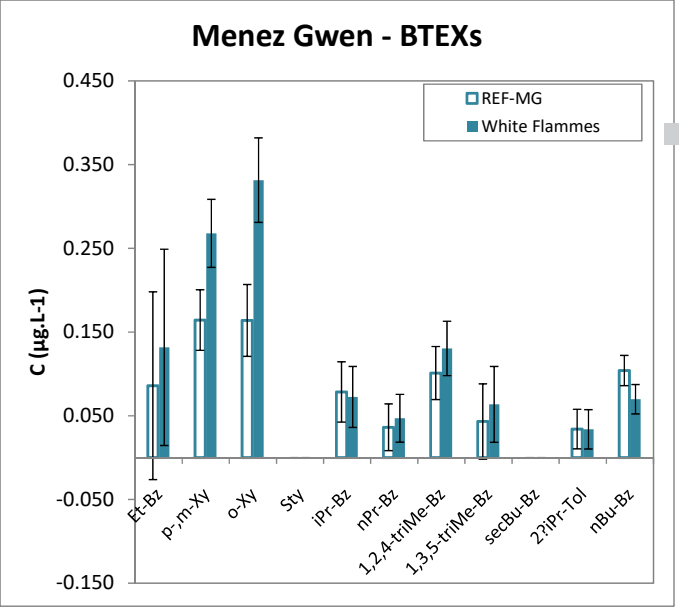


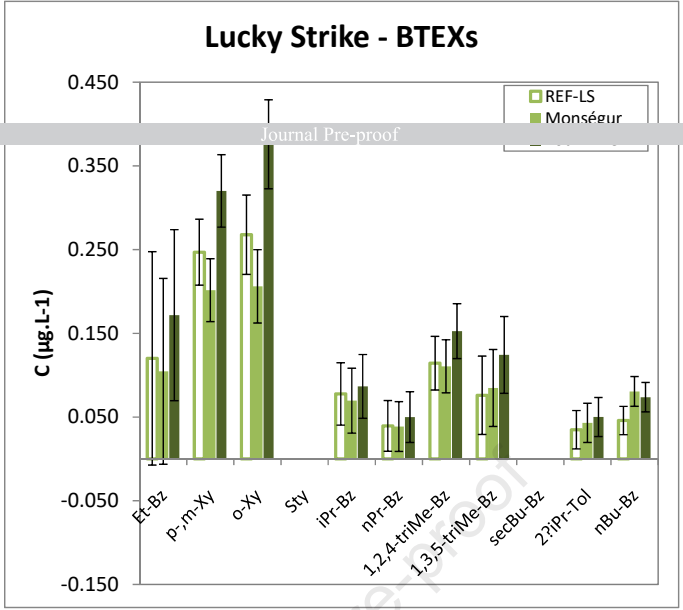


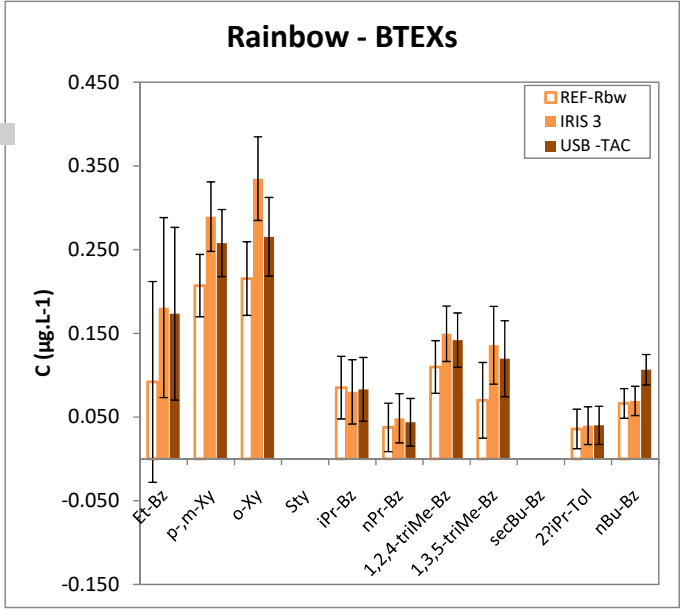


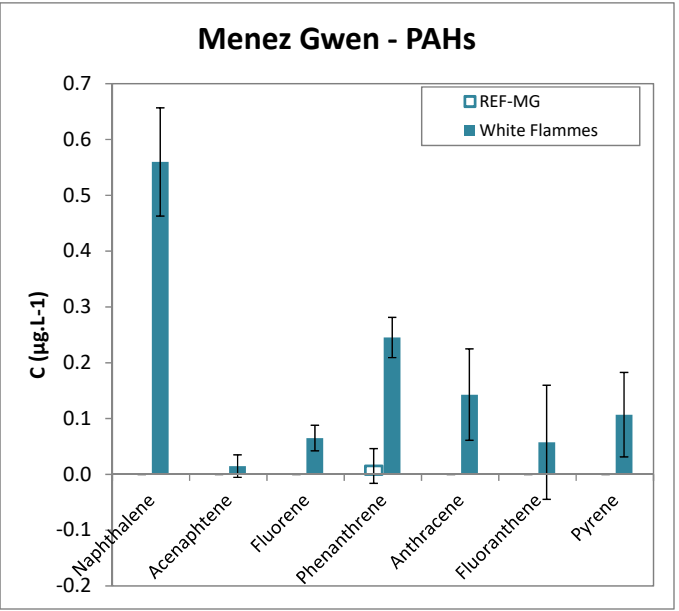


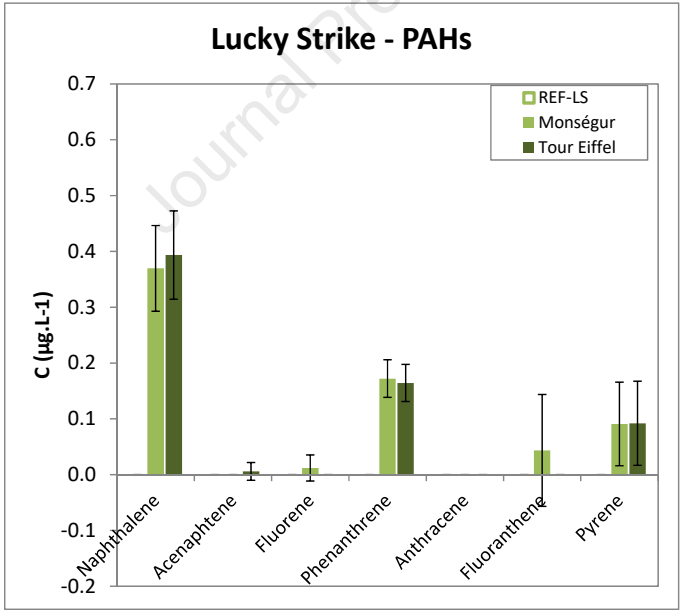


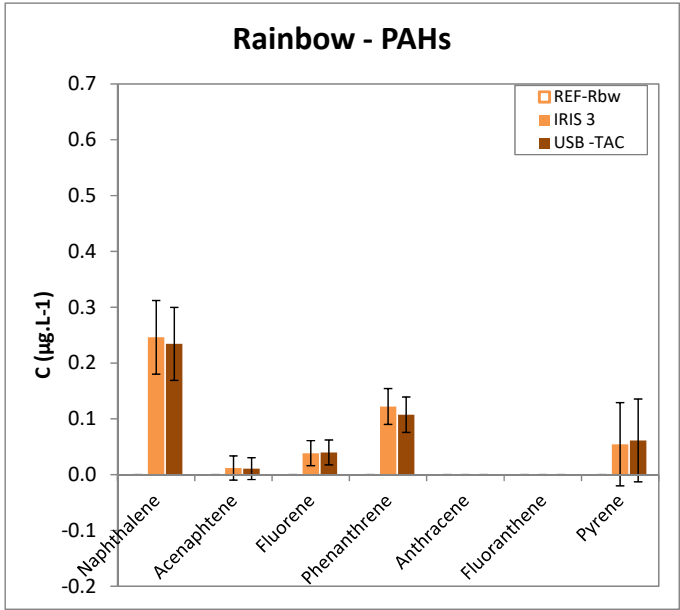

Organic compounds of MAR hydrothermal fluids : concentrations, interests and implications

**Declaration of interests**

☒ The authors declare that they have no known competing financial interests or personal relationships that could have appeared to influence the work reported in this paper.

☐The authors declare the following financial interests/personal relationships which may be considered as potential competing interests: